Ground-based measurement of Galactic Cosmic Rays
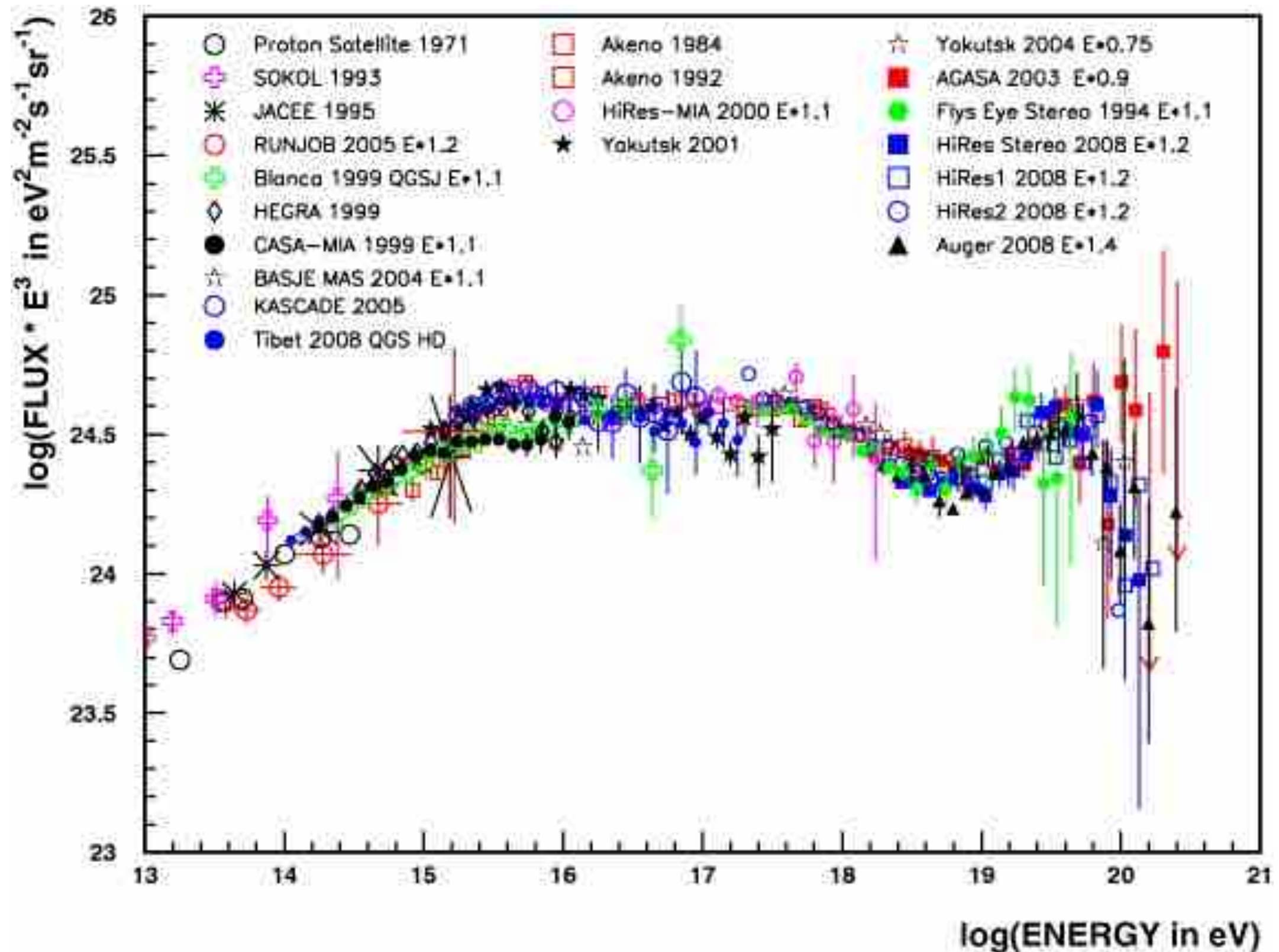
G. Di Sciascio

INFN - Roma Tor Vergata

disciascio@roma2.infn.it

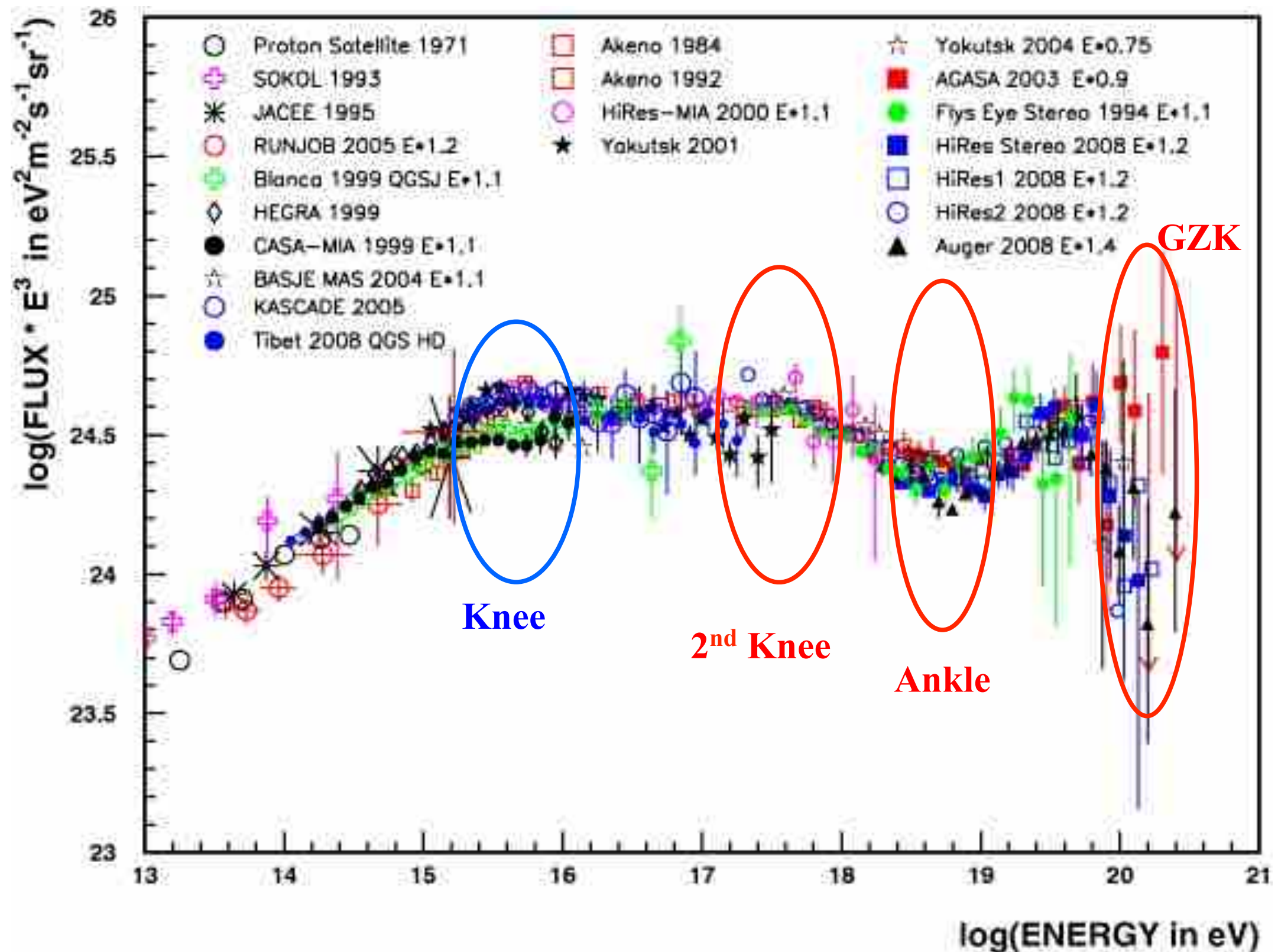*Stato e Prospettive della Fisica delle Astroparticelle*

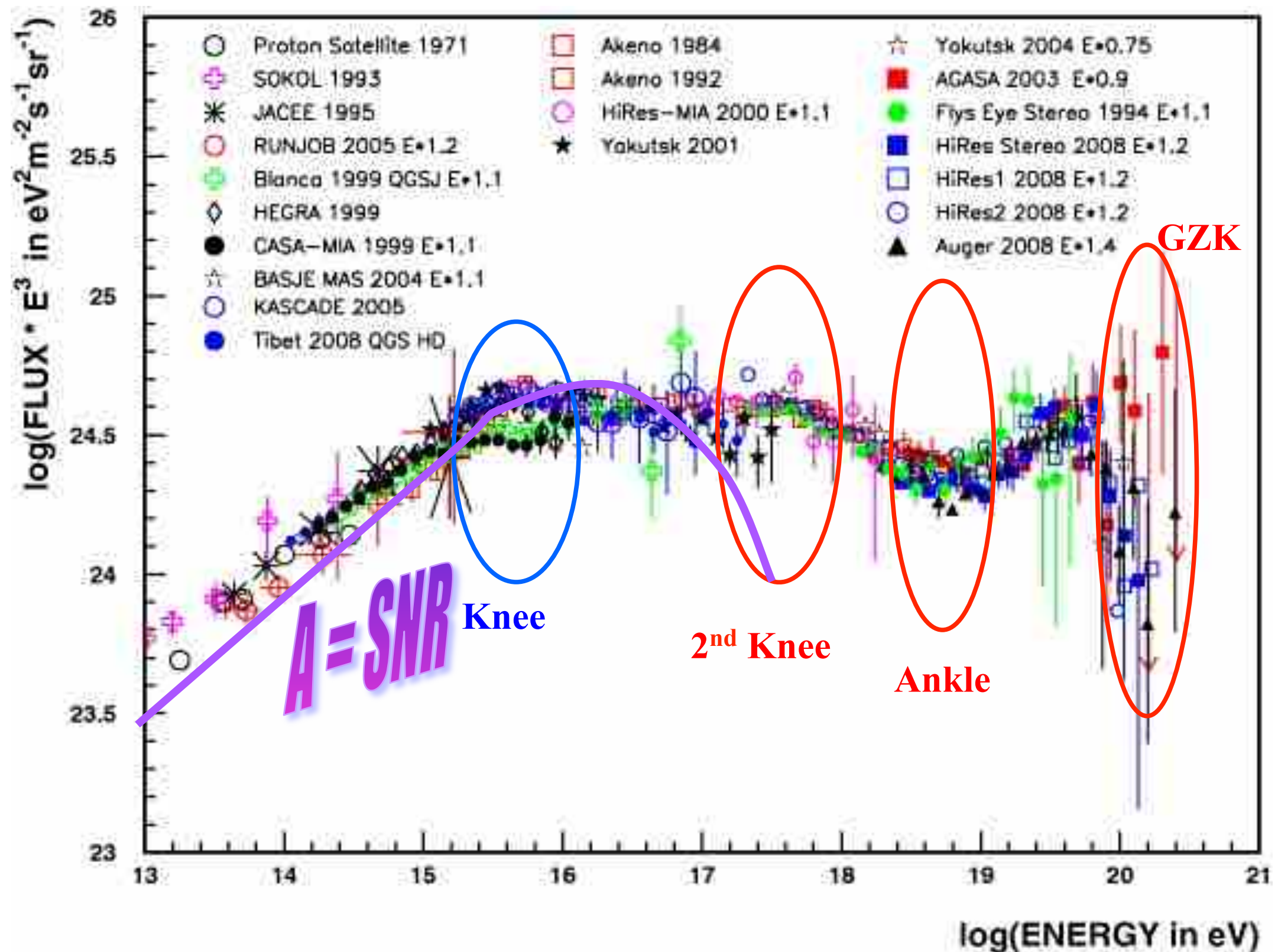Dipartimento di Fisica, Università 'La Sapienza', Roma
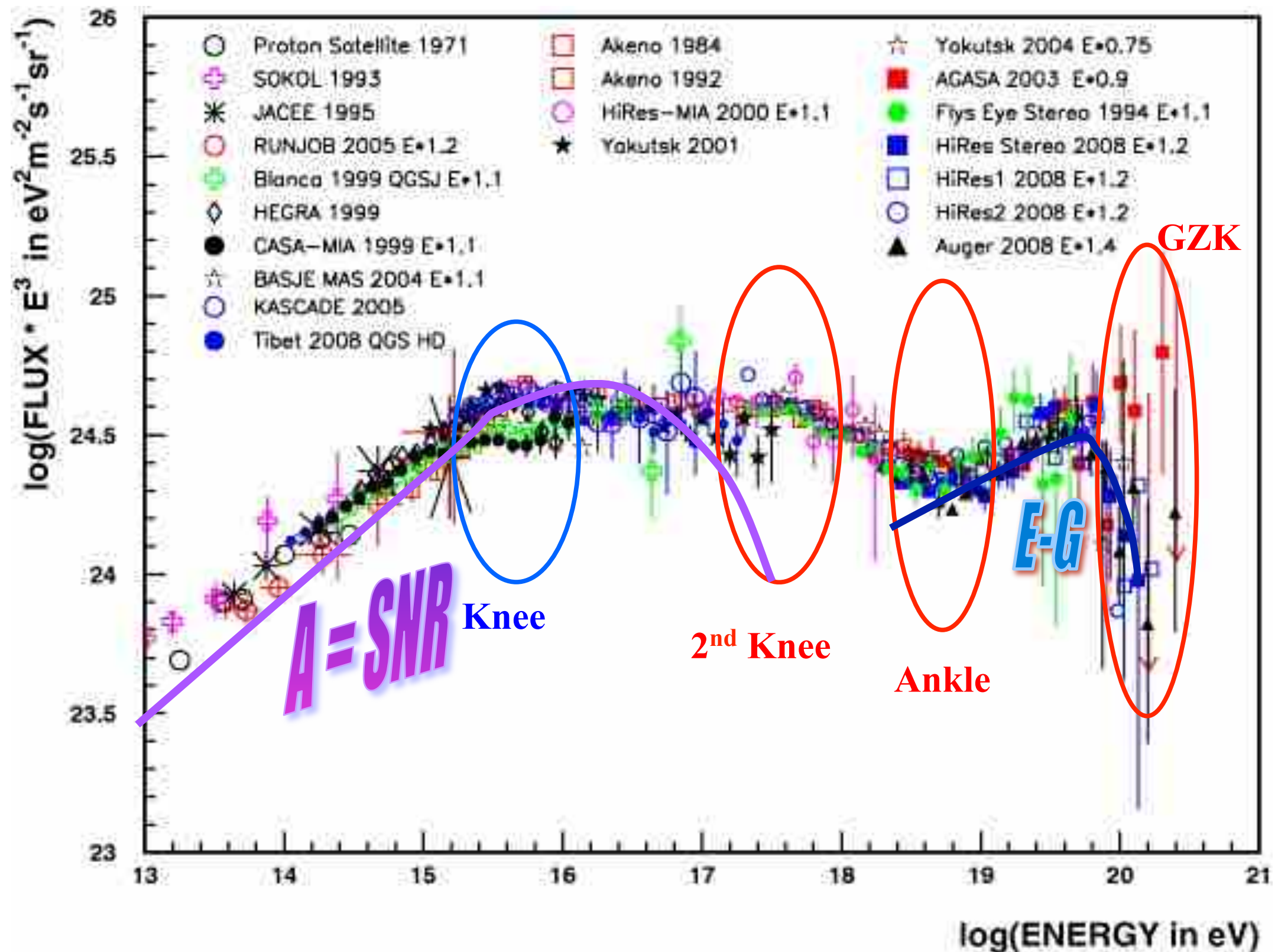
23 Novembre 2017

All-particle energy spectrum
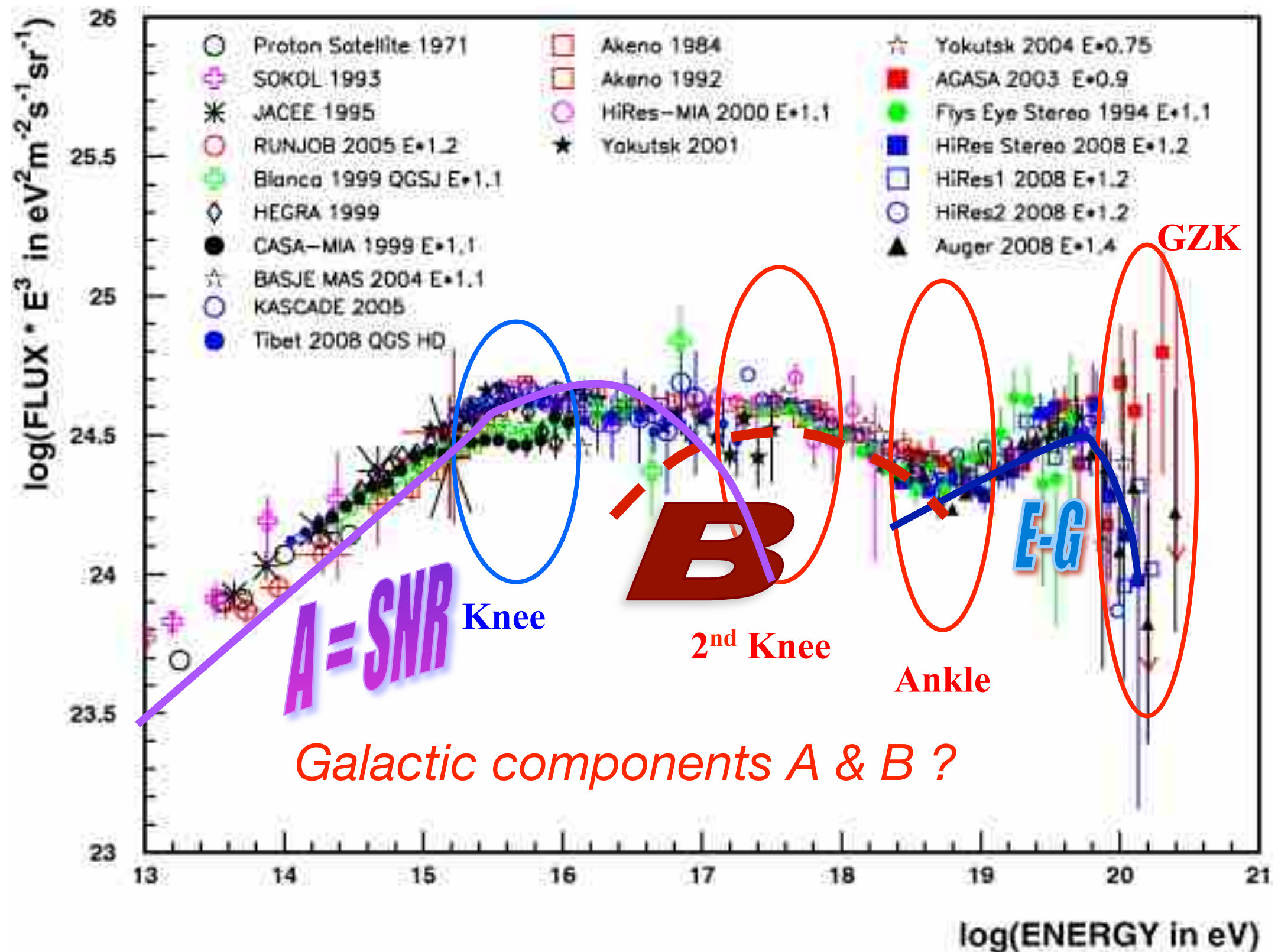
All-particle energy spectrum

All-particle energy spectrum

All-particle energy spectrum
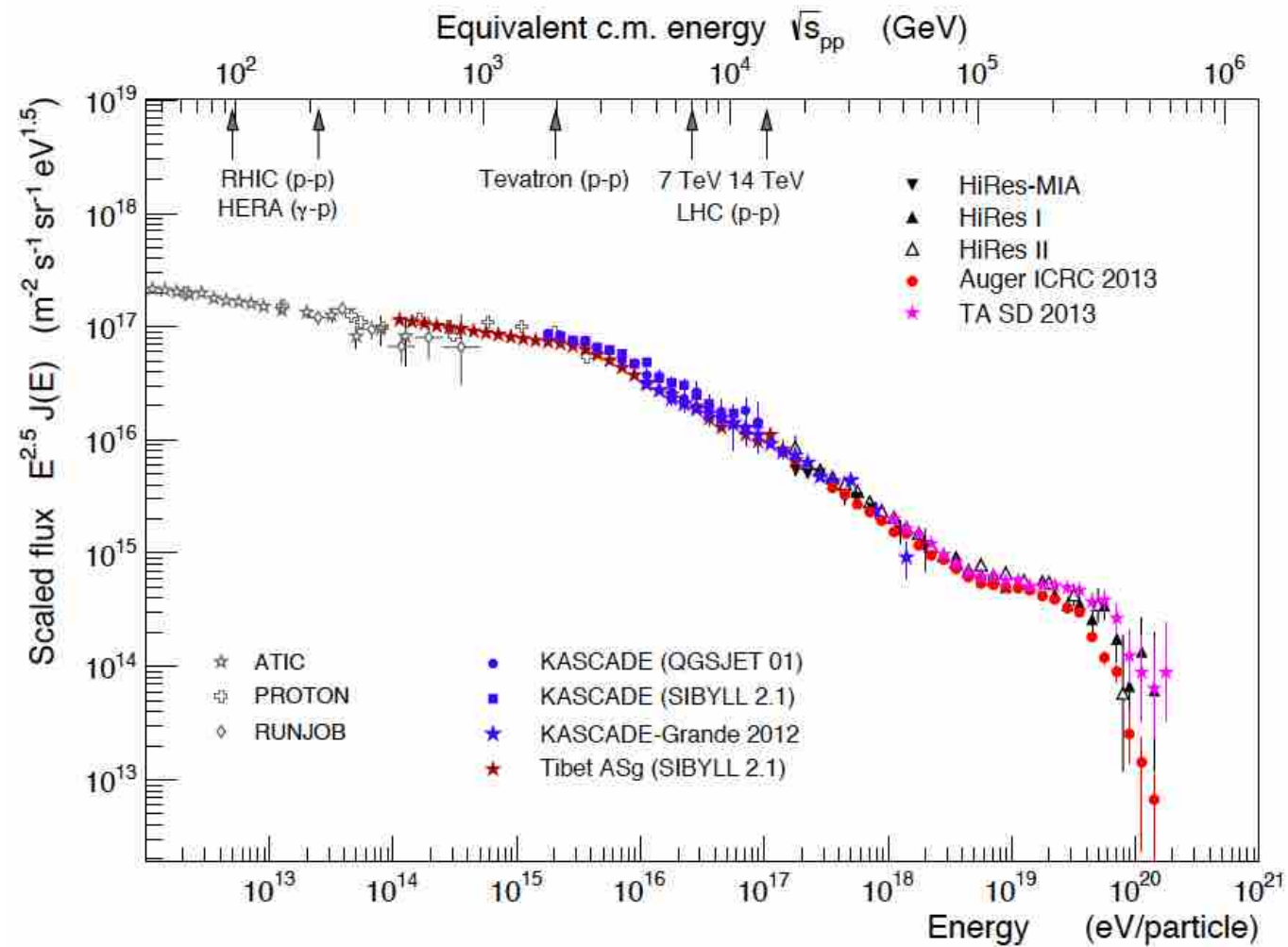
All-particle energy spectrum

Galactic Cosmic Rays

- CRs below 10^{17} eV are predominantly Galactic.

- *Standard paradigm*: Galactic CRs accelerated in SuperNova Remnants

- Galactic CRs via *diffusive* shock acceleration ?
  $n_{CR} \propto E^{-\gamma}$ (at source)

- Energy-dependent *diffusion* through Galaxy
  $n_{CR} \propto E^{-\gamma-\delta}$ (observed)

- Galactic CRs are scrambled by galactic magnetic field over very long time
  ➔ arrival direction *mostly isotropic*
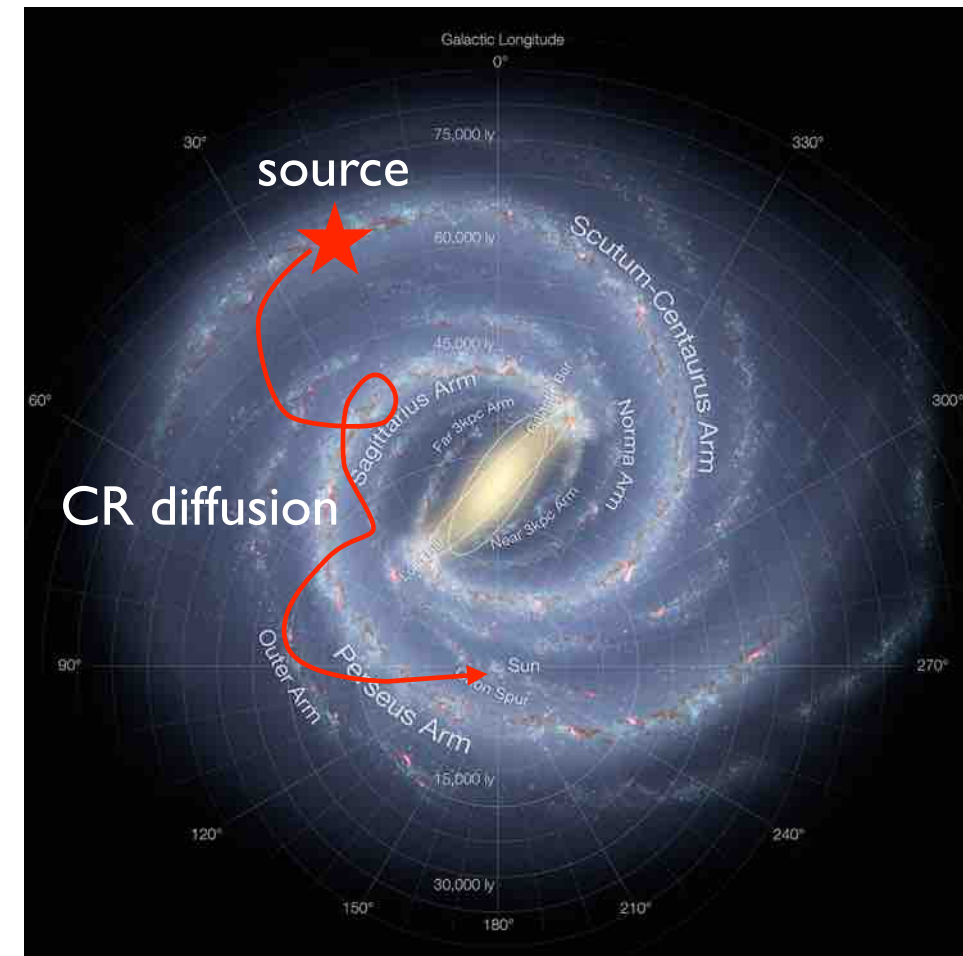
It is beyond any doubt that bulk of the CRs are originated in SNRs where they are accelerated by diffusive shock acceleration process at supernova blast waves driven by expanding SNRs.

The main open questions are: *(1) the total amount of energy channeled into relativistic particles; (2) the final spectrum injected into the ISM; (3) the maximum energy of accelerated particles.*

The *'knee'* in the CR energy spectrum

We'd like CR sources to accelerate (at least) up to that energy

CR knee @ few PeV's Something must happen here...

We would like SNRs to be CR PeVatrons...!

The *'knee'* in the CR energy spectrum
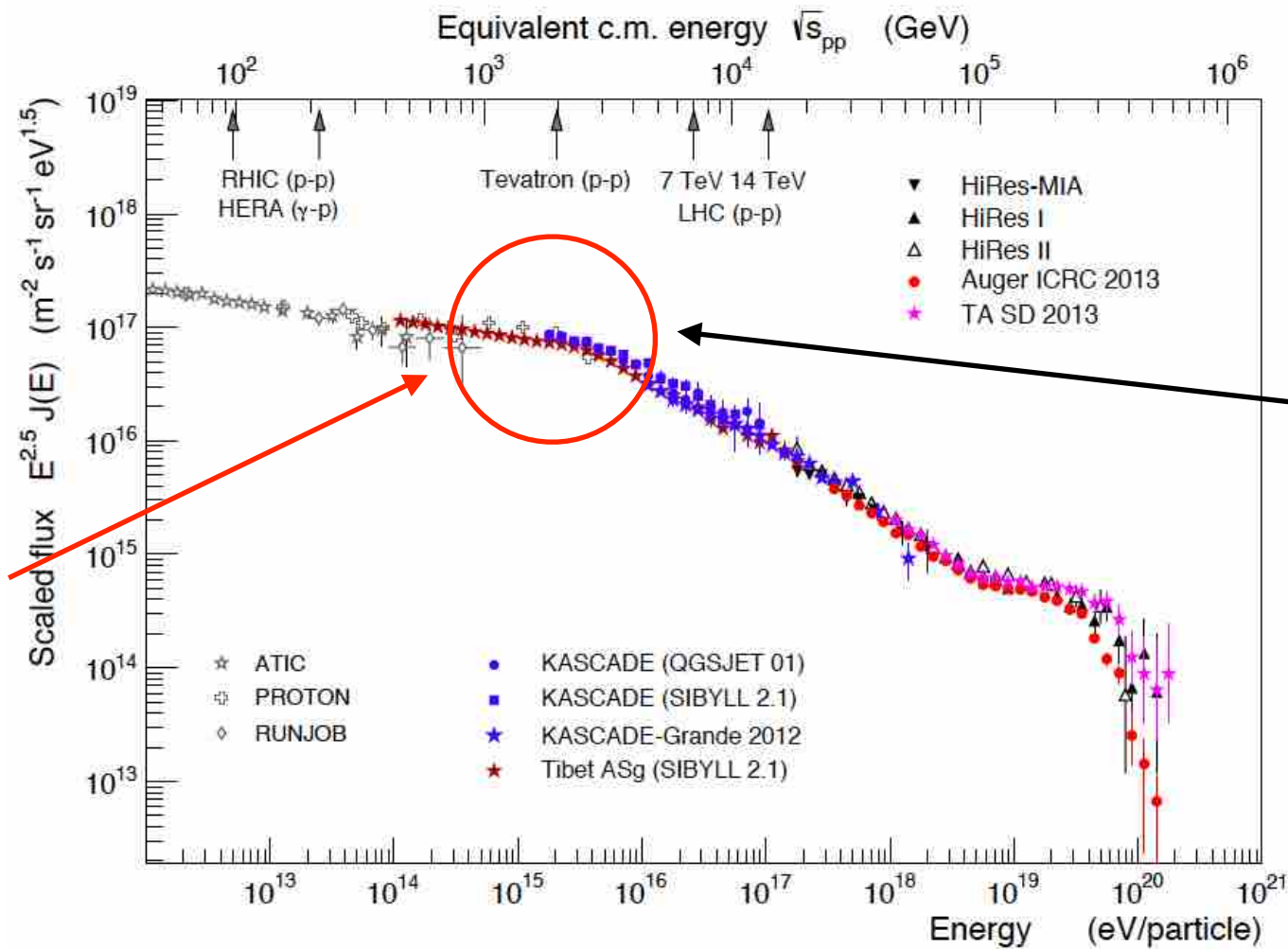
CR knee @ few PeV's Something must happen here...
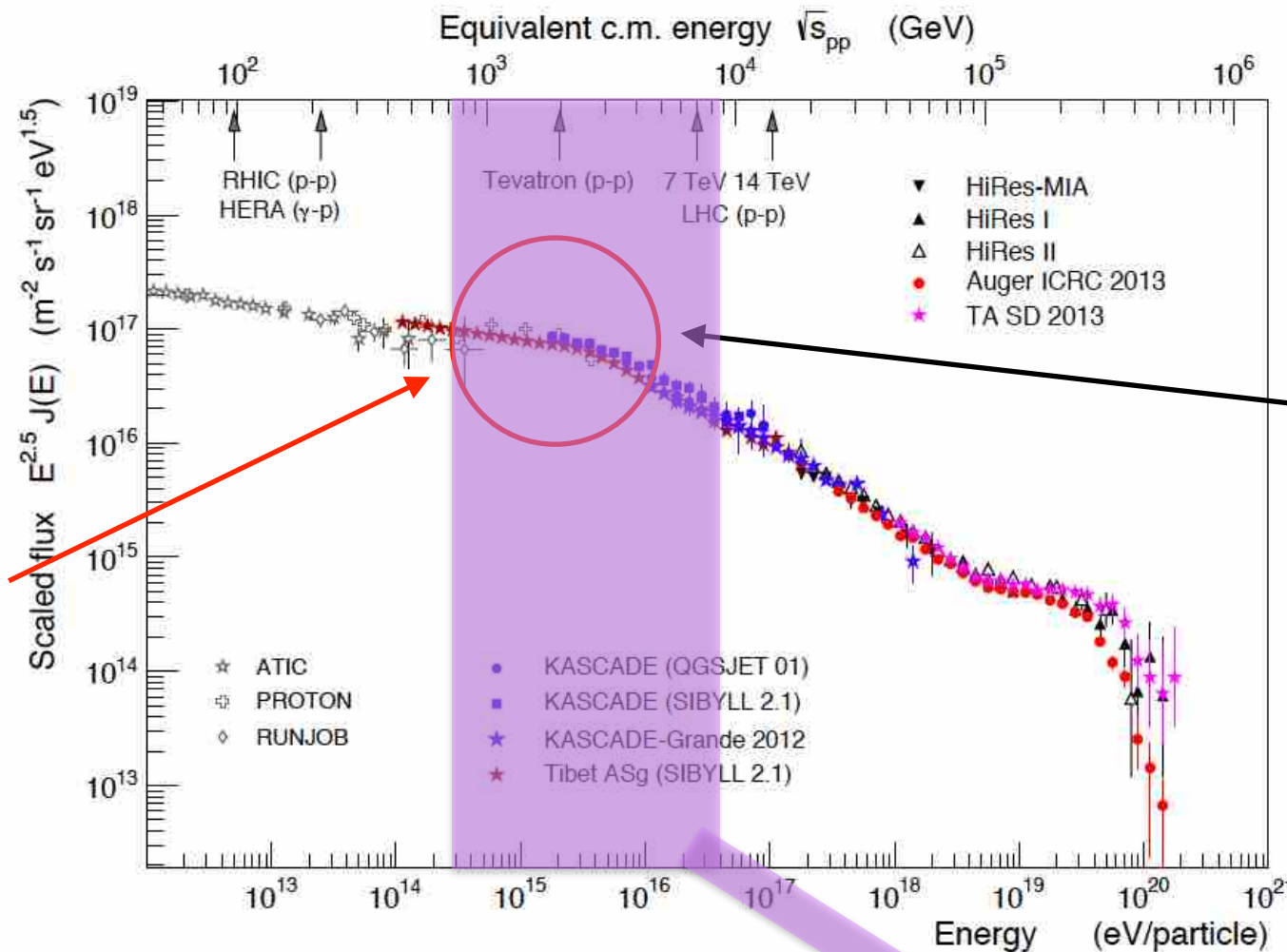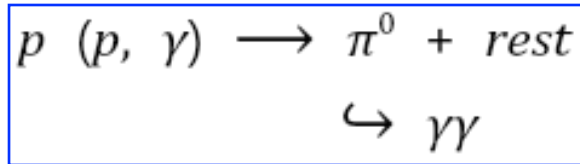
We'd like CR sources to accelerate (at least) up to that energy

We would like SNRs to be CR PeVatrons…!

Hadronic emission: CR sources

$$p \; (p, \gamma) \longrightarrow \pi^0 + rest$$
$$\hookrightarrow \gamma\gamma$$

Gammas from Galactic Cosmic Rays: $E_\gamma \sim E_{CR}/10$

PeV Cosmic Rays Photons > 100 TeV !

The *'knee'* in the CR size spectrum

In 1959 Kulikov & Khristiansen discoved a *'knee'* in the size spectrum of charged particles
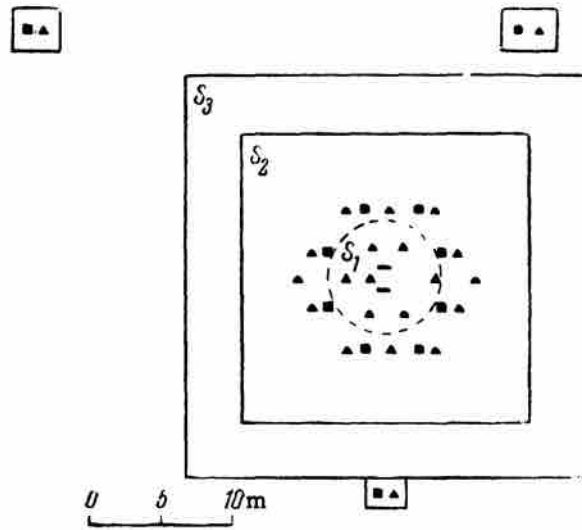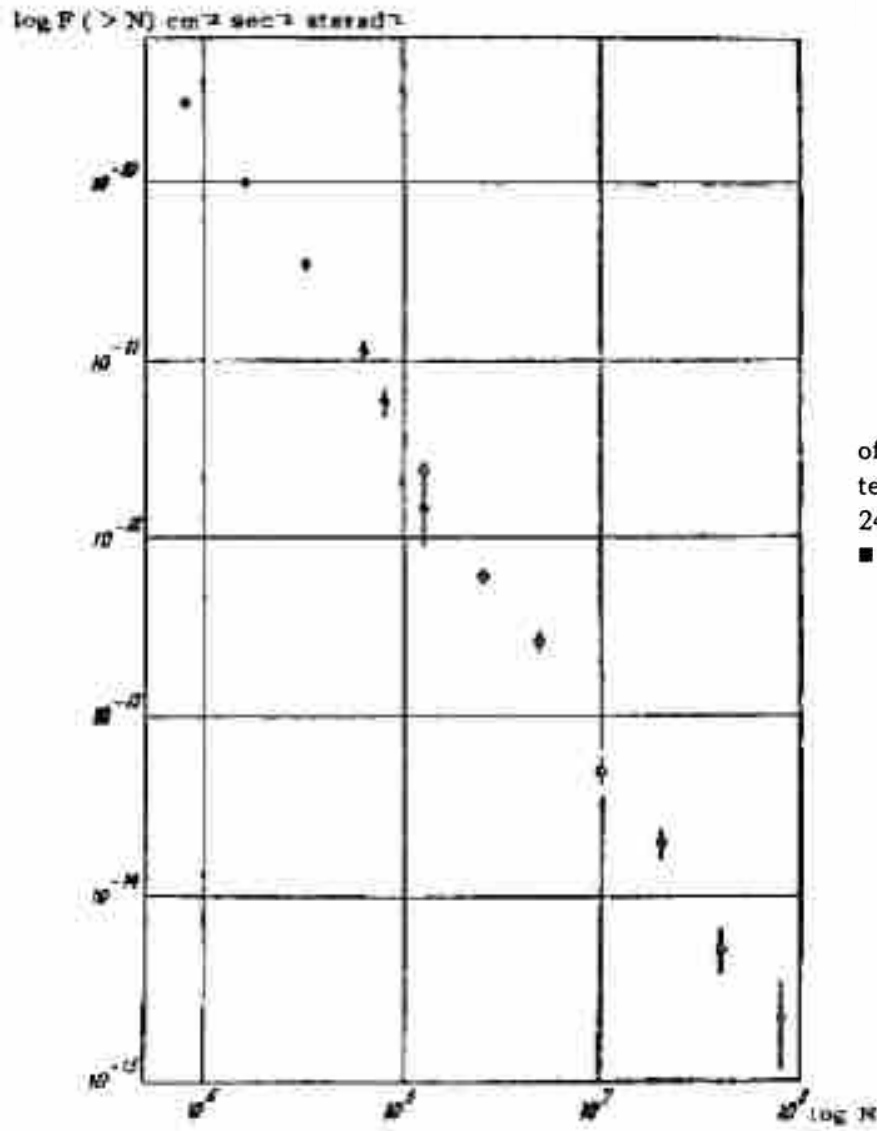
FIG. 1. Diagram of the hodoscope array used for the study of the size spectrum of EAS. ■ — group of 24 hodoscope counters, 330 cm² in area each; ▲ — group of 48 hodoscope counters 24 of area of 100 cm² each, and 24 of area of 24 cm² each, ■ — master groups.

In 1979 the Tien-Shan experiment observed a similar feature in the size spectrum of muons
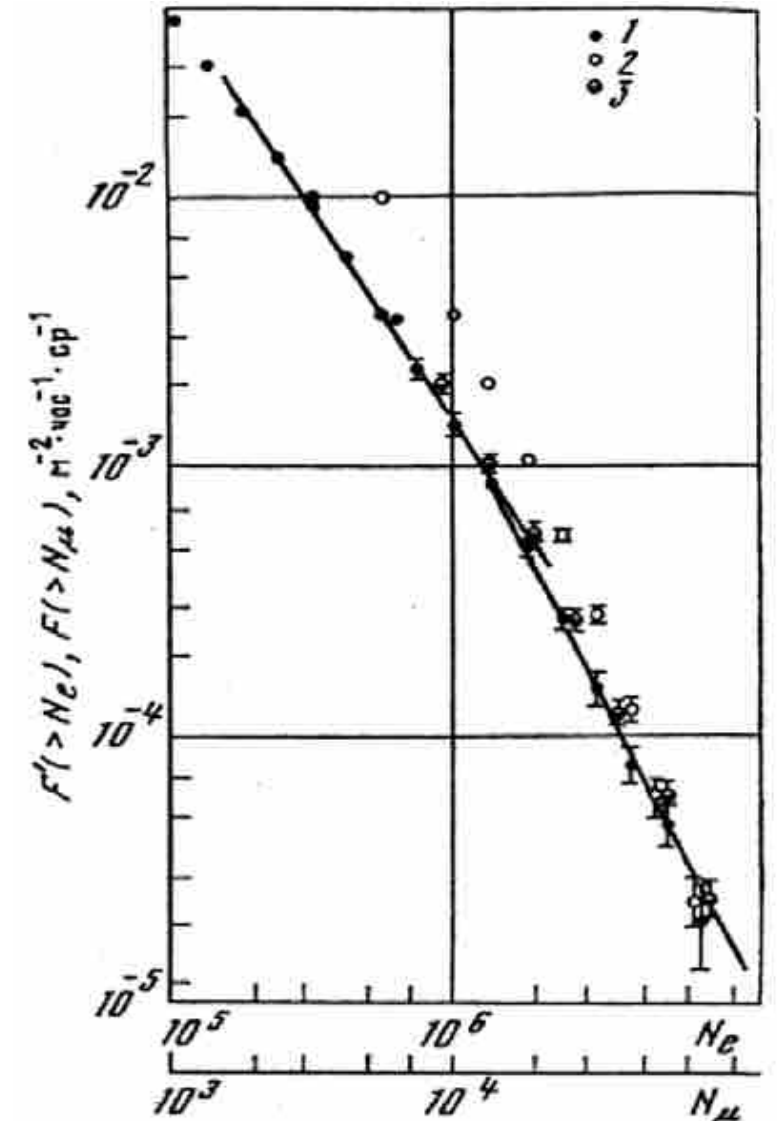
"It is evident that the particles with $E \geq 10^{16}$ eV may have a metagalactic origin.

The observed spectrum is a superposition of the spectra of particles of galactic and metagalactic origin."

Kulikov & Khristiansen, JETP 35 (1959) 441

The origin of the *'knee'*

In 1961 B. Peters postulated a *rigidity cutoff model.*

If E_{max} depends on B then p disappear first, then He, C, O, etc

gyro-radius = Pc / ZeB ≡ R (rigidity) / B

➜ E_{total} (knee) ~ Z × R(knee)

$E_{max} \sim Z \cdot 10^{15}$ eV

Z = 1

Z = 2

Z = 3

$E_{max}(iron) = 26 \times E_{max}(proton)$

FLUX

ENERGY
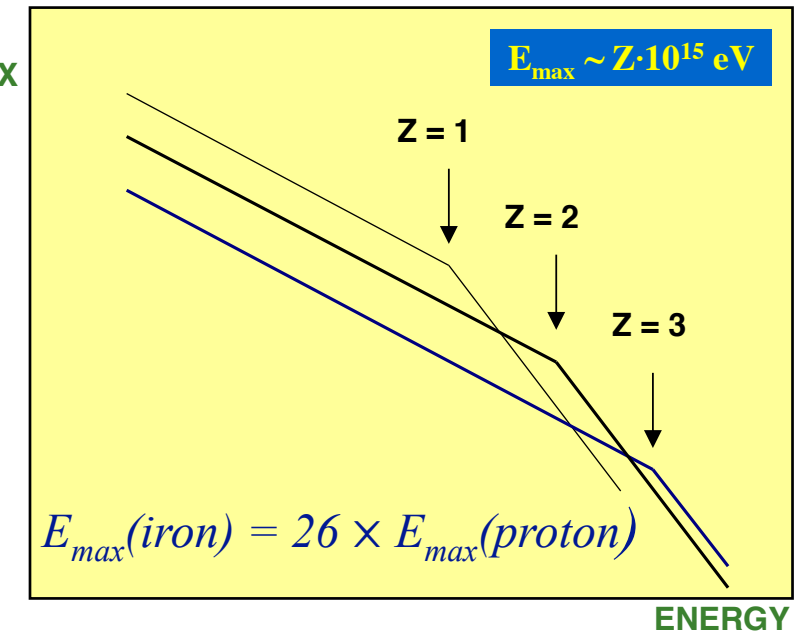
Problem: E_{knee} is higher than expected

Peters cycle: *systematic increase of < A > approaching E_{max}*
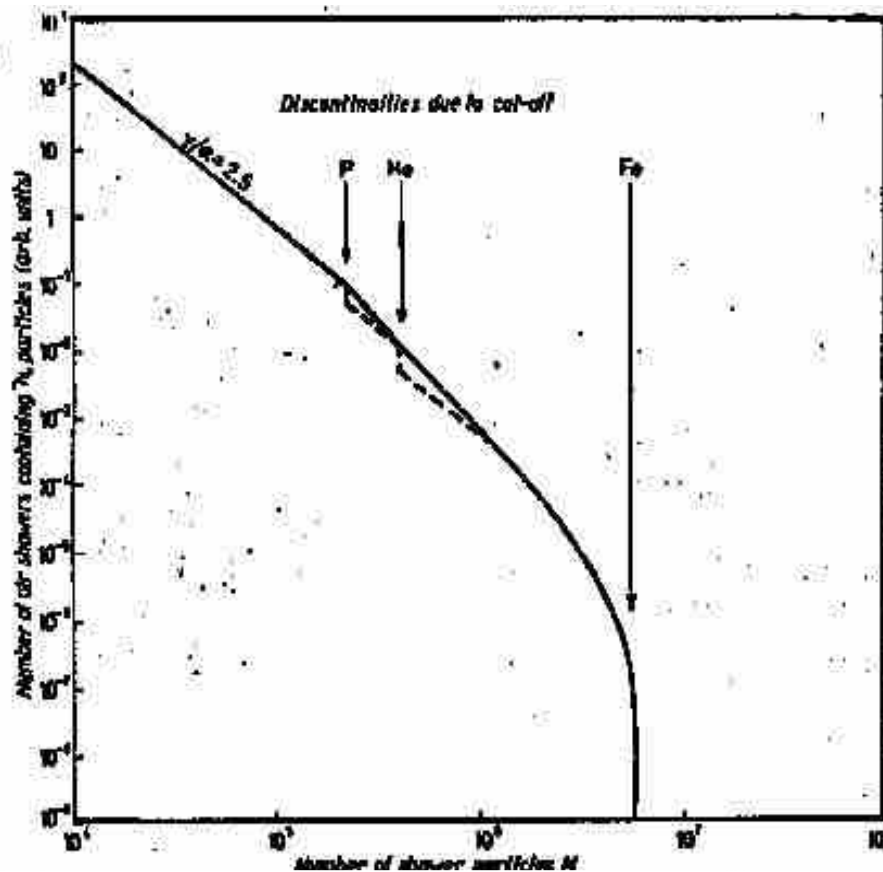
<A> should begin to decrease again for E > 30 x E_{knee}
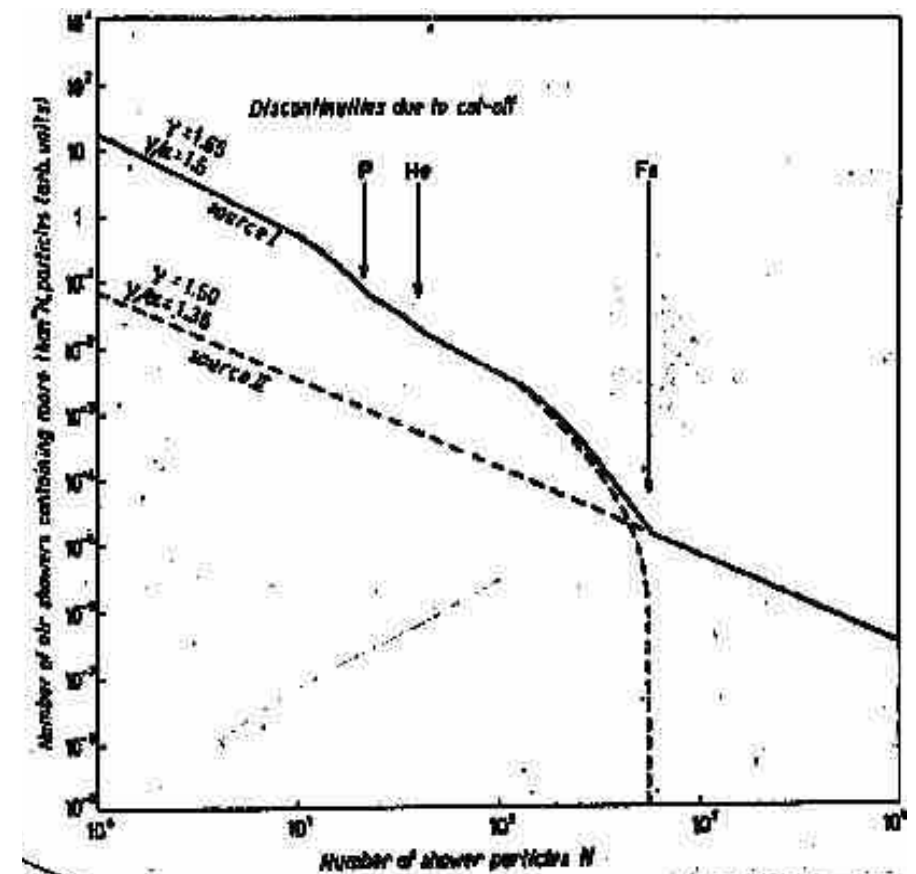
B. Peters, Nuovo Cimento 22 (1961) 800

Knee as end of Galactic population ?

Understanding the origin of the "knee" is the key for a comprehensive theory of the origin of CRs up to the highest observed energies.

In fact, the knee is clearly connected with the issue of the end of the Galactic CR spectrum and the transition from Galactic to extra-galactic CRs.
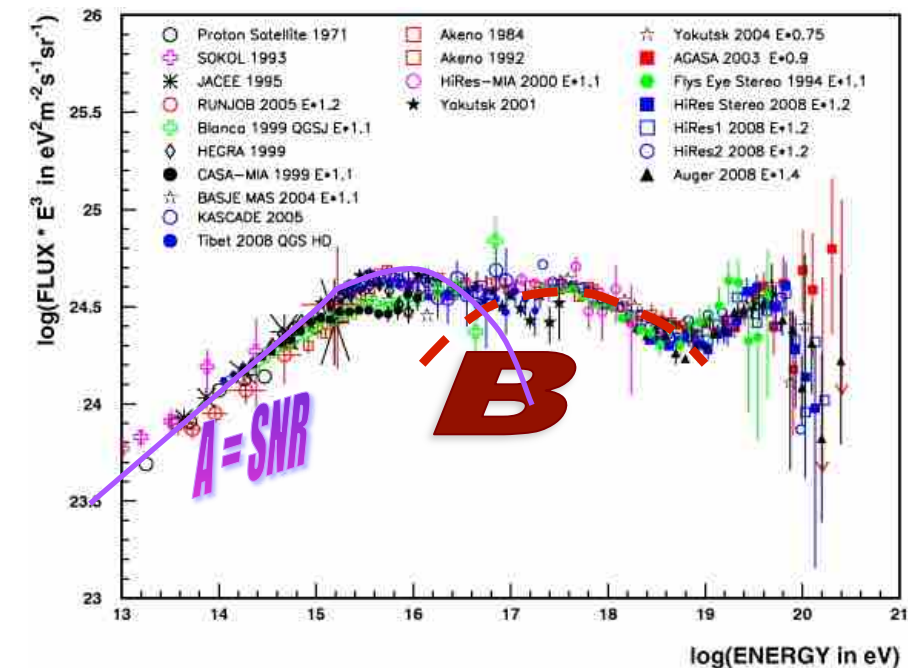
★ *Rigidity* models can be *rigidity-acceleration* models or *rigidity-confinement* models

- *Accelerator feature*: maximum energy of acceleration
  ➜ implies that all accelerators are similar

- *Structure generated by propagation:* ➜ implies that the (main) Galactic CR accelerators must be capable to accelerate to much higher energy

If the "knee" is a *propagation effect*, the Galaxy contains *"super-PeVatrons"* and the study of these objects requires *Gamma-Ray Astronomy at Very High Energy* (100 - 1000 TeV).

➜ Strong interest in the PeV gamma ray (and neutrino) astronomy.

Max energy of accelerated particles

The description of how particles escape from a SNR shock has not been completely understood yet, the reason being the uncertainties related to *how particles reach the maximum energies*.

The maximum energy attainable in SNR shocks is directly related to the magnetic fields that confines the particles at high energies to the shock area.

HILLAS plot

R=acceleration site dimensions

$$\left(\frac{E}{10^{20}\,\mathrm{eV}}\right) < 0.3 \cdot \frac{1}{2} \cdot Z \cdot \beta \cdot \left(\frac{L}{10^{12}\,\mathrm{km}}\right) \cdot \left(\frac{B}{\mathrm{G}}\right)$$

Max energy of accelerated particles

The description of how particles escape from a SNR shock has not been completely understood yet, the reason being the uncertainties related to *how particles reach the maximum energies*.

Morlino arXiv:1706.08275

The maximum energy attainable in SNR shocks is directly related to the magnetic fields that confines the particles at high energies to the shock area.

On a general ground, we have two different scenarios

- $E_{max} \approx Z \times 2 \times 10^{14}$ eV which is the theoretical upper limit under normal magnetic field picture ($\approx 10\ \mu G$).

- $E_{max} \approx Z \times 3 \times 10^{15}$ eV, achievable under amplified magnetic field situation (order of few hundreds μG), the *PeVatron scenario*.

HILLAS plot

R=acceleration site dimensions

$$\left(\frac{E}{10^{20}\ \text{eV}}\right) < 0.3 \cdot \frac{1}{2} \cdot Z \cdot \beta \cdot \left(\frac{L}{10^{12}\ \text{km}}\right) \cdot \left(\frac{B}{\text{G}}\right)$$
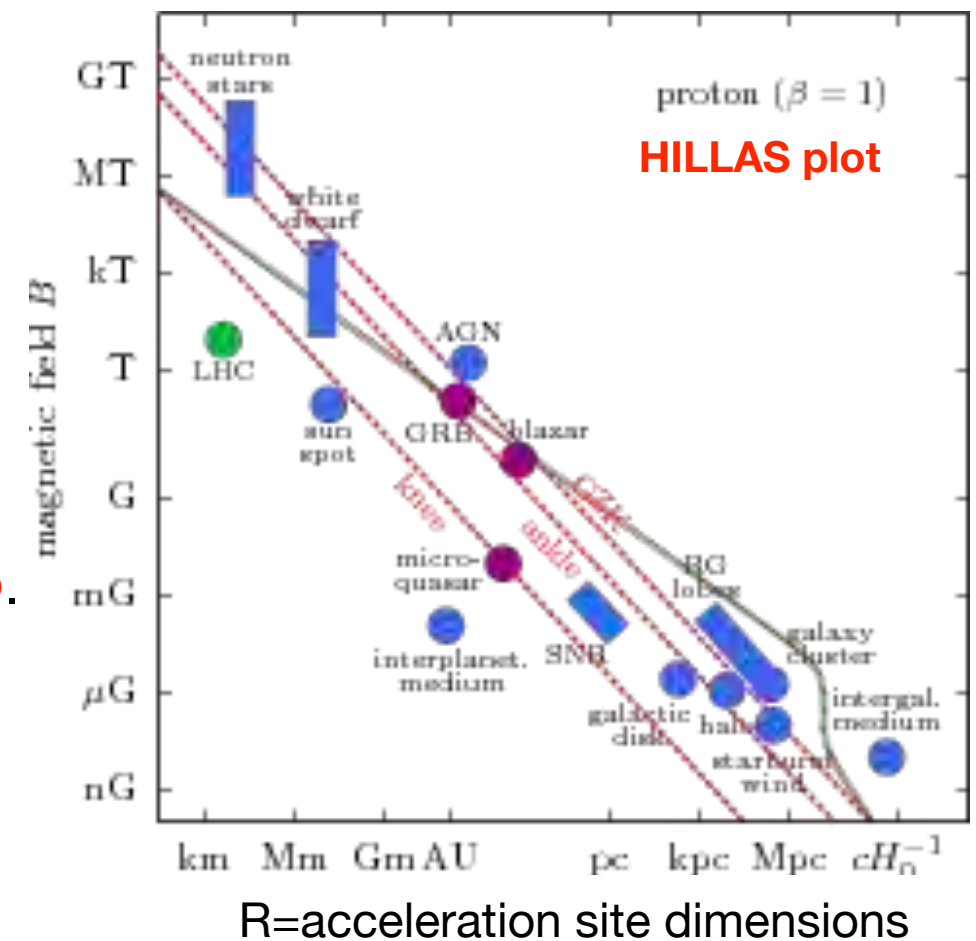
Max energy of accelerated particles

The description of how particles escape from a SNR shock has not been completely understood yet, the reason being the uncertainties related to *how particles reach the maximum energies*.

Morlino arXiv:1706.08275

The maximum energy attainable in SNR shocks is directly related to the magnetic fields that confines the particles at high energies to the shock area.

On a general ground, we have two different scenarios

- $E_{max} \approx Z \times 2 \times 10^{14}$ eV which is the theoretical upper limit under normal magnetic field picture ($\approx 10 \ \mu G$).

- $E_{max} \approx Z \times 3 \times 10^{15}$ eV, achievable under amplified magnetic field situation (order of few hundreds μG), the *PeVatron scenario*.

But "*acceleration up to PeV energies is problematic* in all scenarios considered. This implies that either a different (more efficient) mechanism of magnetic field amplification operates at SNR shocks, or that *the sources of GCR in the PeV energy range should be searched somewhere else*."

Gabici arXiv:1610.07638

HILLAS plot

R=acceleration site dimensions
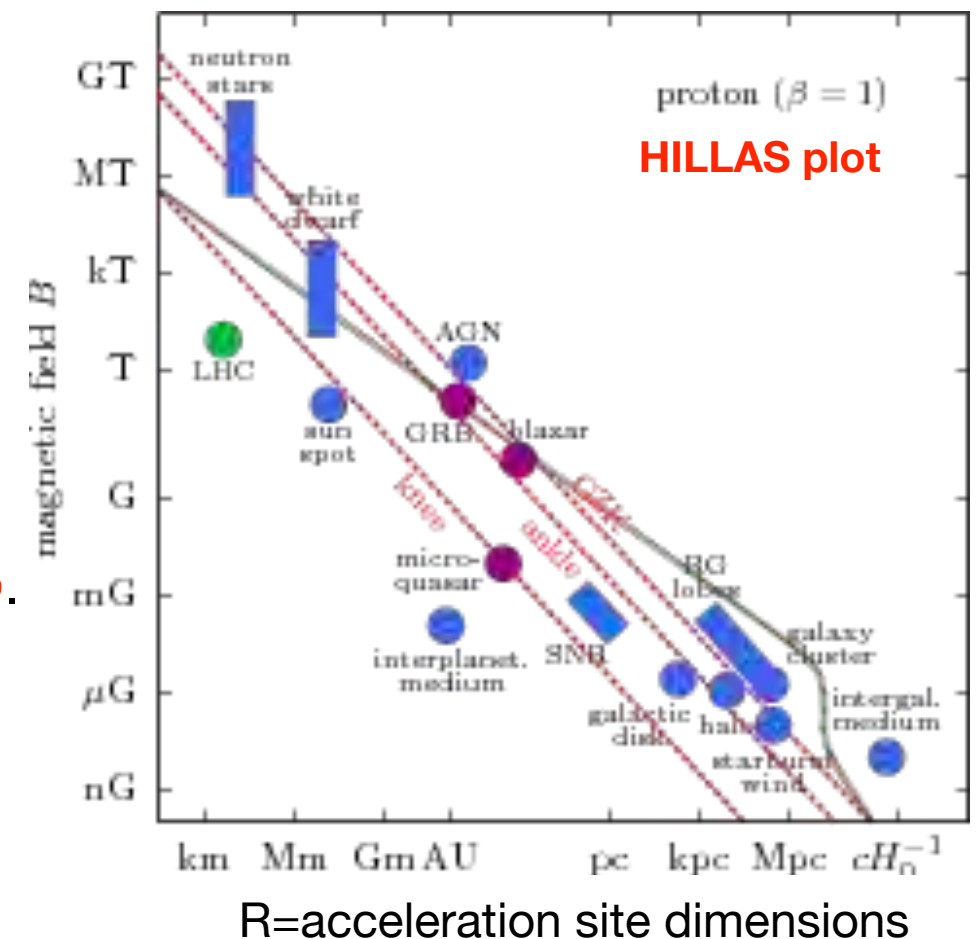
$$\left(\frac{E}{10^{20} \, \text{eV}} \right) < 0.3 \cdot \frac{1}{2} \cdot Z \cdot \beta \cdot \left(\frac{L}{10^{12} \, \text{km}} \right) \cdot \left(\frac{B}{\text{G}} \right)$$

Are SuperNova Remnants CR PeVatrons ?

$f(p) \propto p^{-4}$
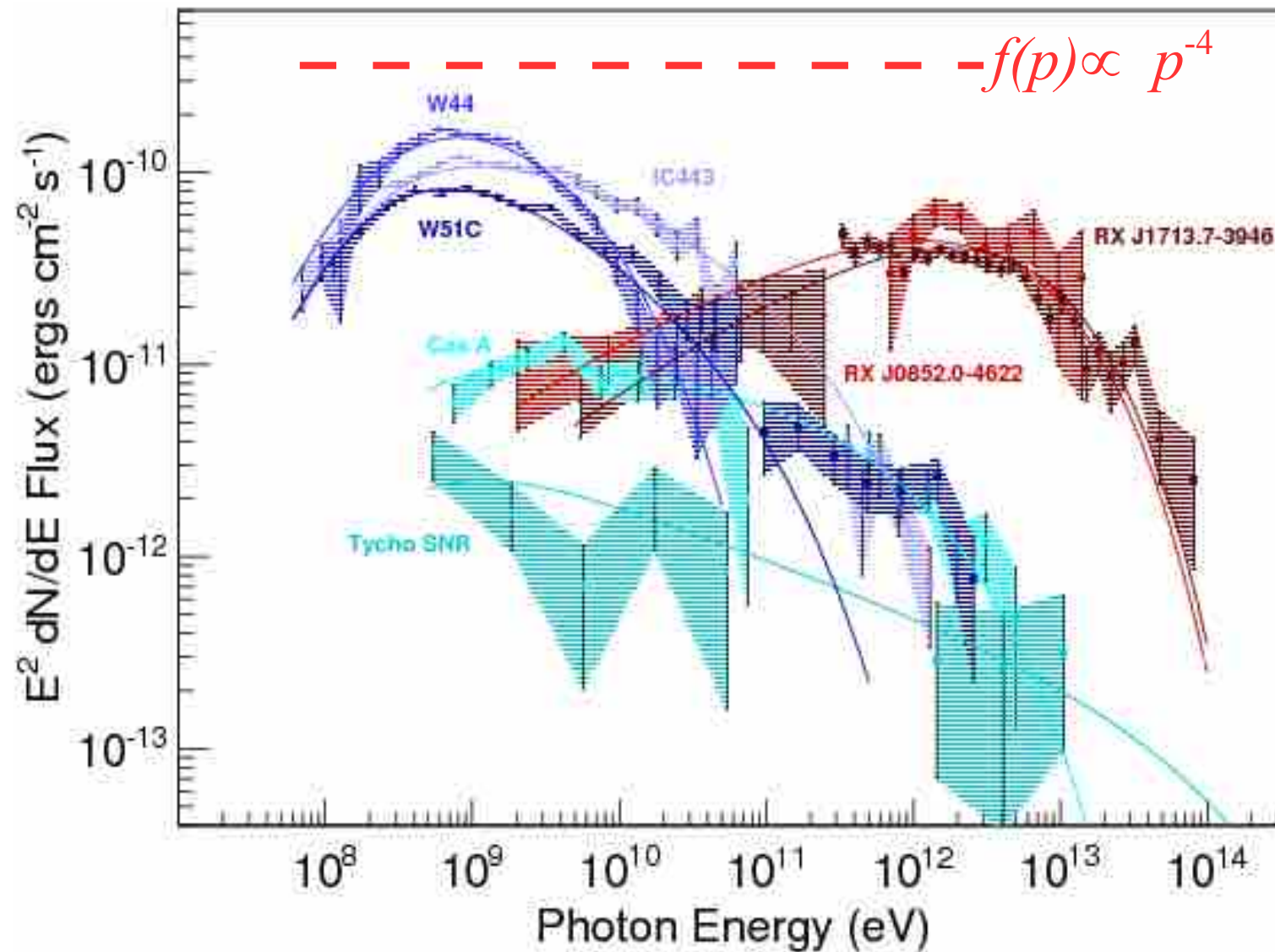
S. Funk, *Ann.Rev.Nucl.Part.Sci.* 65 (2015)

Middle-aged SNRs (~20.000 yrs)
- ✦ **hadronic emission**
- ✦ **steep spectra** $\sim E^{-3}$
- ✦ $E_{max} < 1$ **TeV**

Young SNRs (~2000 yrs)
- ✦ **hadronic/leptonic ?**
- ✦ **hard spectra**
- ✦ $E_{max} \approx 10 - 100$ **TeV**

Very young SNRs (~300 yrs)
- ✦ **hadronic**
- ✦ **steep spectra** $\sim E^{-2.3}$
- ✦ $E_{max} \approx 10 - 100$ **TeV**

a general trend of the γ-ray spectrum with the age ?

Not enough to explain the Knee at ~ PeV

Understanding the origin of the knee

If the knee is a source property we should see a corresponding spectral feature in the gamma-ray spectra of CR sources.
If the knee is the result of propagation, we should observe a *knee that is potentially dependent on location*, because the propagation properties depend on position in the Galaxy.

Vernetto & Lipari: ICRC 2017

Different models to explain the 'knee' and different signatures…

- **Acceleration in SNRs:**
  finite lifetime of shock $E_{max} = Z \cdot 10^{15}$ eV ⟹
  - Eknee $\propto Z$
  - No anisotropy change across the knee region

- **Diffusion process:**
  probability of escape from Galaxy = $f(Z)$ ⟹
  - Eknee $\propto Z$
  - Anisotropy $\propto E^{\delta}$

- **Interaction with bkg particles:**
  Photo-disintegration, etc. ⟹
  - Eknee $\propto A$

- **Change in particle interaction**
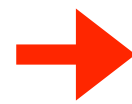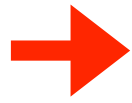
Key elements: *mass composition* and *anisotropy*

Understanding the origin of the knee

If the knee is a source property we should see a corresponding spectral feature in the gamma-ray spectra of CR sources.
If the knee is the result of propagation, we should observe a *knee that is potentially dependent on location*, because the propagation properties depend on position in the Galaxy.

Diffuse gamma ray flux |b| < 5°
- FERMI, l = 25° - 100°
- ARGO-YBJ, l = 25° - 100°
- Milagro, l = 40° - 100°
- CASA-MIA, l = 50° - 200°

C.R. x 10⁻⁴

Vernetto & Lipari: ICRC 2017

Different models to explain the 'knee' and different signatures…

● **Acceleration in SNRs:**
  finite lifetime of shock $E_{max} = Z \cdot 10^{15}$ eV

  ➡ - Eknee $\propto Z$
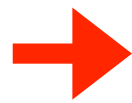 - No anisotropy change across the knee region

● **Diffusion process:**
  probability of escape from Galaxy = $f(Z)$

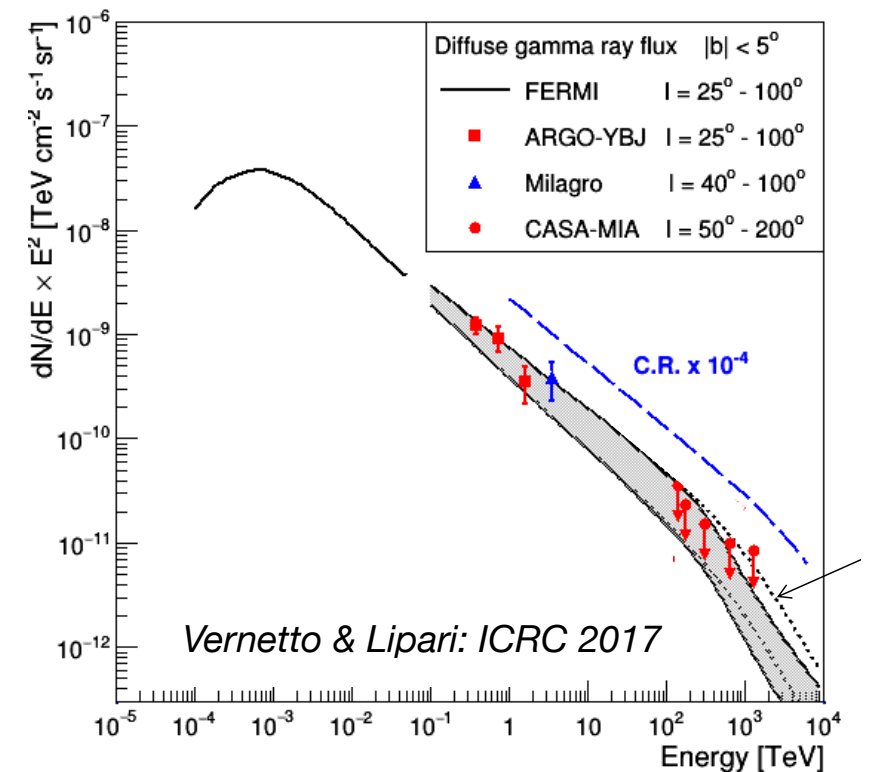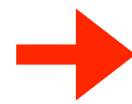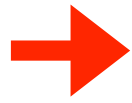 ➡ - Eknee $\propto Z$
  - Anisotropy $\propto E^{\delta}$

● **Interaction with bkg particles:**
  Photo-disintegration, etc.

  ➡ - Eknee $\propto A$

● **Change in particle interaction**

Key elements: *mass composition* and *anisotropy*

Experimental results still conflicting !

All-particle energy spectrum
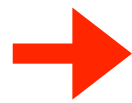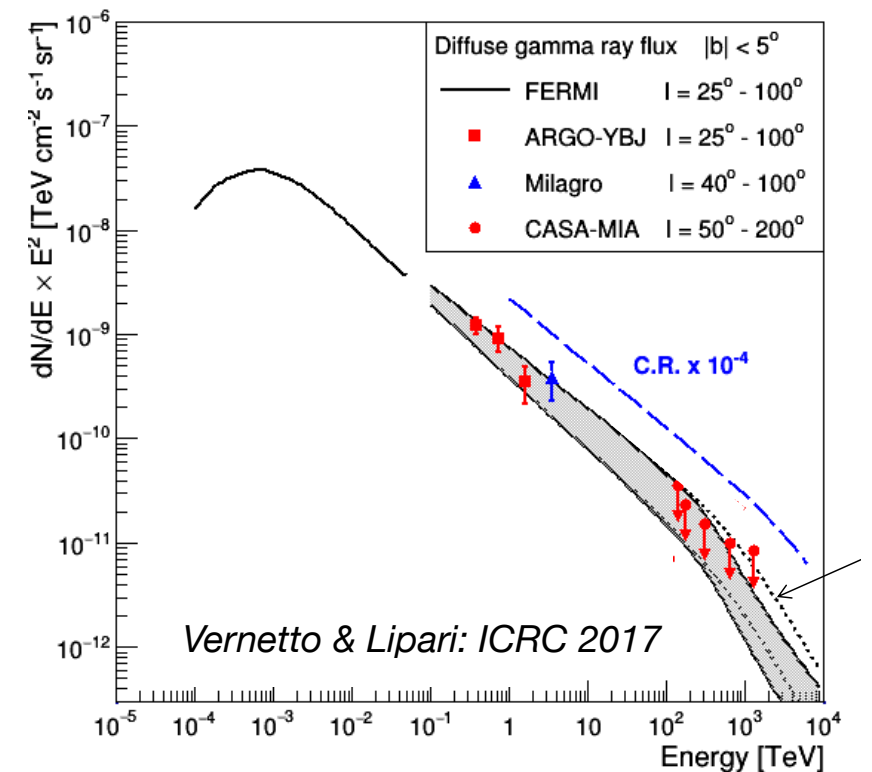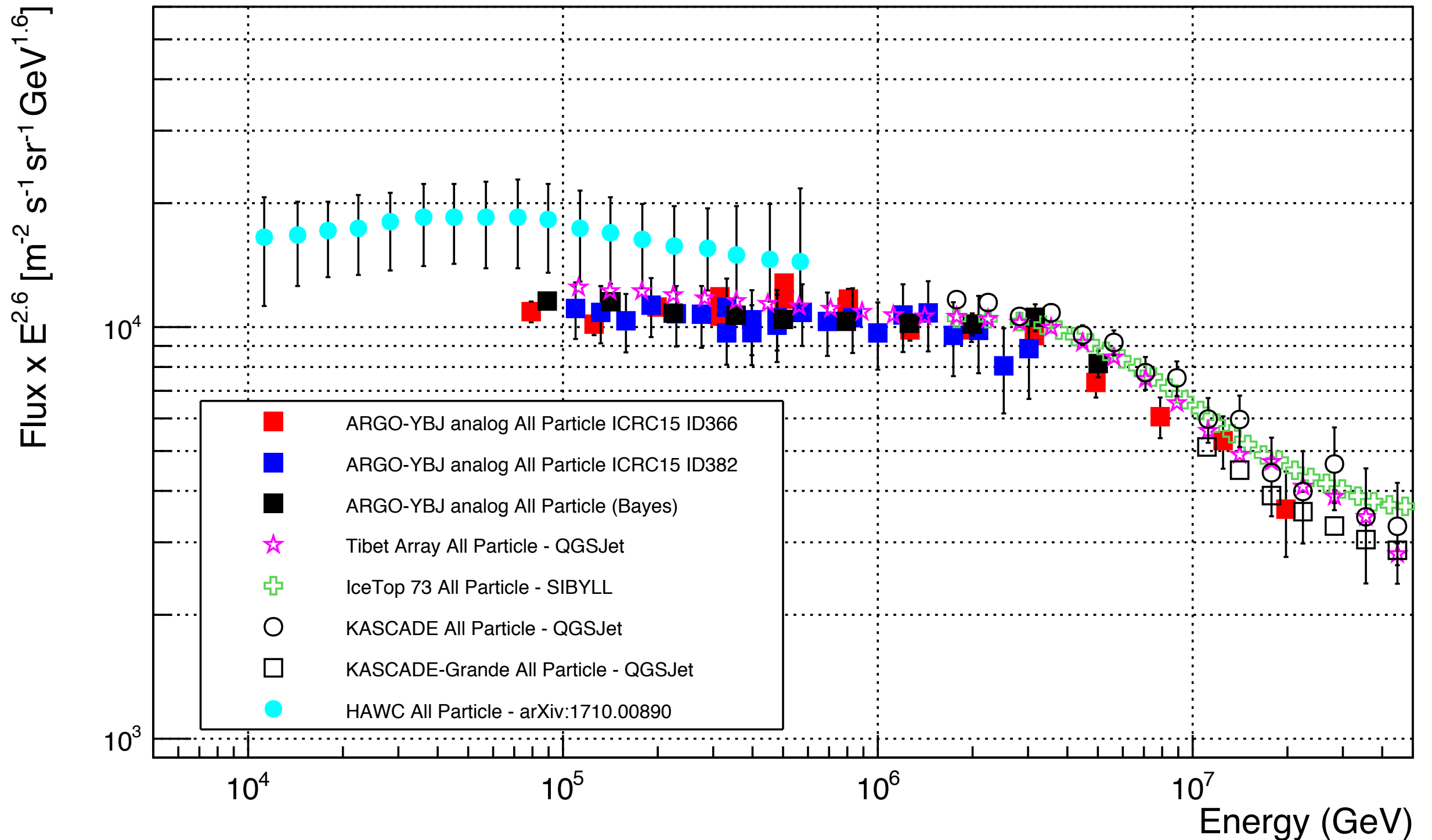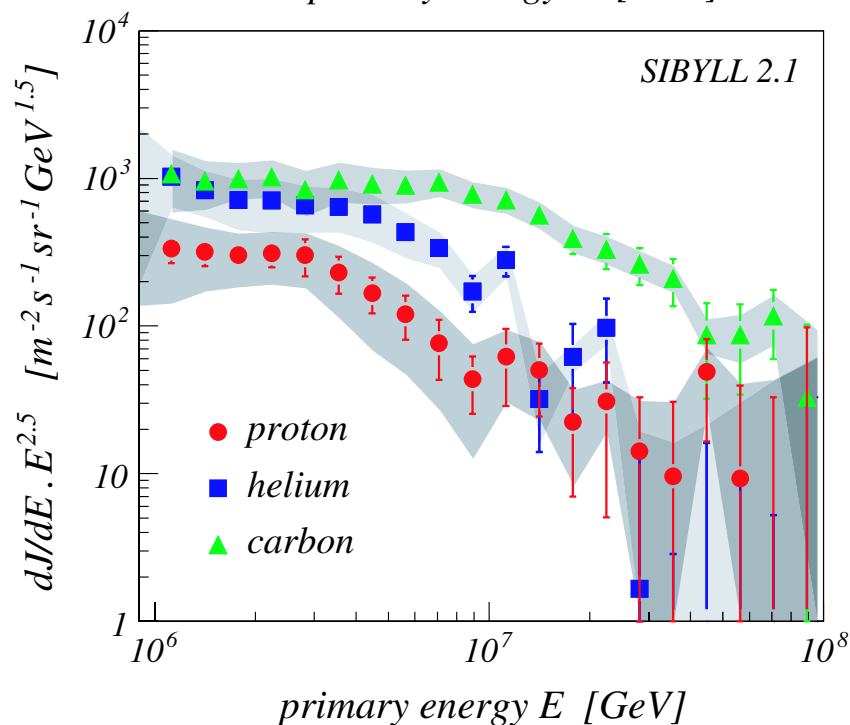
KASCADE

The knee in the all-particle spectrum is due to the *bending of the proton component*

QGSJet 01

proton
helium
carbon

SIBYLL 2.1

proton
helium
carbon

○ AMS   ✚ Sokol-2   **proton spectrum**
★ BESS   ● JACEE
▲ Caprice   ■ RUNJOB
✳ Ryan   △ Tibet
✕ HEGRA

▲ KASCADE proton, QGSJet 01 analysis
▼ KASCADE proton, SIBYLL 2.1 analysis
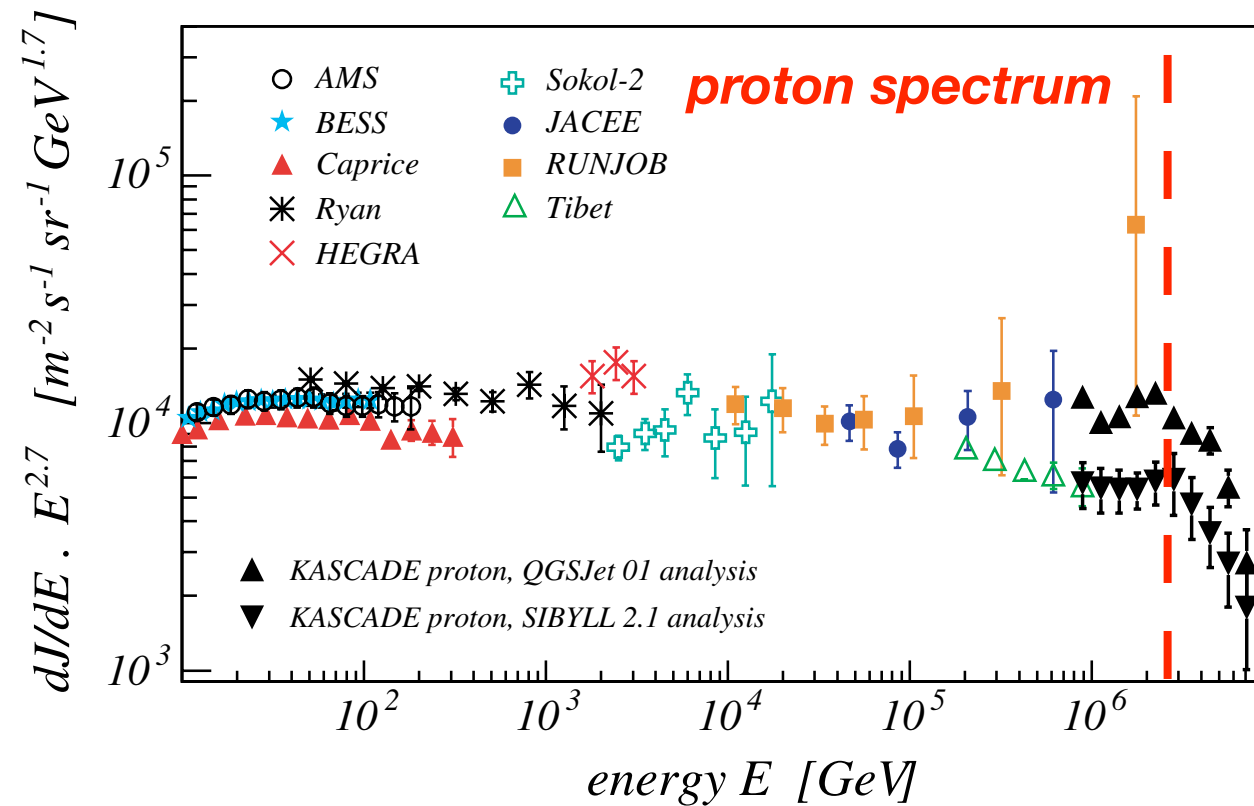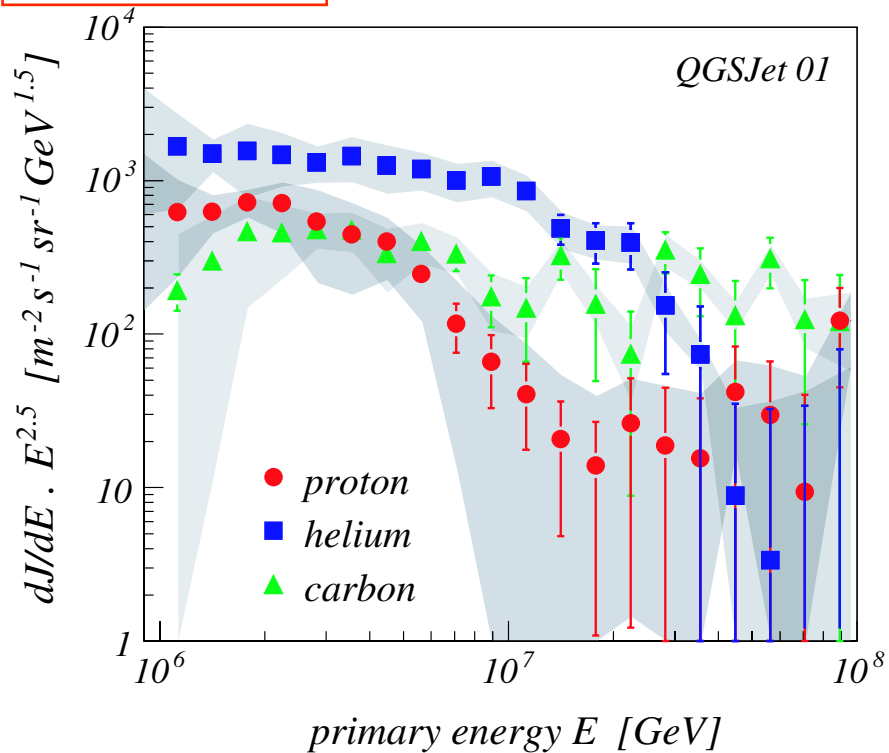
from the analysis of the nearly vertical shower set: The knee is observed at an energy around ≈5 PeV with a change of the index $\Delta\gamma \approx 0.4$. Considering the results of the mass group spectra, in all analyses an appearance of knee-like features in the spectra of the light elements is ascertained. In all solutions the positions of the knees in these spectra is shifted to higher energy with increasing element number.

sea level

Astroparticle Physics 24 (2005) 1
Astroparticle Physics 31 (2009) 86

Composition at the knee - 2

1400 m asl

Astroparticle Physics 12 (1999) 1-17

Astroparticle Physics 12 (1999) 1-17

The cosmic ray composition between 10^{14} and 10^{16} eV

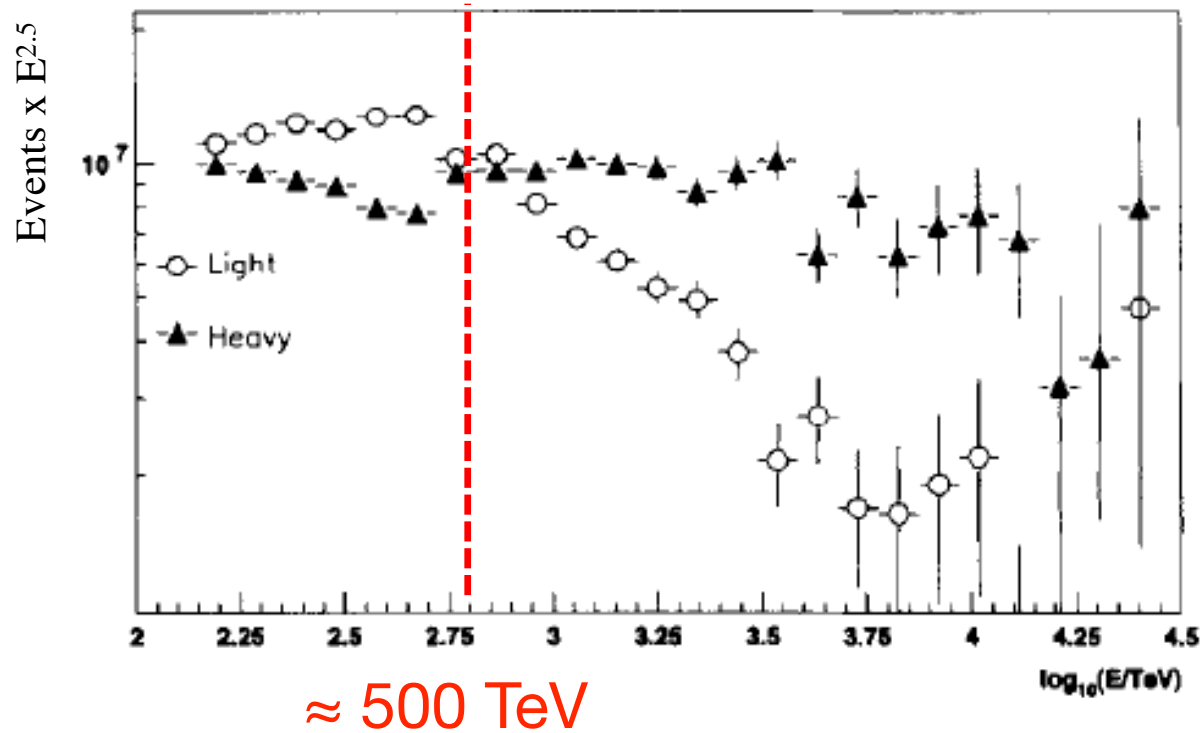M.A.K. Glasmacher [a], M.A. Catanese [a,1], M.C. Chantell [b], C.E. Covault [b], J.W. Cronin [b], B.E. Fick [b], L.F. Fortson [b,2], J.W. Fowler [b], K.D Green [b,3], D.B. Kieda [c], J. Matthews [a,4], B.J. Newport [b,5], D.F. Nitz [a,6], R.A. Ong [b], S. Oser [b], D. Sinclair [a], J.C. van der Velde [a]

≈ 500 TeV

Physics Letters B 632 (2006) 58

Tibet ASγ

4300 m asl   ≈ 500 TeV

The composition measured by CASA-MIA near 10^{14} eV is consistent with direct measurements by other experiments, and becomes heavier through the knee region of the spectrum. At 10^{16} eV, the data closely resemble simulated iron-induced events, in at energy.
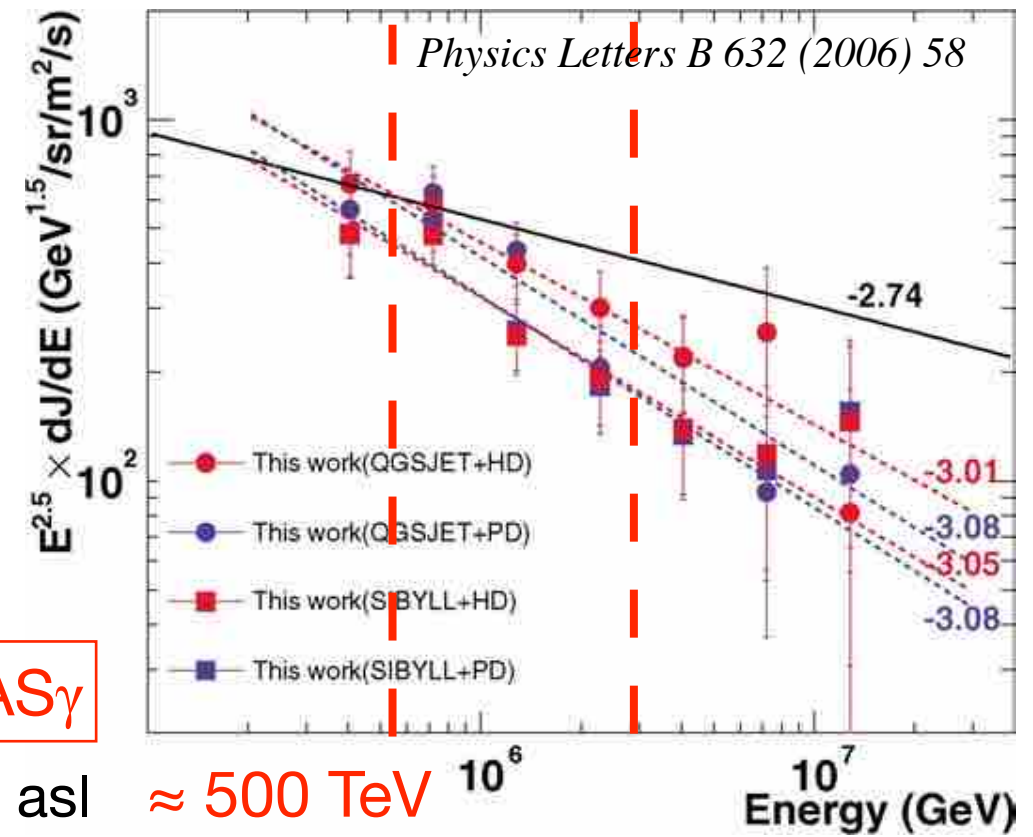
Strong dependence from hadronic models !
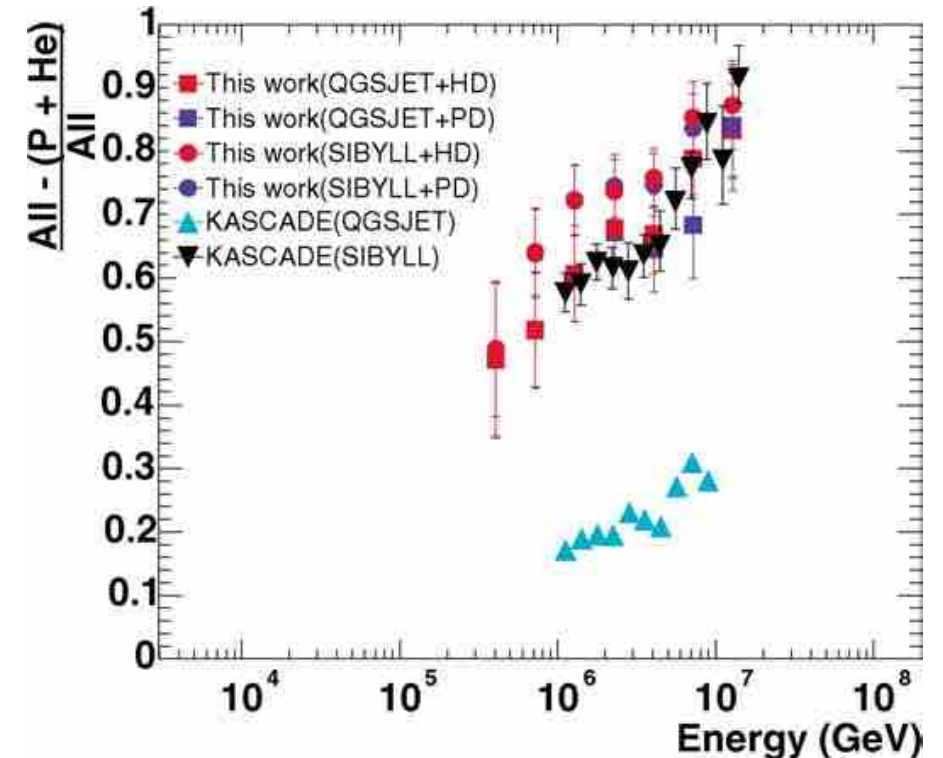
Composition at the knee - 3

ApJ 612 (2004) 268

≈ 400 TeV

The measured $\langle \ln A \rangle$ increases with energy over the energy range of $10^{14.5}-10^{16}$ eV. This is consistent with our former Cerenkov light observations and the measurements by some other groups. The observed $\langle \ln A \rangle$ is consistent with the expected features of a model in which the energy spectrum of each component is steepened at a fixed rigidity of $10^{14.5}$ V.
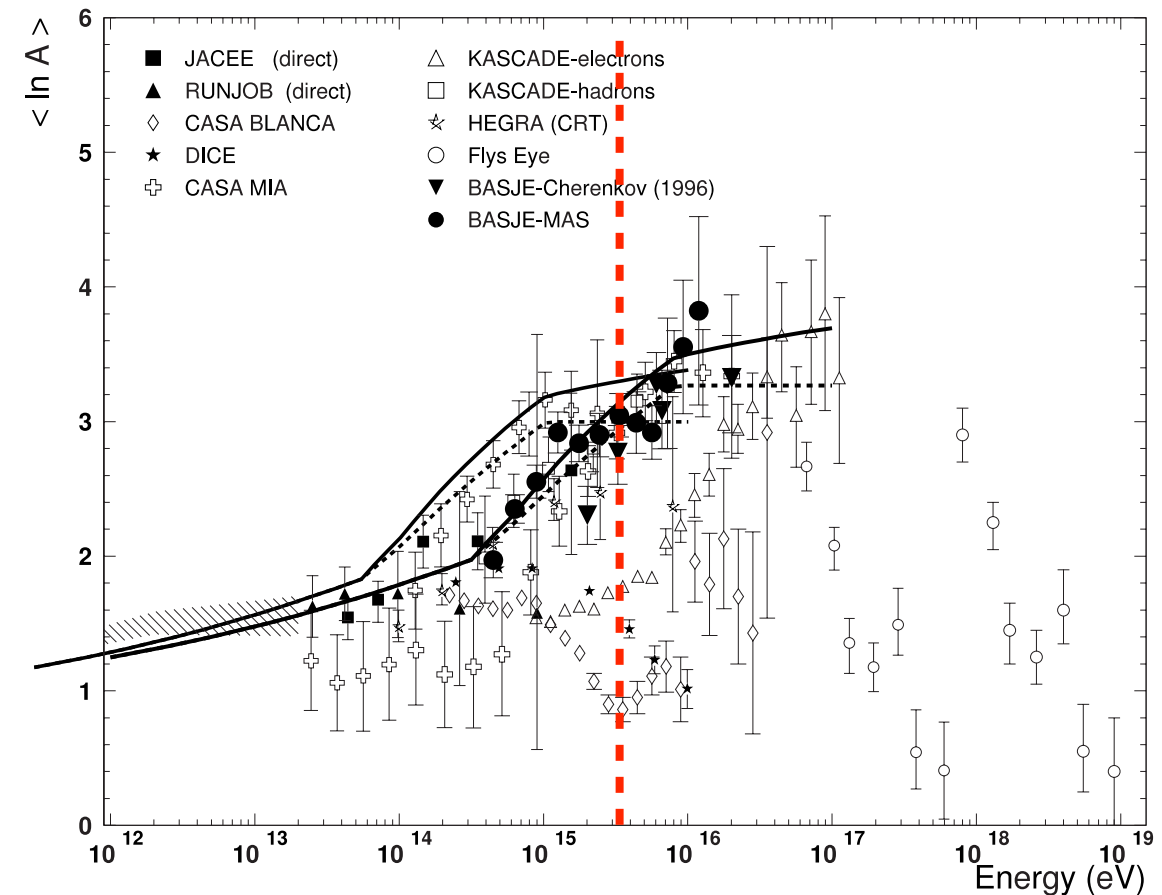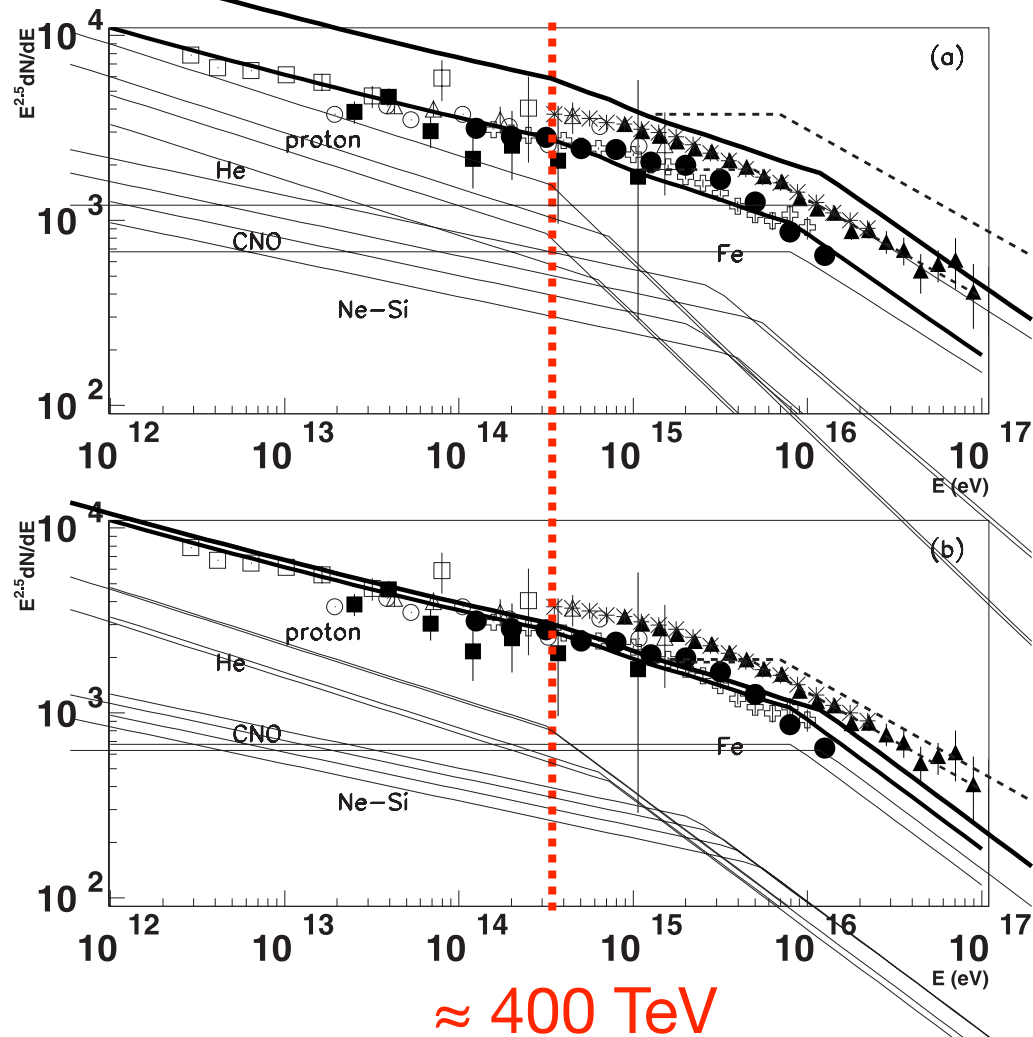
Finally, we conclude that the actual model suggests that the dominant component above 10^{15} eV is heavy and that the $\langle \ln A \rangle$ increases with the energy to about 3.5 at 10^{16} eV.

Chacaltaya 5200 m asl

Light component spectrum (3 TeV - 5 PeV) by ARGO-YBJ

ARGO-YBJ reports evidence for a proton knee starting at about 700 TeV

Legend:
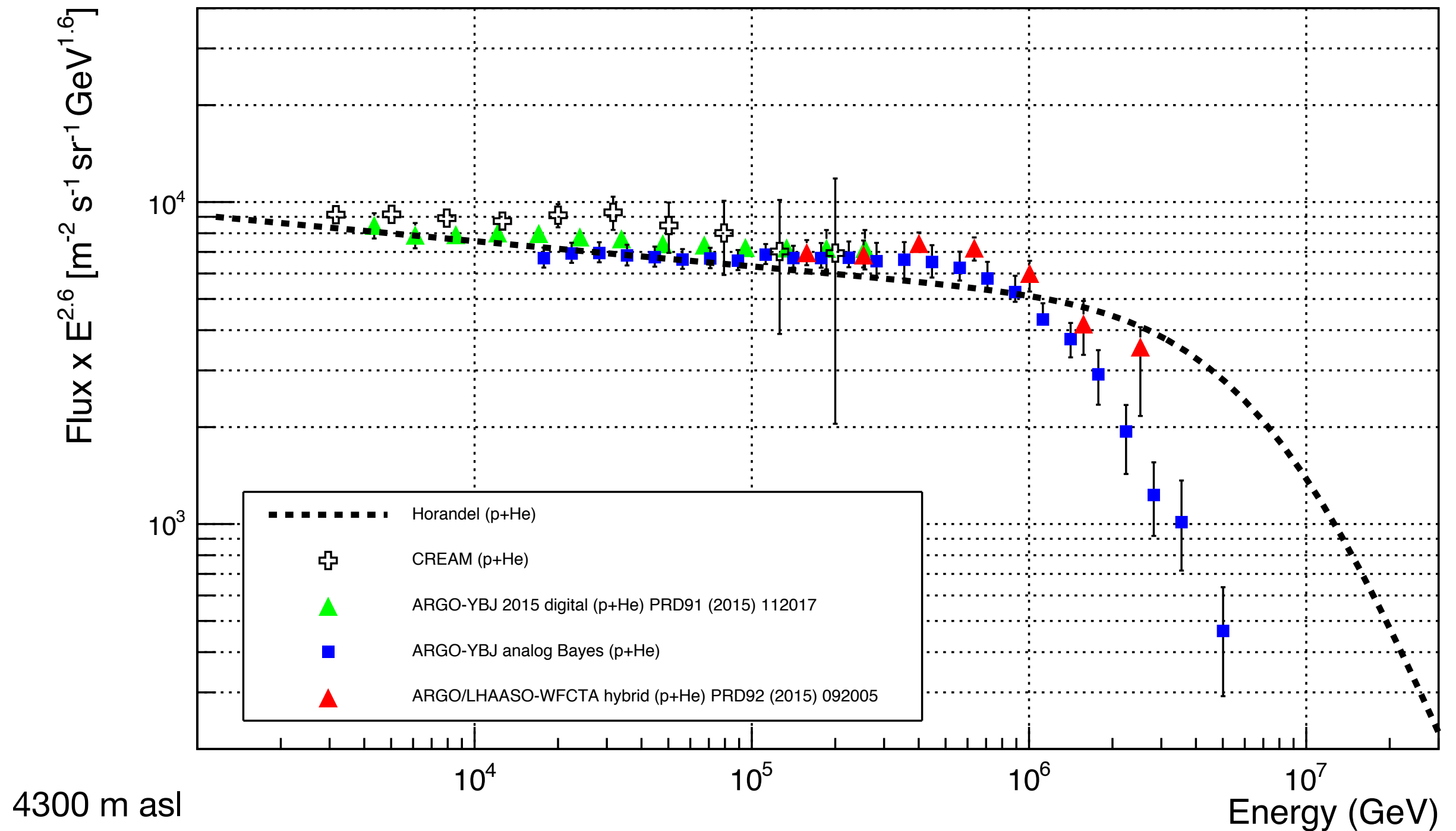- **Horandel (p+He)** — dashed line
- **CREAM (p+He)** — open cross
- **ARGO-YBJ 2015 digital (p+He) PRD91 (2015) 112017** — green triangle
- **ARGO-YBJ analog Bayes (p+He)** — blue square
- **ARGO/LHAASO-WFCTA hybrid (p+He) PRD92 (2015) 092005** — red triangle

Y-axis: Flux x $E^{2.6}$ [m^{-2} s^{-1} sr^{-1} $GeV^{1.6}$]

X-axis: Energy (GeV)

4300 m asl

KASCADE-Grande

Astrop. Phys. 36 (2012) 183

QGSJET II   KASCADE-Grande

~15% systematic uncertainty in flux (energy independent)

- spectrum all-particle *not a single power law*

- hardening of the spectrum above 10^{16} eV

- steepening close to 10^{17} eV (2.1 σ)
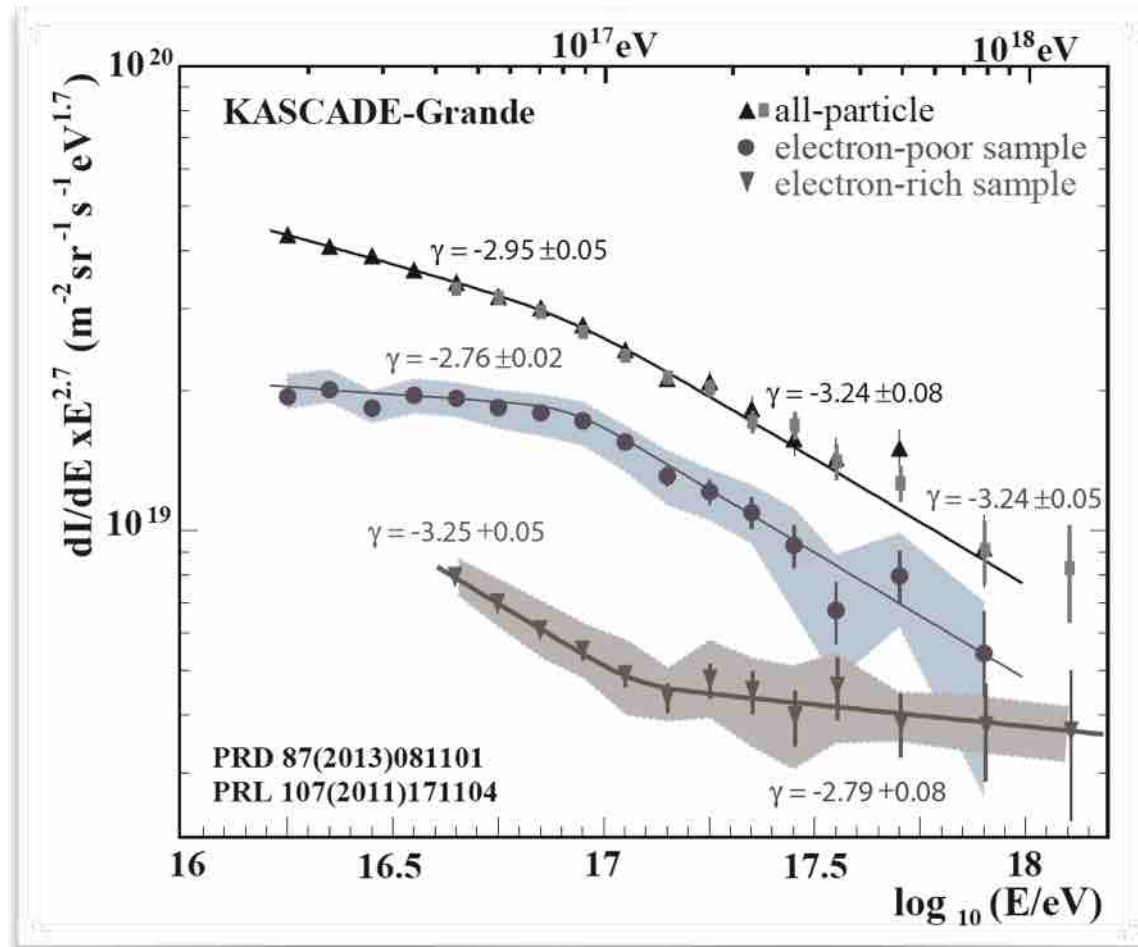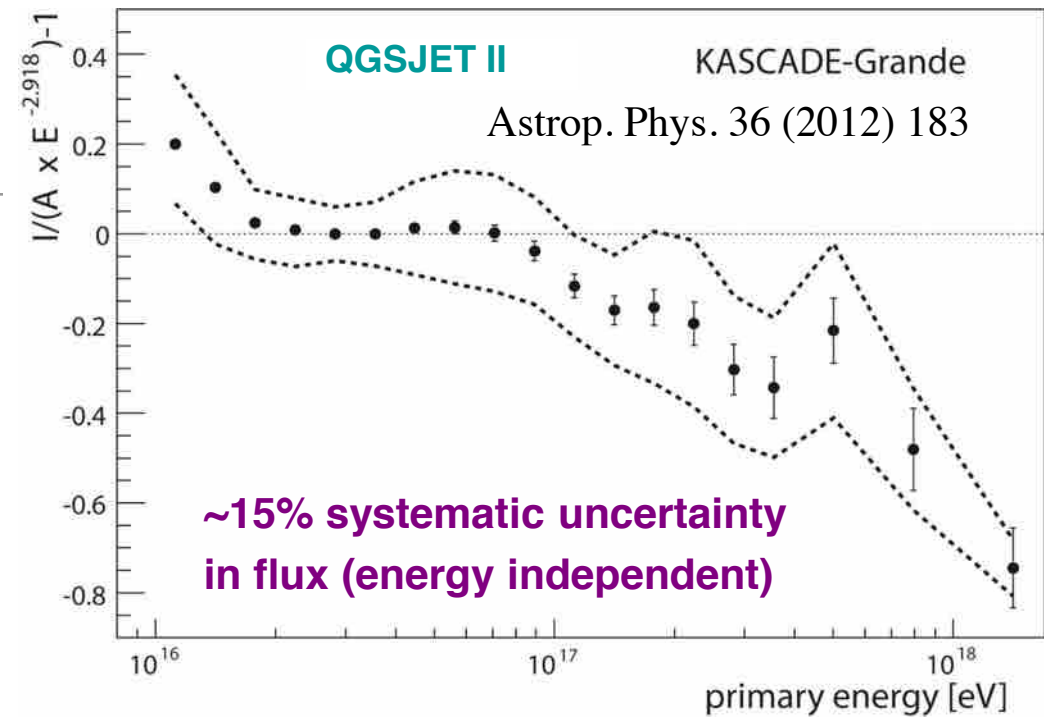
- steepening due to heavy primaries (3.5 σ)

- hardening at $10^{17.08}$ eV (5.8 σ) in light spectrum

- slope change from γ = -3.25 to γ = -2.79 !

Phys.Rev.Lett. 107 (2011) 171104

Phys.Rev.D (R) 87 (2013) 081101
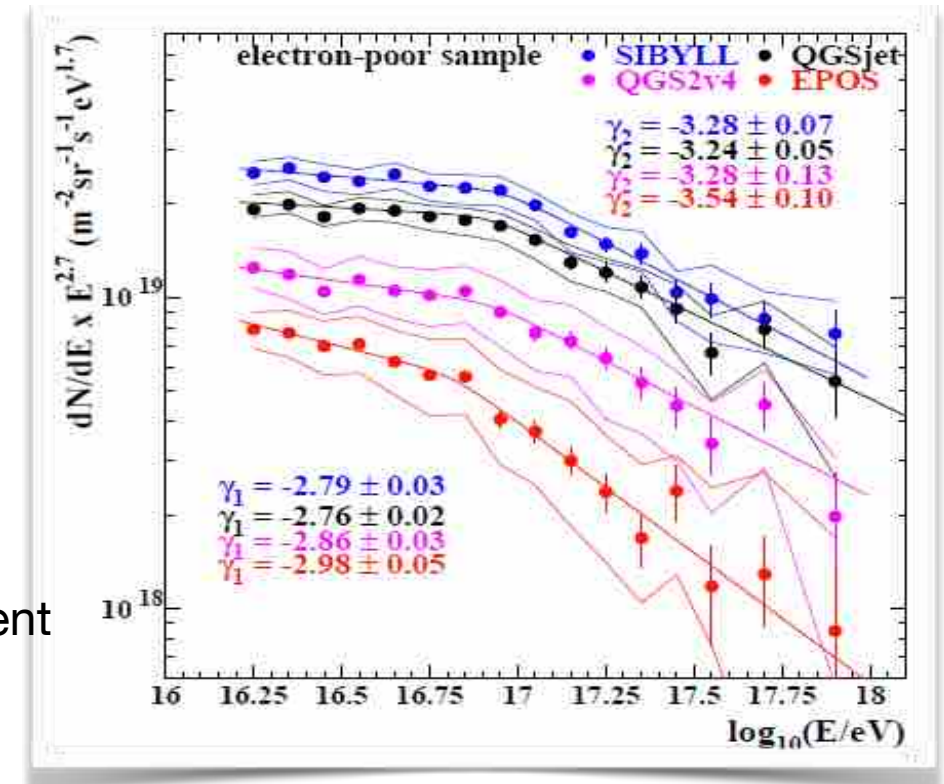
✦ **relative abundances different** for different high-energy hadronic interaction models

Adv. Sp. Res. 53 (2014) 1456

How do we measure composition at ground ?

Strictly speaking, *no air shower experiment measures the primary composition of cosmic rays.*

Instead, one or more *mass sensitive observables* can be measured and the data can then be interpreted in terms of primary mass by a comparison to air shower simulations using hadronic interaction models.

Since different air shower observables react differently to changes in the characteristics of hadronic interactions, one may hope to diminish the model dependence of primary mass estimates *by comparing the results from different observables.*

At least two orthogonal measurements are needed to estimate the energy and mass of the primary CR.

Measuring electron and muon numbers (and their fluctuations) simultaneously at ground has become the first and most commonly employed technique applied to infer the cosmic ray composition from EAS data.
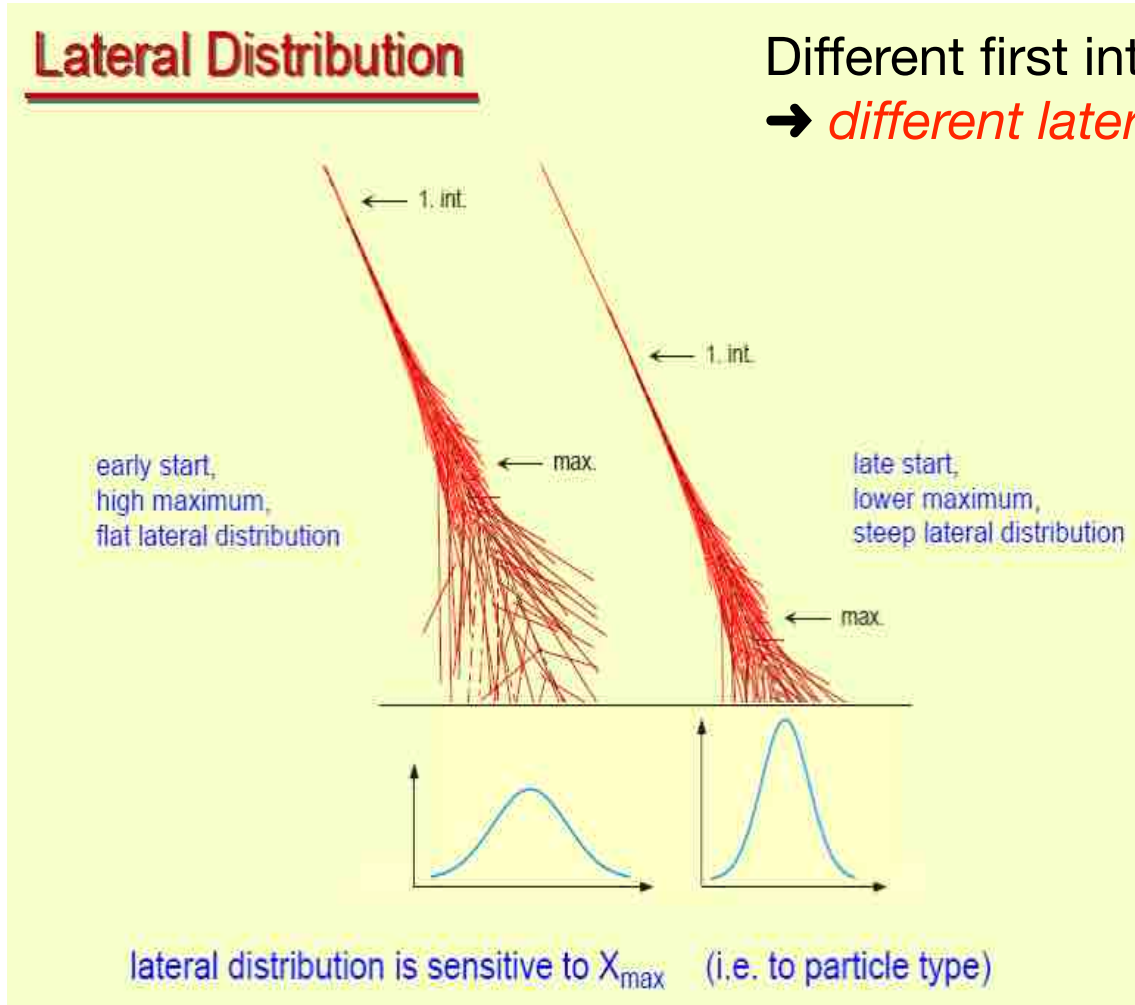
2D shower size distribution
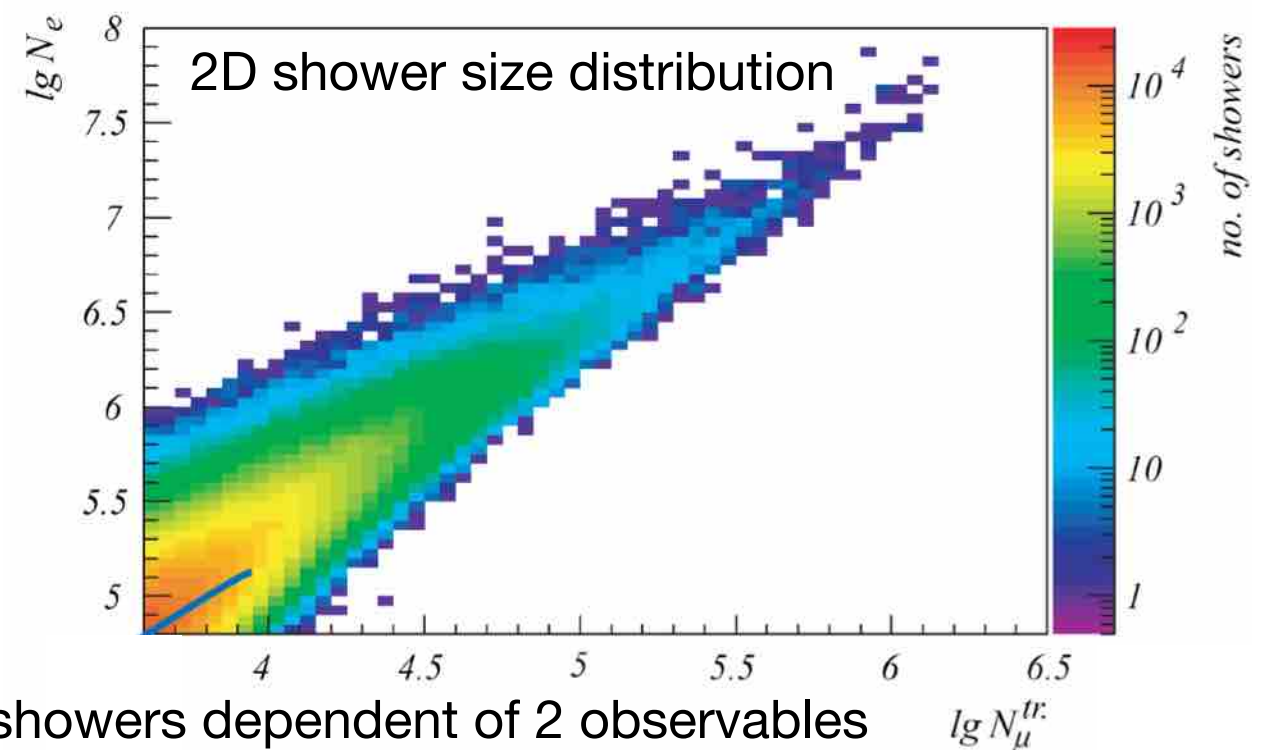
Frequency of showers dependent of 2 observables

Ground-based observations

proton　E=10¹⁴ eV　**iron**

The different approaches to investigate the chemical composition are commonly based on the fact that *inelastic cross section of the nucleus of mass A is proportional to $A^{2/3}$*, which leads to the long interaction mean free path (m.f.p.) of protons and short m.f.p. of nuclei.

Lateral Distribution
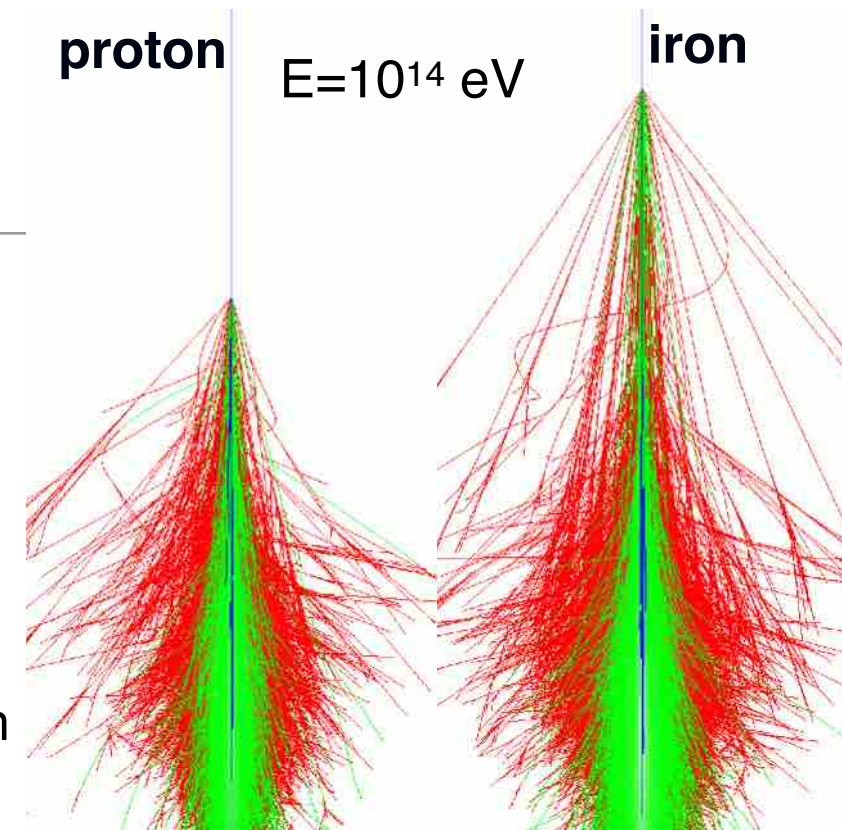
Different first interaction atmospheric depth
➜ *different lateral distribution*

1. int.

1. int.

early start,
high maximum,
flat lateral distribution

← max.

late start,
lower maximum,
steep lateral distribution

← max.

lateral distribution is sensitive to X_{max}　(i.e. to particle type)

Nuclei develop higher in atmosphere (smaller X_{max}) than protons producing flatter lateral distributions.

The showers can be classified in terms of the density ratio at two distances from the shower core

$$\rho(25\text{-}35m) \, / \, \rho(0\text{-}10m)$$

Short m.f.p. of nuclei ➡

Characteristics of early development:
- Large lateral spread
- Muon rich events
- Soft secondary energy spectrum
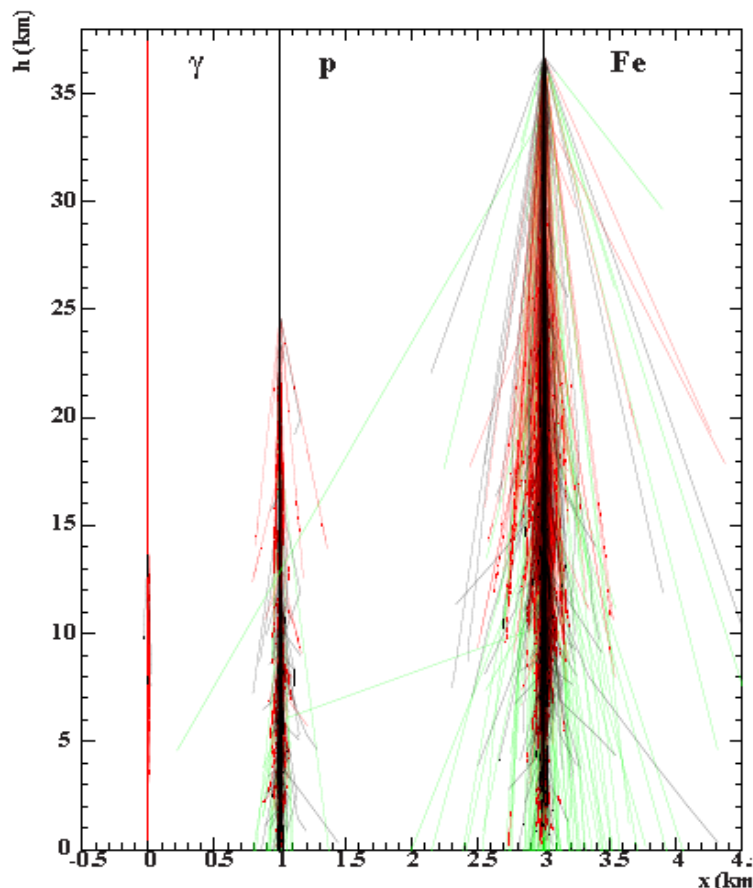
The superposition model

The major differences between showers induced by different primary masses have a rather simple cause.

The discriminating power originates from the fact that a primary nucleus of mass A and energy E_0 can in good approximation be treated as a superposition of A protons of energy $E' = E_0/A$ (*superposition model*).

The resulting EAS is the sum of A separate p-induced EAS all starting at the same point.

For any additive measurable quantity Q the model predicts A times the average value for the quantity computed in a proton shower of energy $E' = E_0/A$

$$\langle Q^A(E)\rangle = A \cdot \langle Q^p(E/A)\rangle$$

$$N_\mu = \left(\frac{E_0}{E_{crit}^\pi}\right)^\beta \quad\Longrightarrow\quad N_\mu^A = A \cdot \left(\frac{E_0}{A \cdot E_{crit}^\pi}\right)^\beta = A^{1-\beta} \cdot N_\mu^p$$

$$= N_\mu^p \cdot A^{0.15}$$

The superposition model

The major differences between showers induced by different primary masses have a rather simple cause.

The discriminating power originates from the fact that a primary nucleus of mass A and energy E_0 can in good approximation be treated as a superposition of A protons of energy $E' = E_0/A$ (*superposition model*).

The resulting EAS is the sum of A separate p-induced EAS all starting at the same point.

For any additive measurable quantity Q the model predicts A times the average value for the quantity computed in a proton shower of energy $E' = E_0/A$

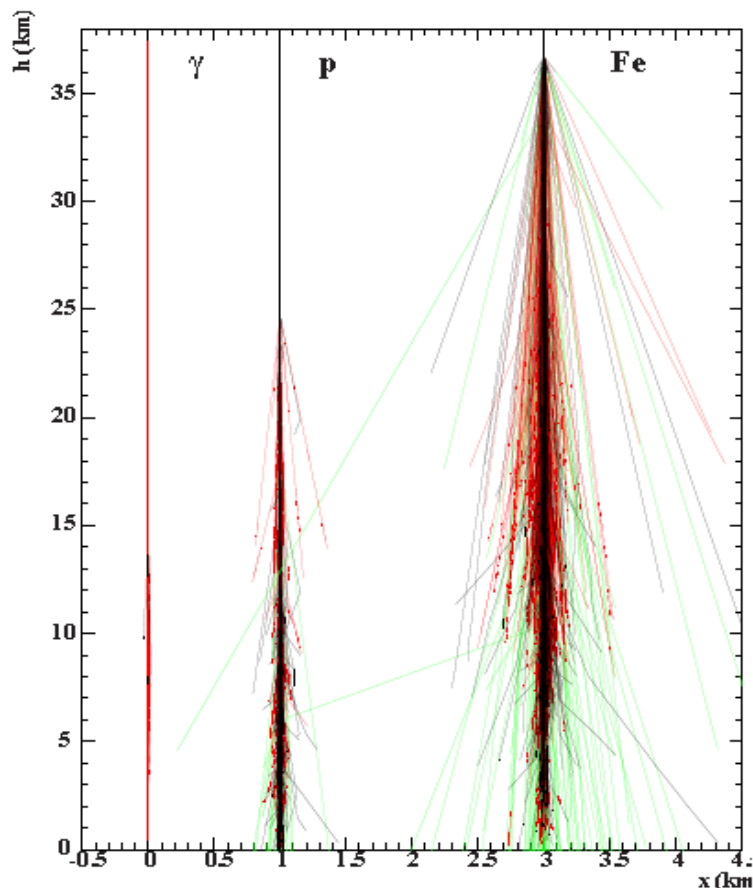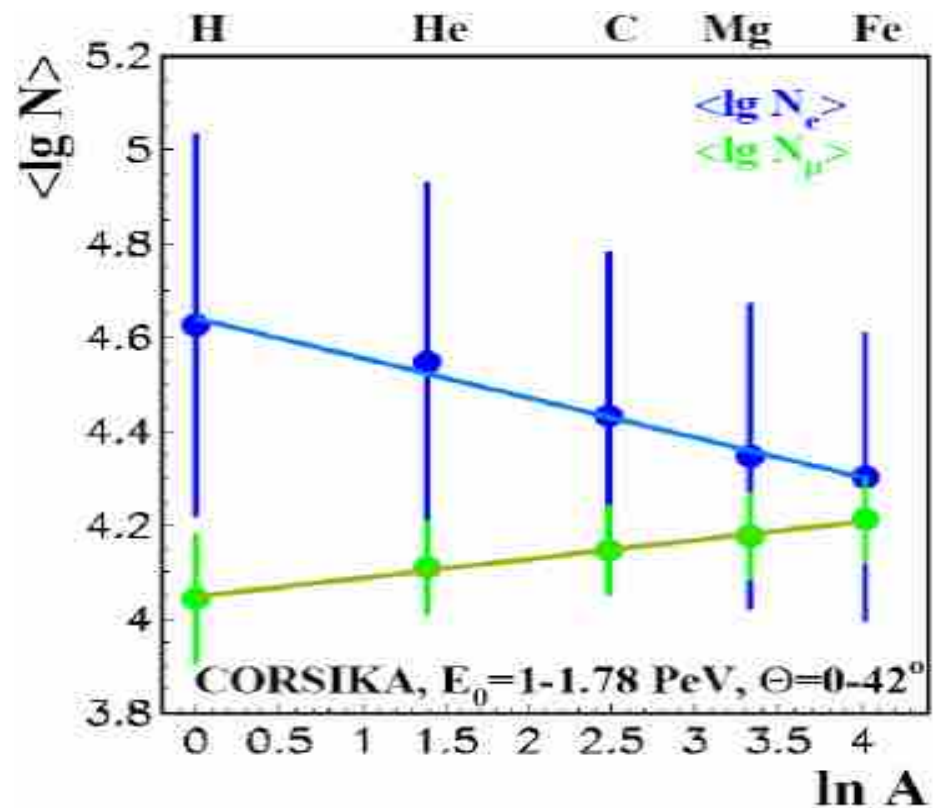$$\langle Q^A(E) \rangle = A \cdot \langle Q^p(E/A) \rangle$$

$$N_\mu = \left(\frac{E_0}{E_{crit}^\pi} \right)^\beta \quad \Longrightarrow \quad N_\mu^A = A \cdot \left(\frac{E_0}{A \cdot E_{crit}^\pi} \right)^\beta = A^{1-\beta} \cdot N_\mu^p$$

$$= N_\mu^p \cdot A^{0.15}$$

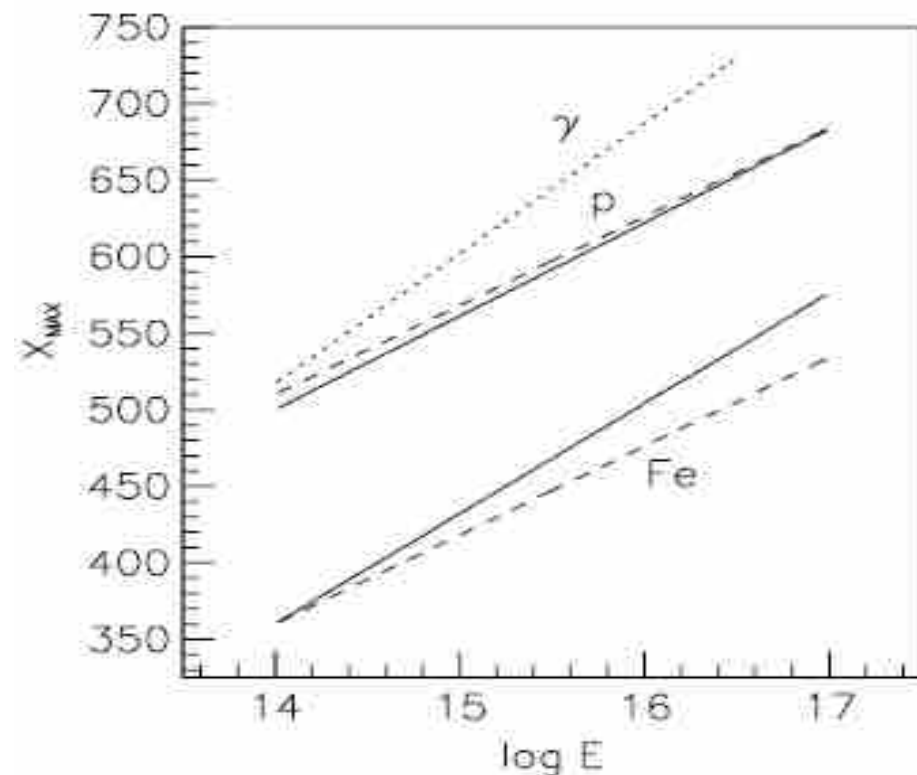*Number of muons is a mass sensitive observable*

Nucleus-air interactions

Showers induced by heavy primaries generate more secondary particles, each of smaller energy, and due to the faster attenuation of the electromagnetic component with a smaller number of electrons at the observation level (after the EAS maximum). Simultaneously the number of muons is larger.

Increasing the mass A

★ More secondary particles with less energy → less electrons (after max), more μ

★ Surviving hadrons have less energy

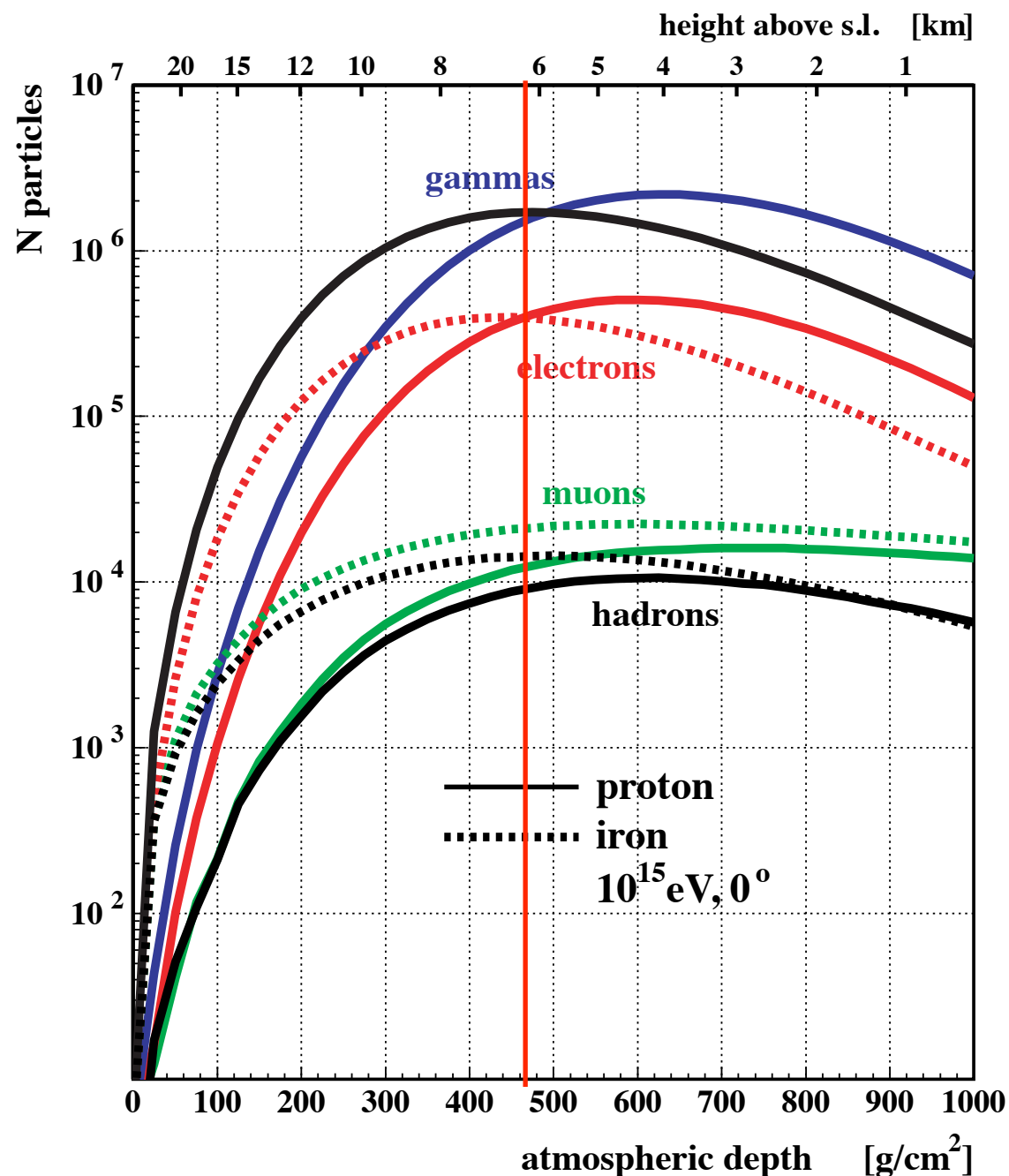★ Larger deflection angles → flatter lateral distributions of secondary particles

The lower energy nucleons generate fewer interactions and so lose less energy to e.m. components.

Showers by nuclei dissipate their energy faster than protons, thus having shallower (smaller) X_{max}.

Particles at ground

The number of electrons *at shower maximum* is nearly independent on the primary mass

$$N^A_{e,\max} \approx N^p_{e,\max}$$

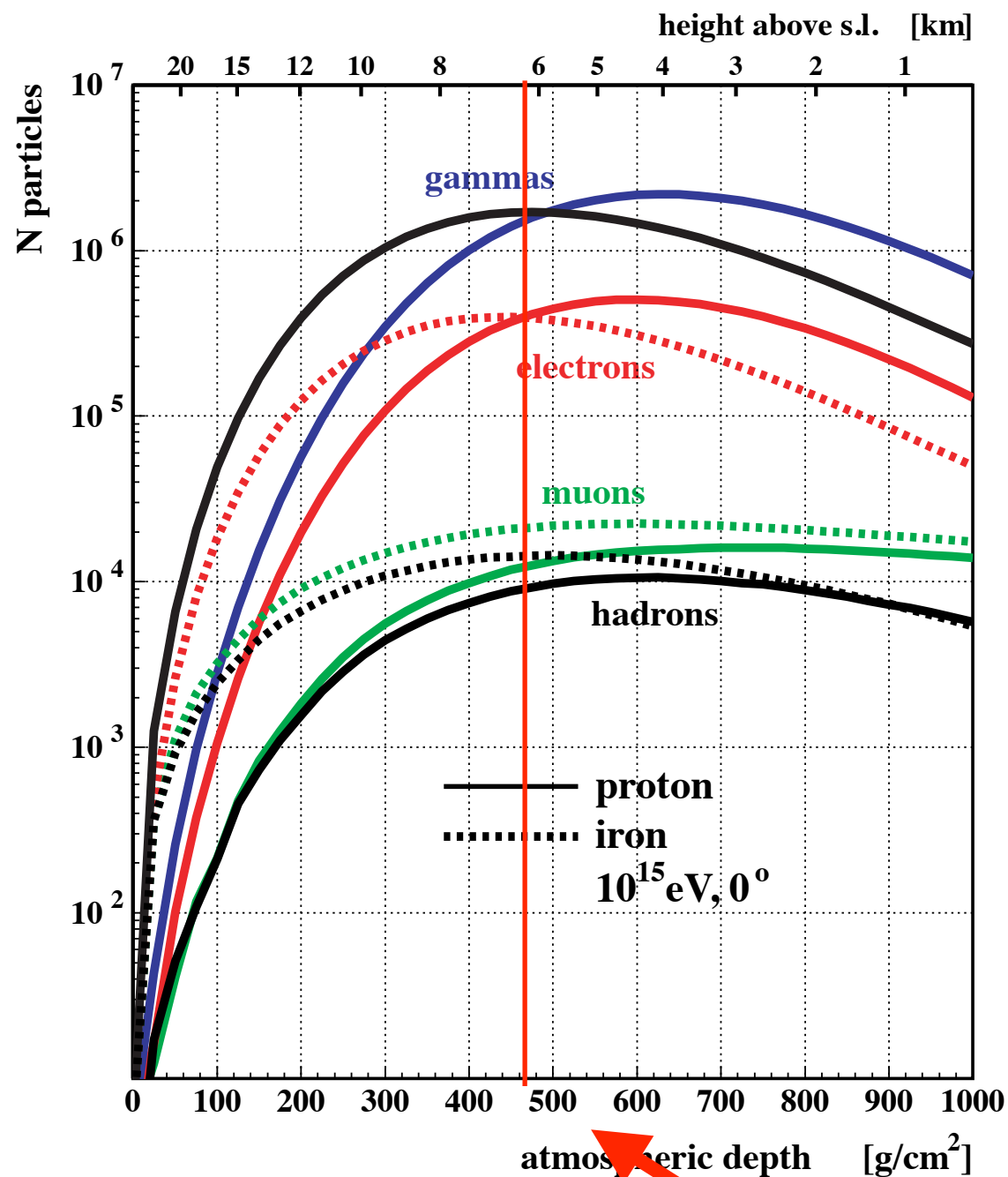$$N^A_\mu \approx N^p_{\mu,\max} A^{1-\beta} \qquad \beta \approx 0.8 \text{ - } 0.9$$

★ The number of electrons at shower maximum gives a good estimate of the primary energy independent of the composition.

★ The number of muons can be used to infer the mass of the primary particle, since it grows with $A^{1-\beta}$.

Moreover, the evolution of the muon number with energy, $dN\mu/d\ln E$, is a good tracer of changes in the primary composition.

A constant composition gives $dN\mu/d\ln E = \beta$ and any departure from that behavior can be interpreted as a change of the average mass of the primaries.

Particles at ground

The number of electrons *at shower maximum* is nearly independent on the primary mass

$$N^A_{e,\max} \approx N^p_{e,\max}$$

$$N^A_\mu \approx N^p_{\mu,\max} A^{1-\beta} \qquad \beta \approx 0.8 - 0.9$$

★ The number of electrons at shower maximum gives a good estimate of the primary energy independent of the composition.

★ The number of muons can be used to infer the mass of the primary particle, since it grows with $A^{1-\beta}$.

Moreover, the evolution of the muon number with energy, $dN\mu/d\ln E$, is a good tracer of changes in the primary composition.

A constant composition gives $dN\mu/d\ln E = \beta$ and any departure from that behavior can be interpreted as a change of the average mass of the primaries.
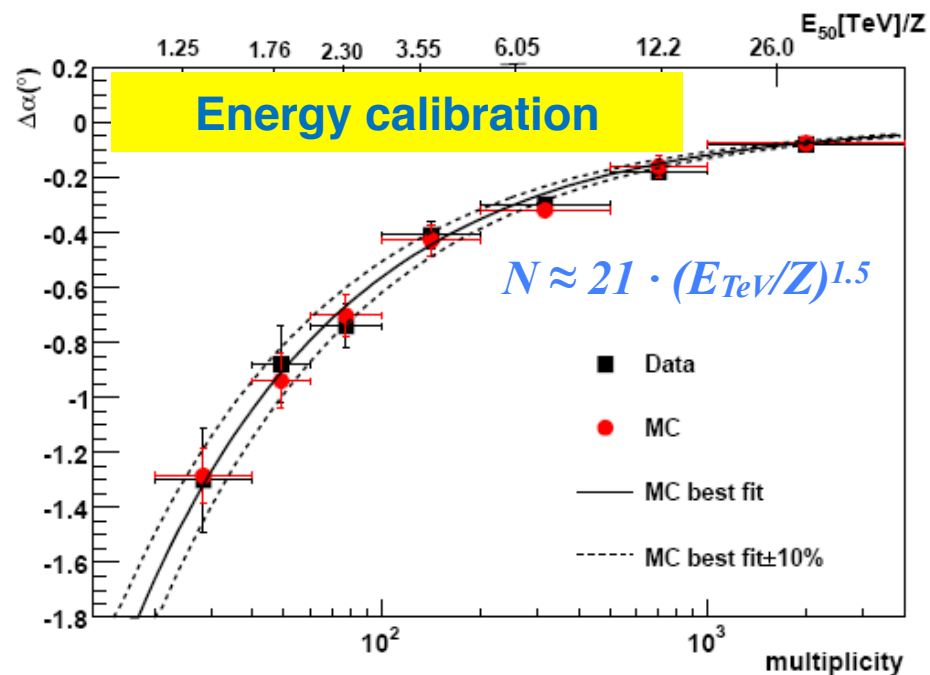
High Altitude > 4000 m asl !!!

Calibration of the energy scale

(p+He) spectrum (2 - 700) TeV
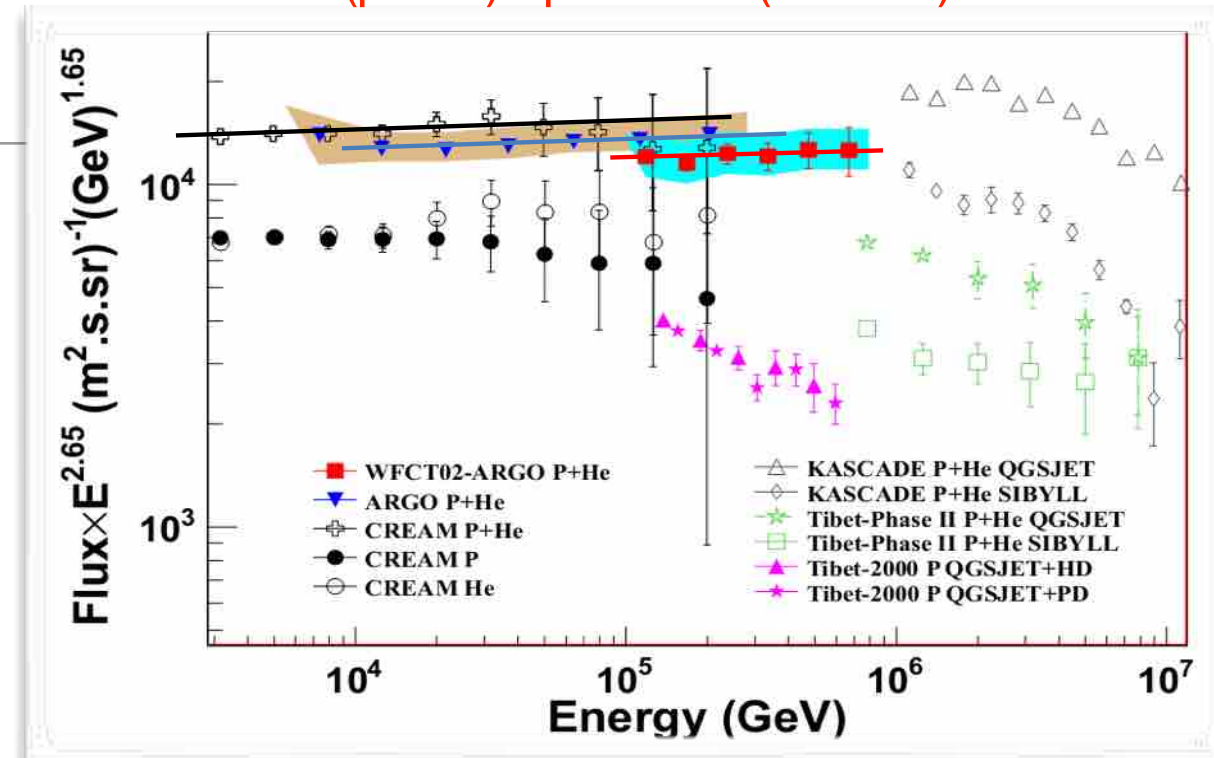

Chin. Phys. C 38, 045001 (2014)

ARGO-YBJ: *Moon shadow* tool
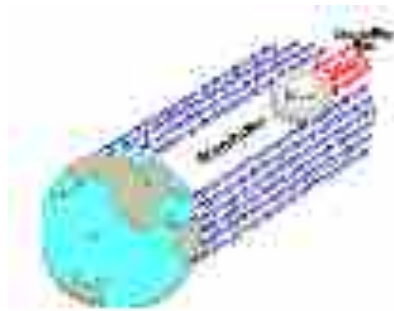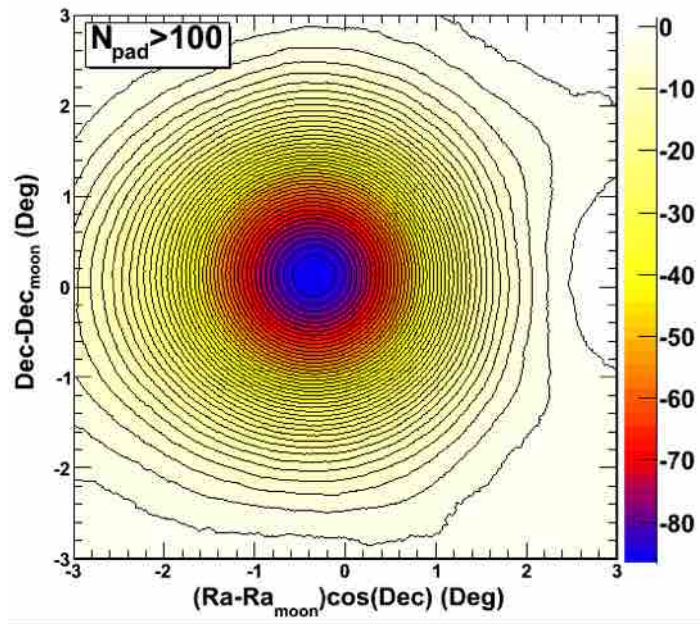
PRD 84 (2011) 022003

The energy scale uncertainty is estimated at 10% level in the energy range 1 – 30 (TeV/Z).

- CREAM: $1.09 \times 1.95 \times 10^{-11}$ (E/400 TeV)$^{-2.62}$
- ARGO-YBJ: 1.95×10^{-11} (E/400 TeV)$^{-2.61}$
- Hybrid: $0.92 \times 1.95 \times 10^{-11}$ (E/400 TeV)$^{-2.63}$

Single power-law: 2.62 ± 0.01

Flux at 400 TeV:

$1.95 \times 10^{-11} \pm 9\%$ (GeV^{-1} m^{-2} sr^{-1} s^{-1})

The 9% difference in flux corresponds to a difference of ± 4% in energy scale between different experiments.

Measurement of the elemental composition

Unfortunately, the experimental situation is more complicated, because surface detectors do not observe the number of electrons at shower maximum !

Since heavy primaries reach their shower max at smaller depths than light ones, the number of electrons on ground is expected to be composition sensitive, with a larger electron number for air showers initiated by light primaries.

$$N_e(E_0, A) = \alpha(A) E_0^{\beta(A)},$$

$$\text{where } \alpha(A) = 197.5 A^{-0.521} \text{ and } \beta(A) = 1.107 A^{0.035}$$

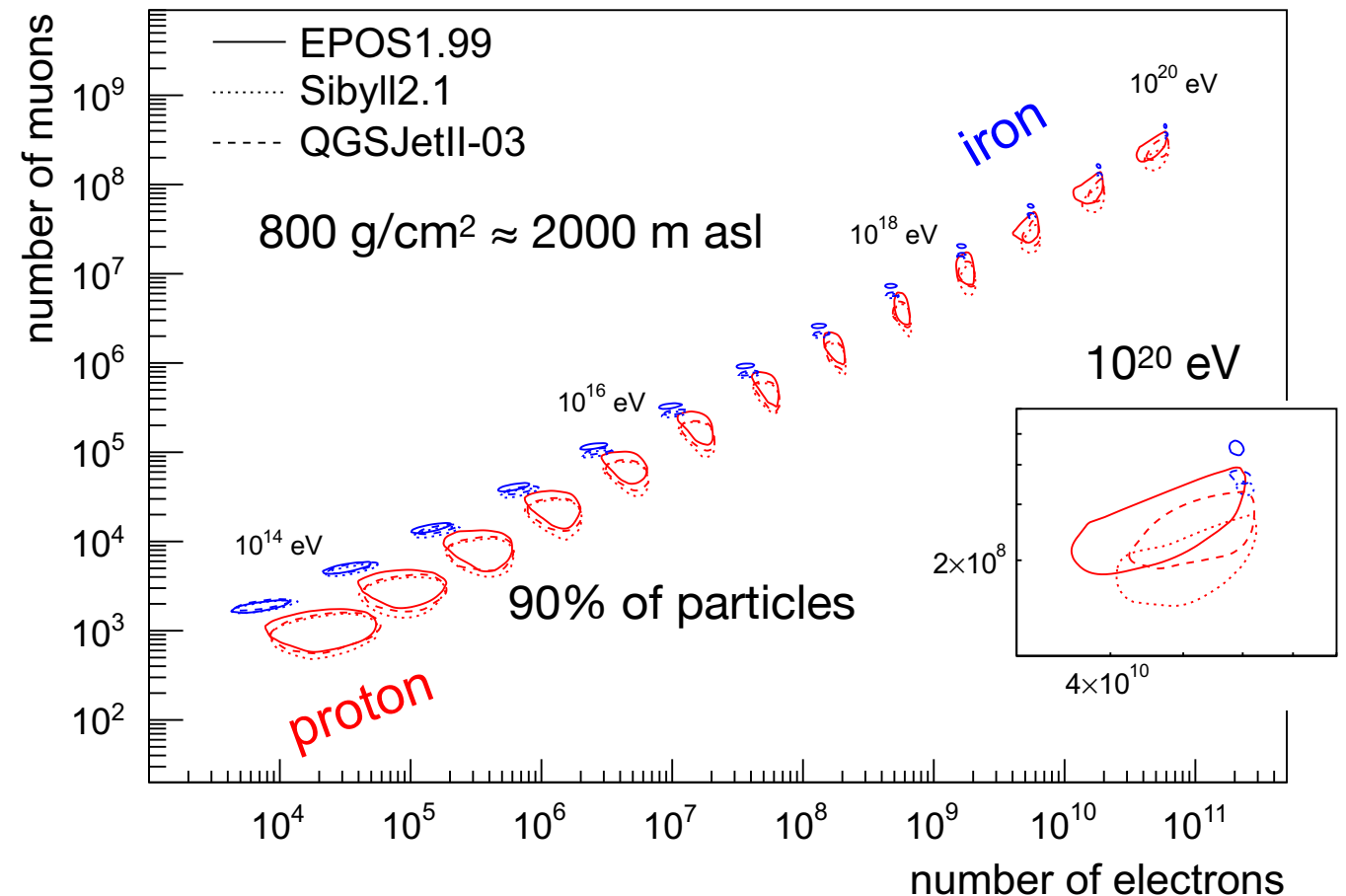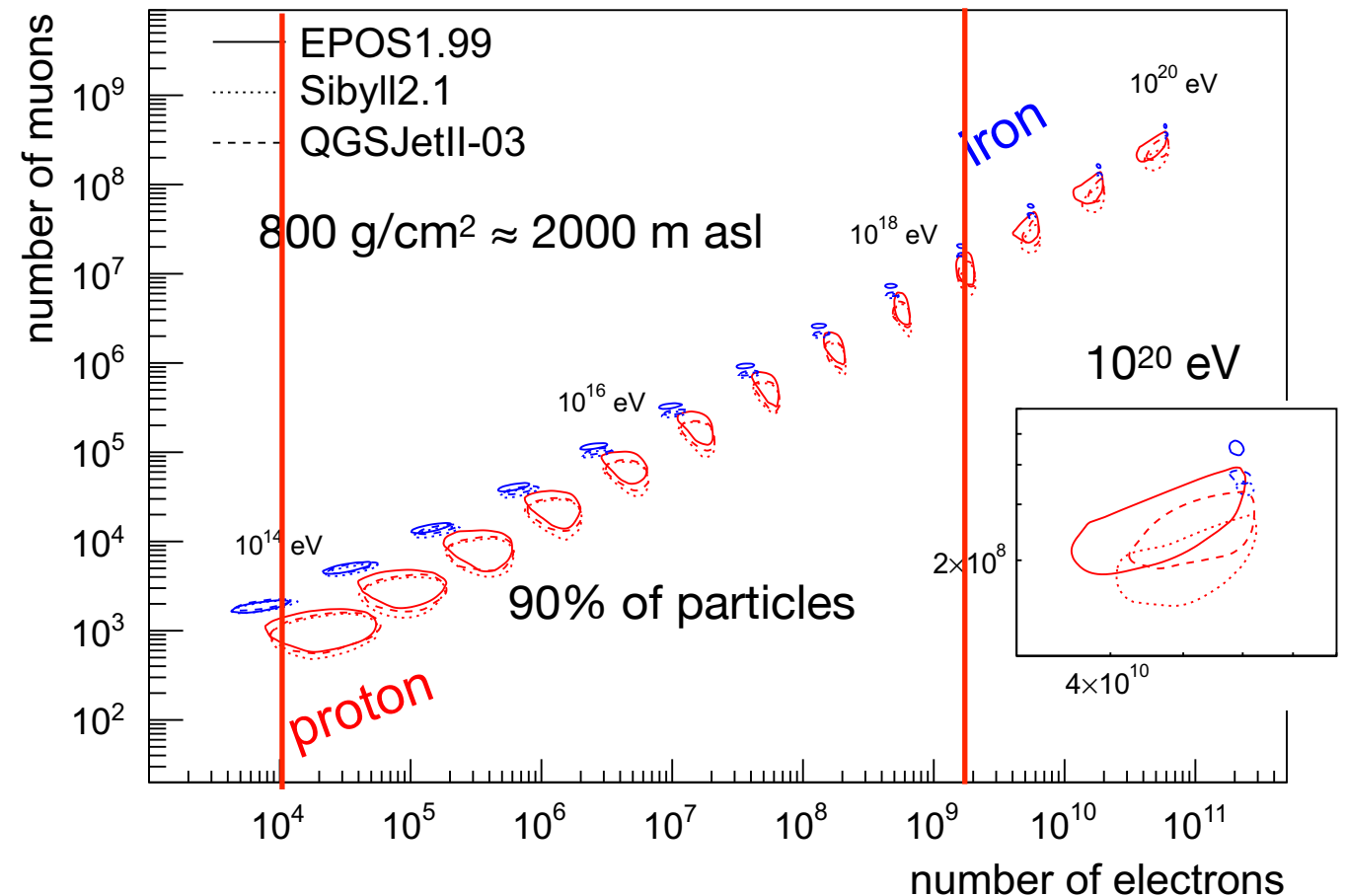We must assume a given composition but we want to measure it ➜ degeneracy !

Measurement of the elemental composition

Unfortunately, the experimental situation is more complicated, because surface detectors do not observe the number of electrons at shower maximum !

Since heavy primaries reach their shower max at smaller depths than light ones, the number of electrons on ground is expected to be composition sensitive, with a larger electron number for air showers initiated by light primaries.

$$N_e(E_0, A) = \alpha(A) E_0^{\beta(A)},$$

where $\alpha(A) = 197.5 A^{-0.521}$ and $\beta(A) = 1.107 A^{0.035}$.

We must assume a given composition but we want to measure it ➜ degeneracy !

The $\ln N_\mu$-$\ln N_e$ observables are basically *rotated* from the desired quantities, $\ln A$ and $\ln E$.

Due to the steeply falling cosmic ray spectrum, this rotation causes a complication in the analysis of air shower data, because *showers of equal ln N_e are enriched in light elements*.
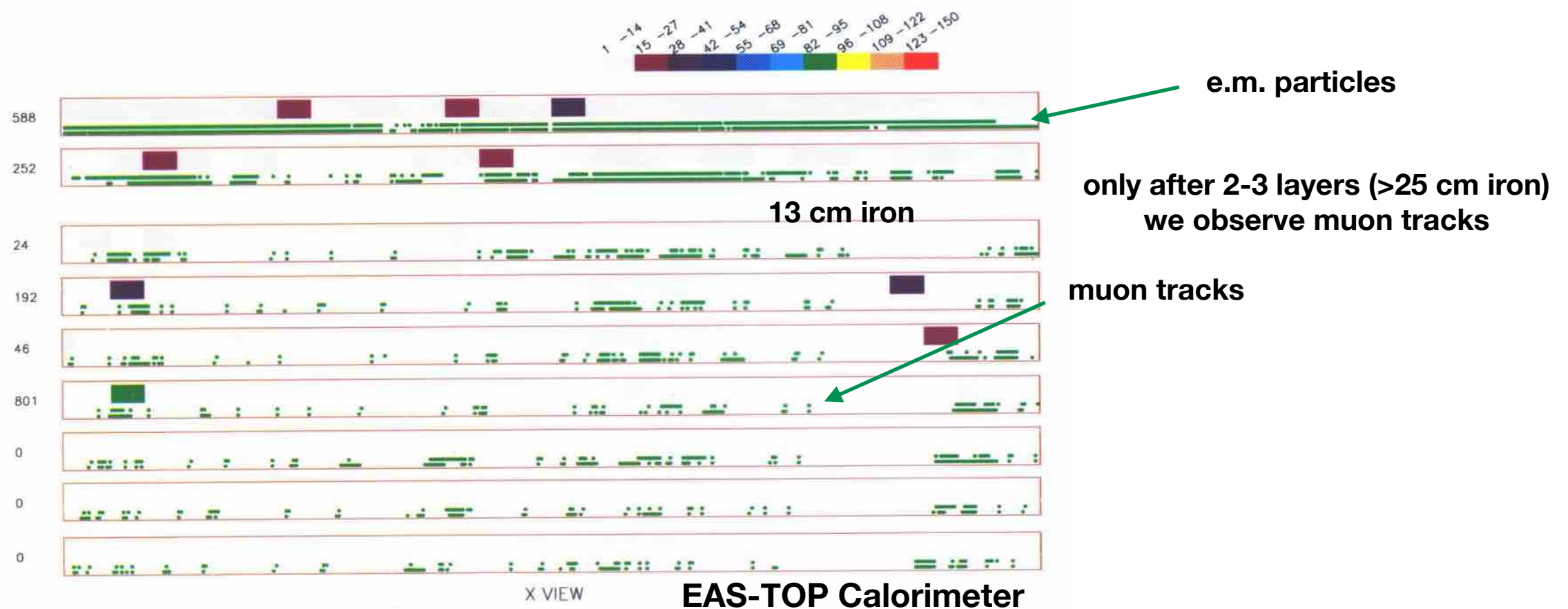
Muon detection

To discriminate between different masses the determination of the *exact number of muons* is mandatory !

In the most classical approach, electron-muon discrimination is achieved by employing a combination of unshielded and *shielded* (under 2-3 m of concrete) scintillation detectors at ground.
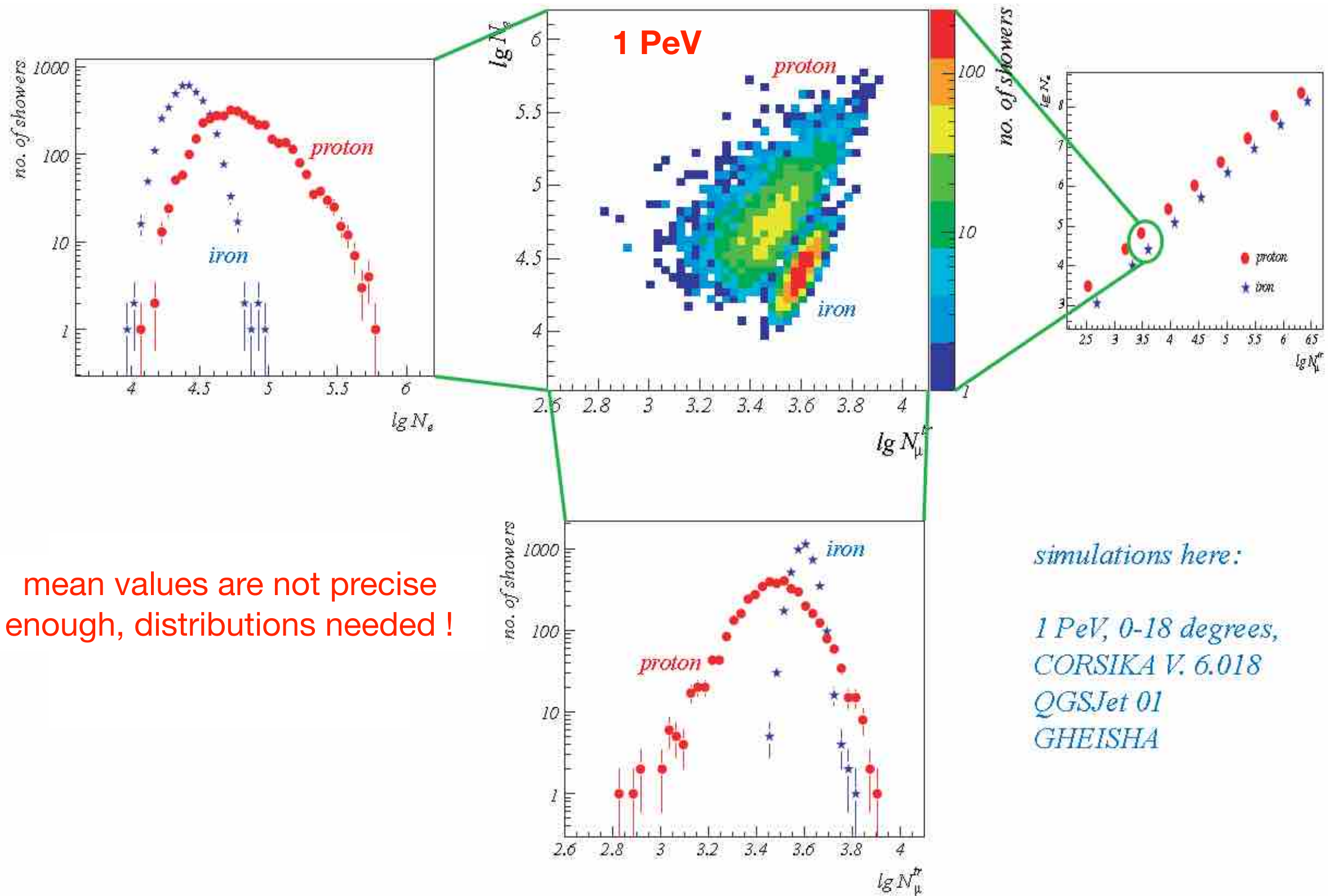
The e.m. particles are more numerous than the muons and the muon lateral distribution is much wider than the electron one ➜ *low density* ➜ *large fluctuations* ➜ *large detection area needed*

but typically used *only a few hundreds m²*


e.m. particles

13 cm iron

only after 2-3 layers (>25 cm iron) we observe muon tracks

muon tracks

EAS-TOP Calorimeter

The main problem is the punch-through by high energy e.m. particles which mimic muons

Understanding fluctuations

1 PeV

mean values are not precise
enough, distributions needed !

simulations here:

1 PeV, 0-18 degrees,
CORSIKA V. 6.018
QGSJet 01
GHEISHA

KASCADE: Unfolding procedures

Energy spectra of 5 mass groups reconstructed (p,He,CNO, MgSI, Fe)
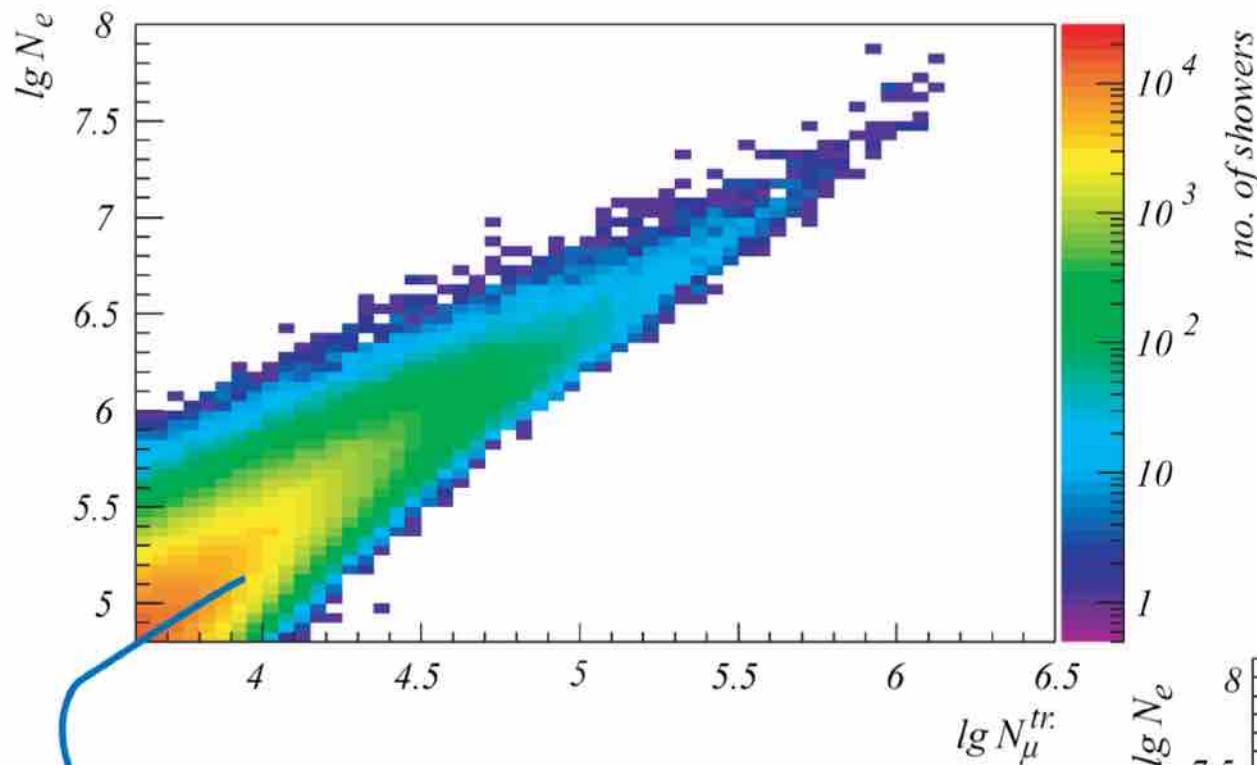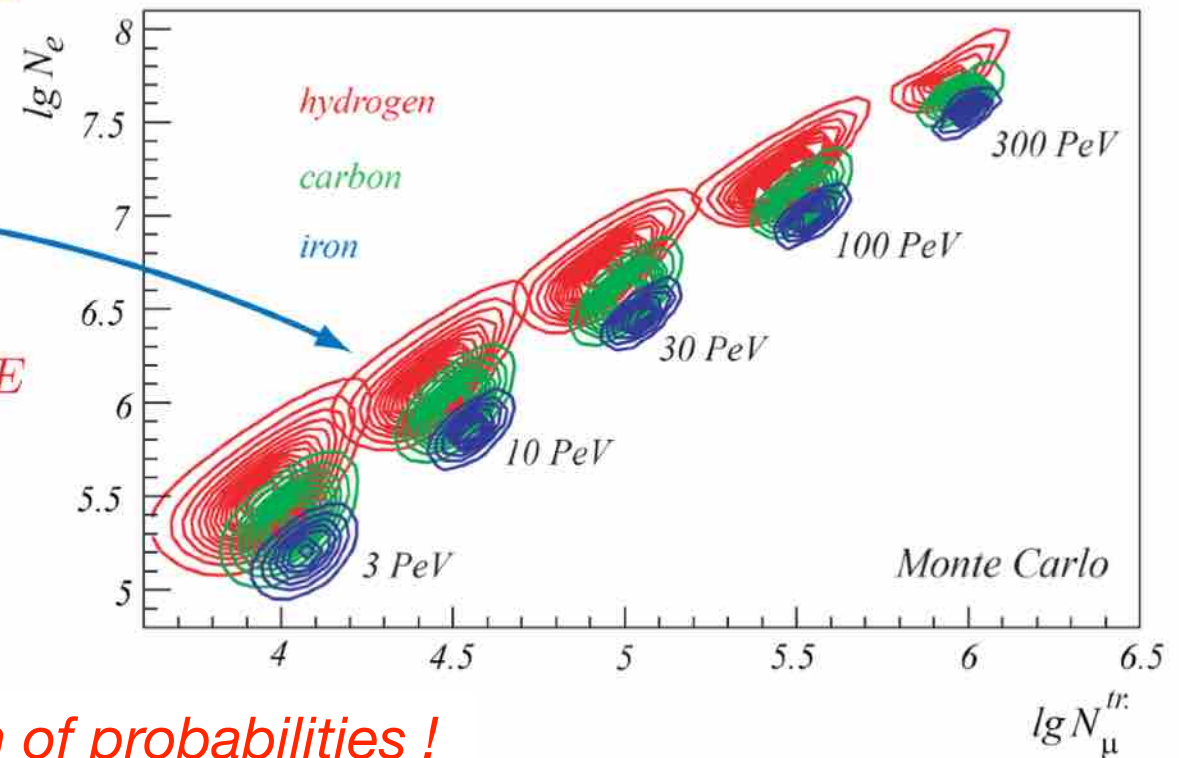

2-dimensional shower size distribution

frequency of showers dependent on 2 observables

zenith angle < 18° , eff. measurement time: 900 days

$$\frac{dJ}{d\lg N_e \, d\lg N_\mu^{tr}} =$$

$$\sum_A \int_{-\infty}^{+\infty} \frac{dJ_A}{d\lg E} \, p_A(\lg N_e, \lg N_\mu^{tr} \mid \lg E) \, d\lg E$$

→ *system of coupled integral equations*

MC simulations needed for determination of probabilities !

→ *Strong dependence on hadronic interaction models*
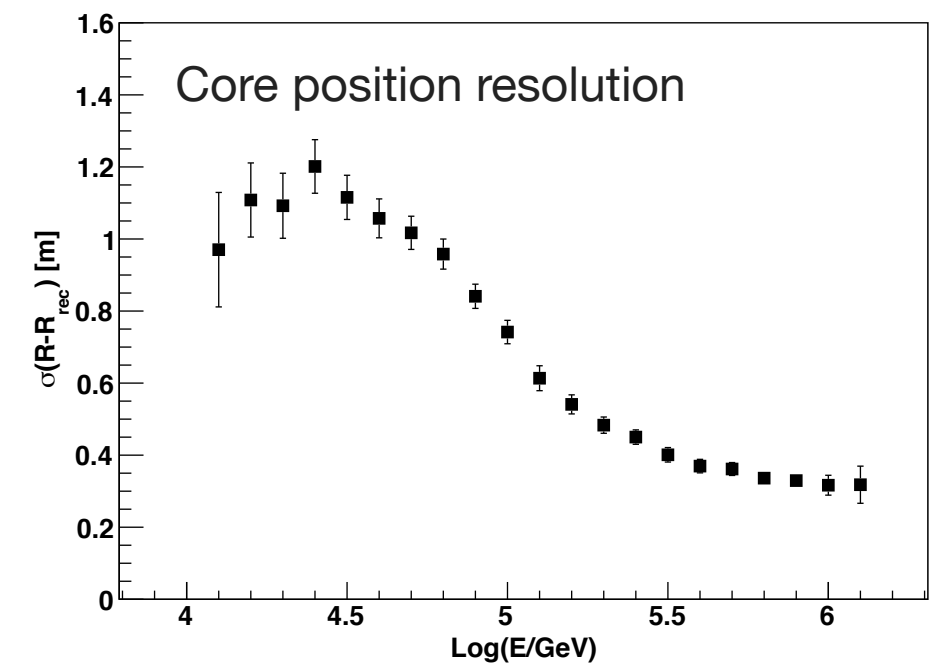
The light-component spectrum (0.3 - 5 PeV)

The high segmentation of the read-out allows to access the LDF down to the shower core.
Discrimination Light/Heavy based on the measurement of the LDF at different distances from the core

ARGO-YBJ
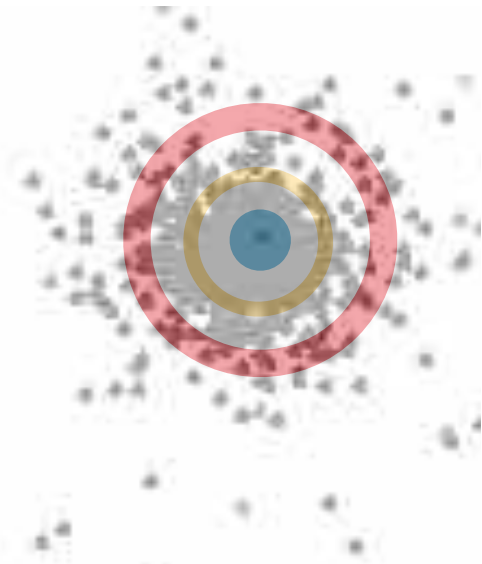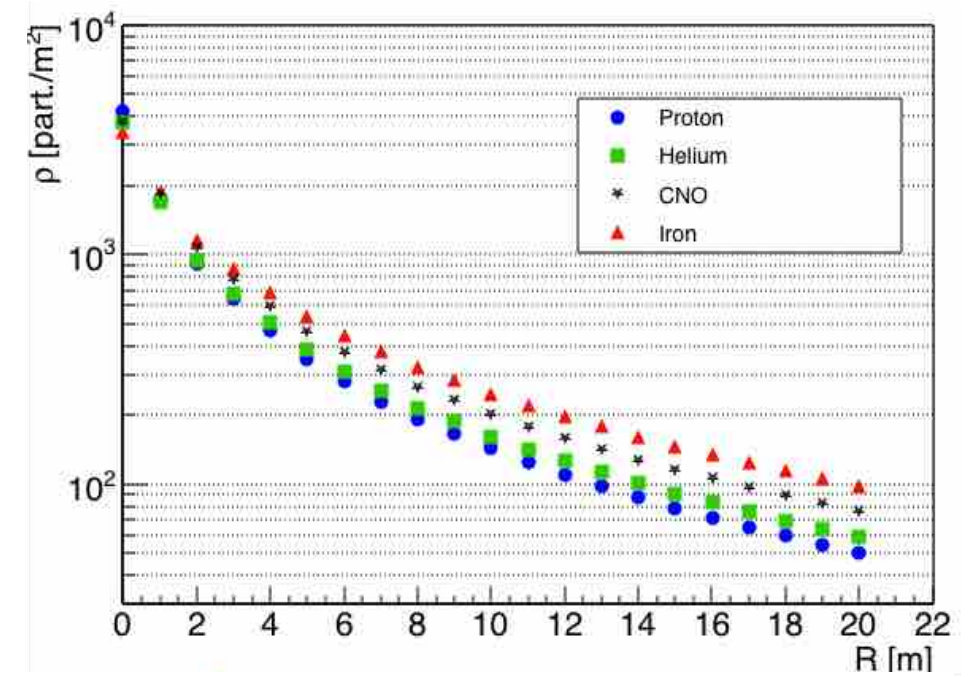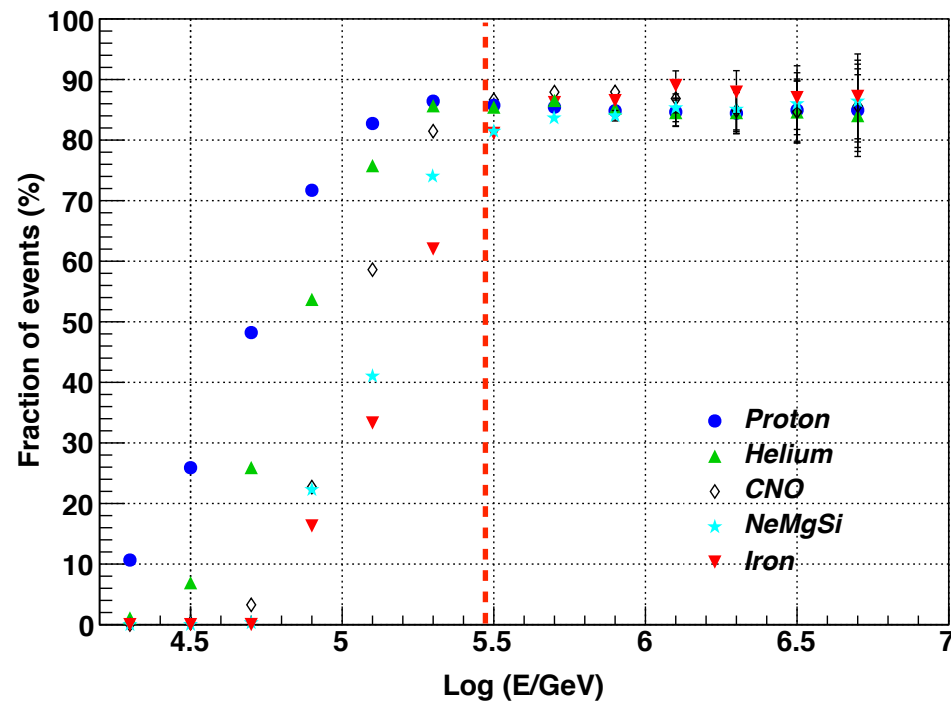
$$\beta_5 = \rho_5/\rho_0$$

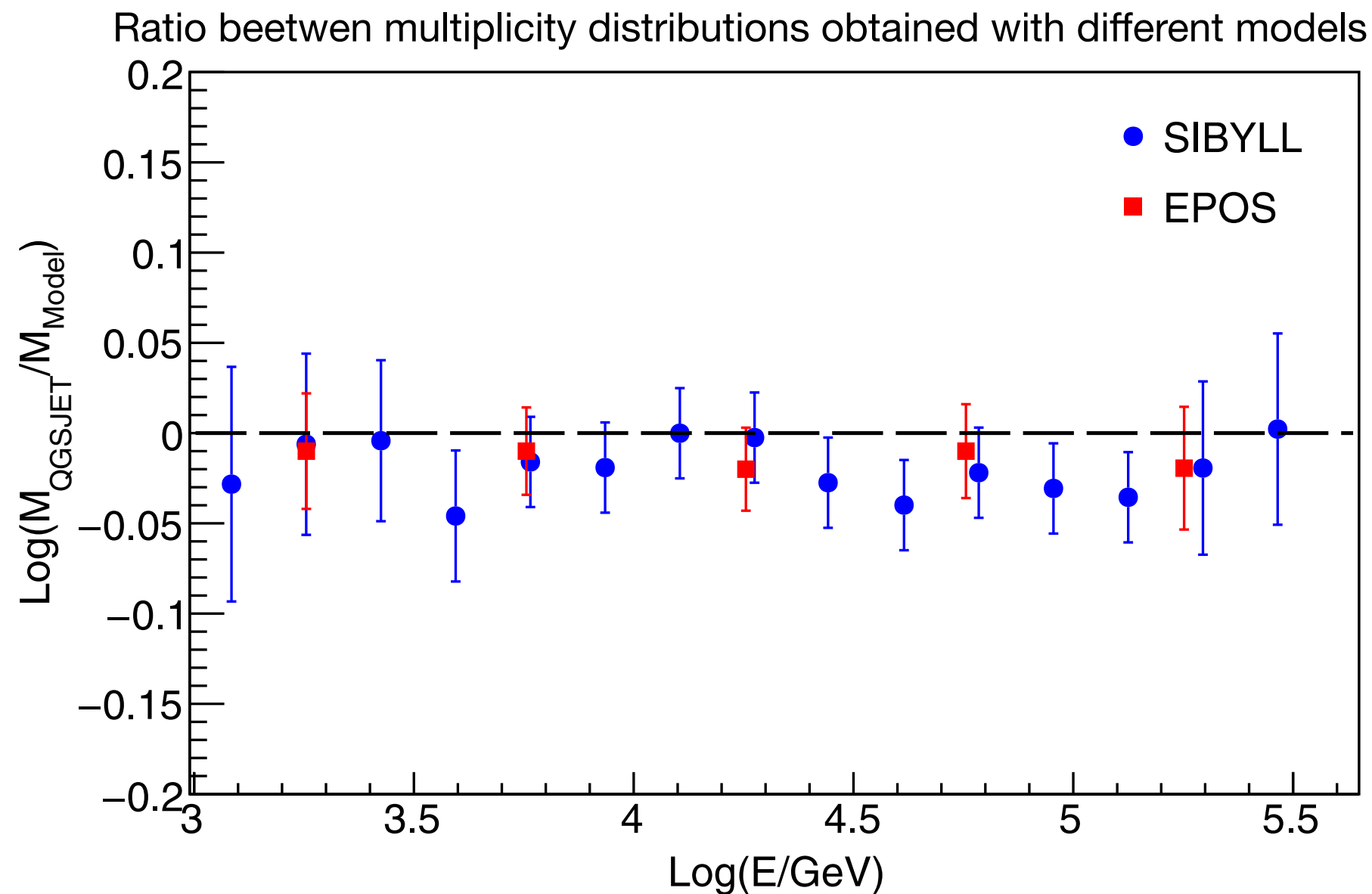$$\beta_{10} = \rho_{10}/\rho_0$$

Hadronic Interaction Models

Corsika v 6980 + Fluka + EGS4
- QGSJET II.03
- SIBYLL 2.1
- EPOS 1.99

Not muons but lateral distribution ➜ topology

Ratio beetwen multiplicity distributions obtained with different models

Wide Field of View Cherenkov Telescopes

The goal: measurement of the CR energy spectrum and composition in the range 10^{13} - 10^{18} eV

Why Wide FoV Cherenkov telescopes at high altitude ?

High altitude
(1) Measure EASs near maximum development points to reduce fluctuations.

(2) Use an unbiased trigger threshold for heavy components of primaries.

(3) Low energy theshold and wide energy range ($10^{13} \rightarrow 10^{18}$ eV).

Cherenkov signal
(4) Measure the electromagnetic component which is less dependent on hadronic interaction models than the muon component.

(5) Good separation capability between the different masses.

(6) Good energy resolution (<20%).

Chin. Phys. C 38, 045001 (2014)
Phys. Rev. D 92, 092005 (2015)

First example of *hybrid measurement*: Cherenkov telescope + EAS array (ARGO-YBJ)

ARGO-YBJ + WFCTA

A prototype of the future LHAASO telescopes has been operated in combination with ARGO-YBJ

- ▸ 4.7 m^2 spherical mirror composed of 20 hexagon-shaped segments
- ▸ 256 PMTs (16 × 16 array)
- ▸ 40 mm Photonis hexagonal PMTs (XP3062/FL)
- ▸ pixel size 1°
- ▸ FOV: 14° × 14°
- ▸ Elevation angle: 60°

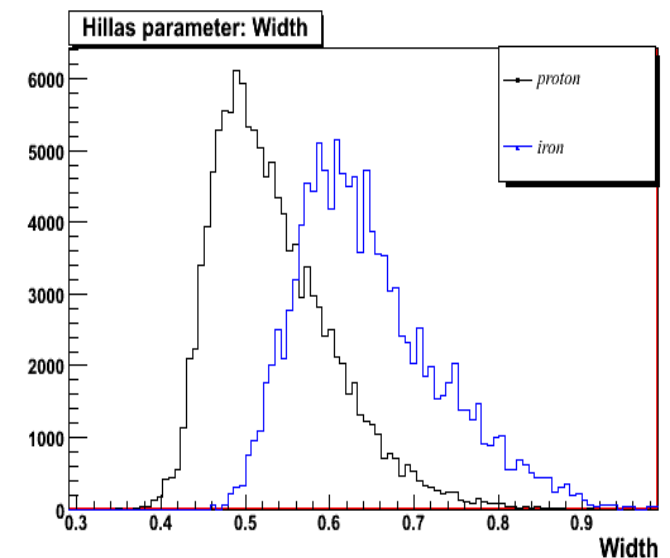❖ *ARGO-YBJ:* core reconstruction & lateral distribution in the core region
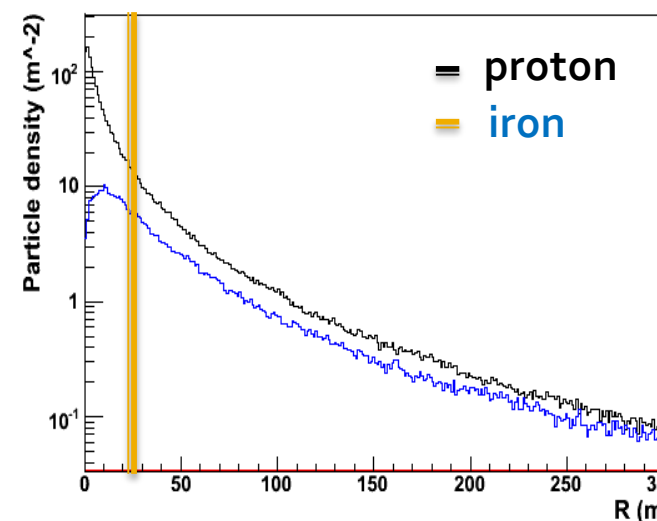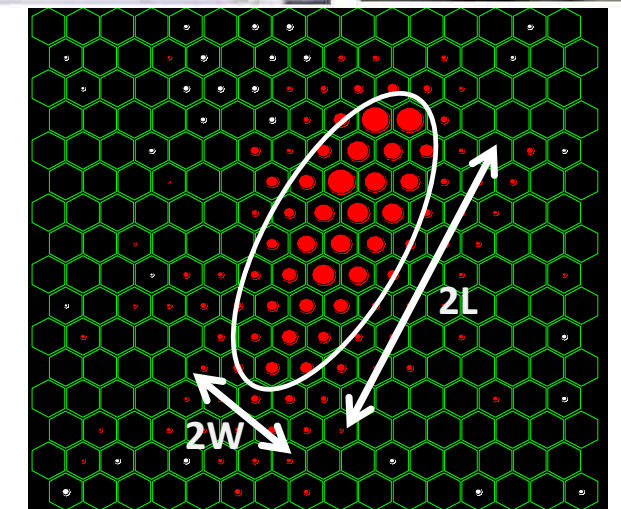
  → mass sensitive

❖ *Cherenkov telescope:* longitudinal information

  Hillas parameters → mass sensitive

- ● angular resolution: 0.2°
- ● shower core position resolution: 2 m

Phys. Rev. D 92, 092005 (2015)

Light component (p + He) selection

- Contamination of heavier component < 5 %
- Energy resolution: ~25% constant with energy
- Uncertainty : ~25% on flux

$$p_L = log_{10}(N_{max}) - 1.44 \cdot log_{10}(E_{rec}/TeV)$$

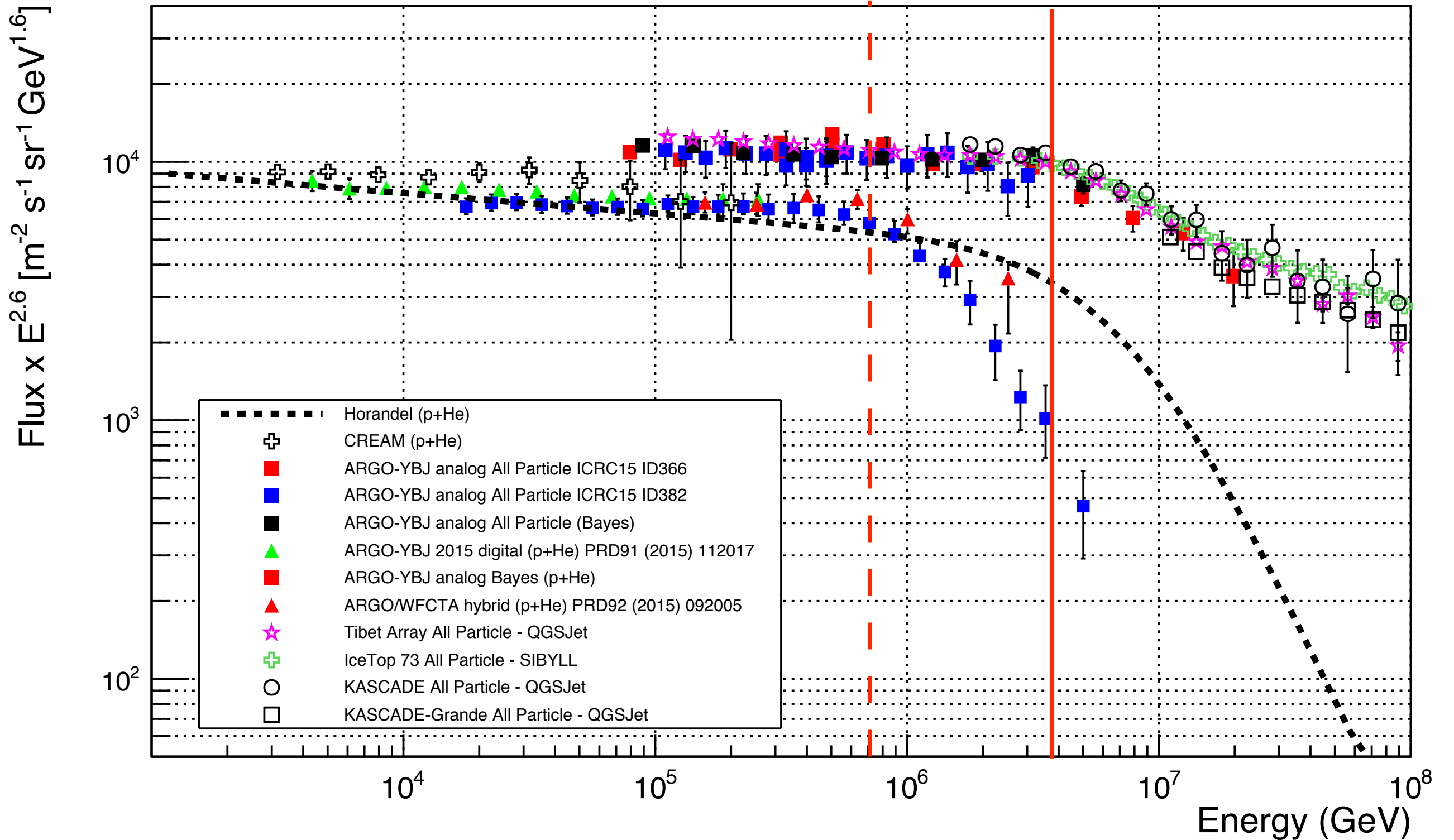$$p_C = L/W - 0.0091(R_p/1\,m) - 0.14 \cdot log_{10}(E_{rec}/TeV)$$

Events for which $p_L \leq -0.91$ and $p_C \leq 1.3$ are rejected

$p_L > -0.91 \,||\, p_C > 1.3$
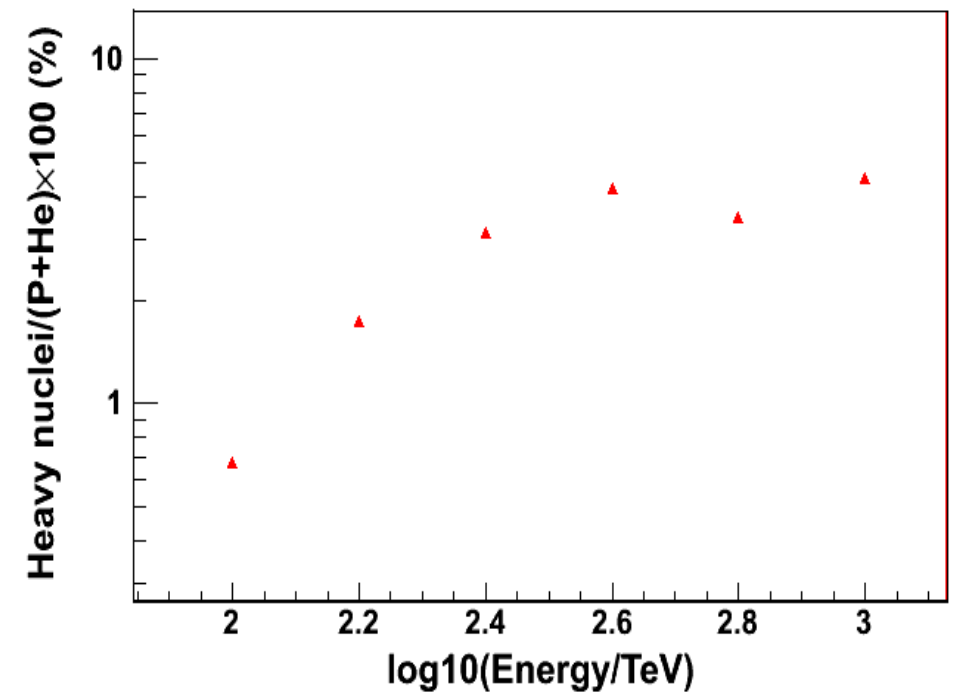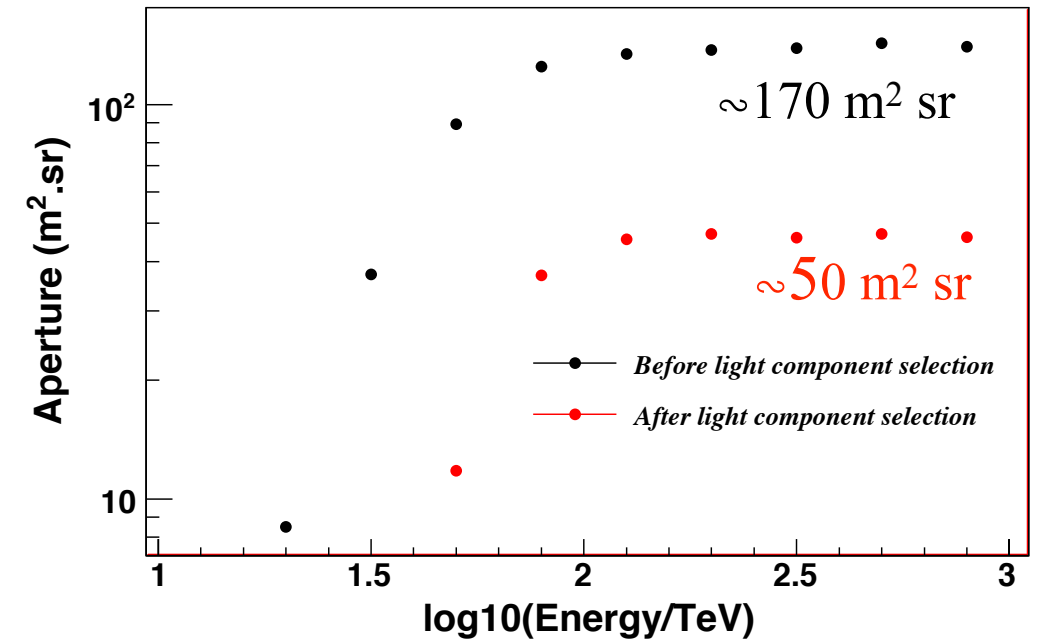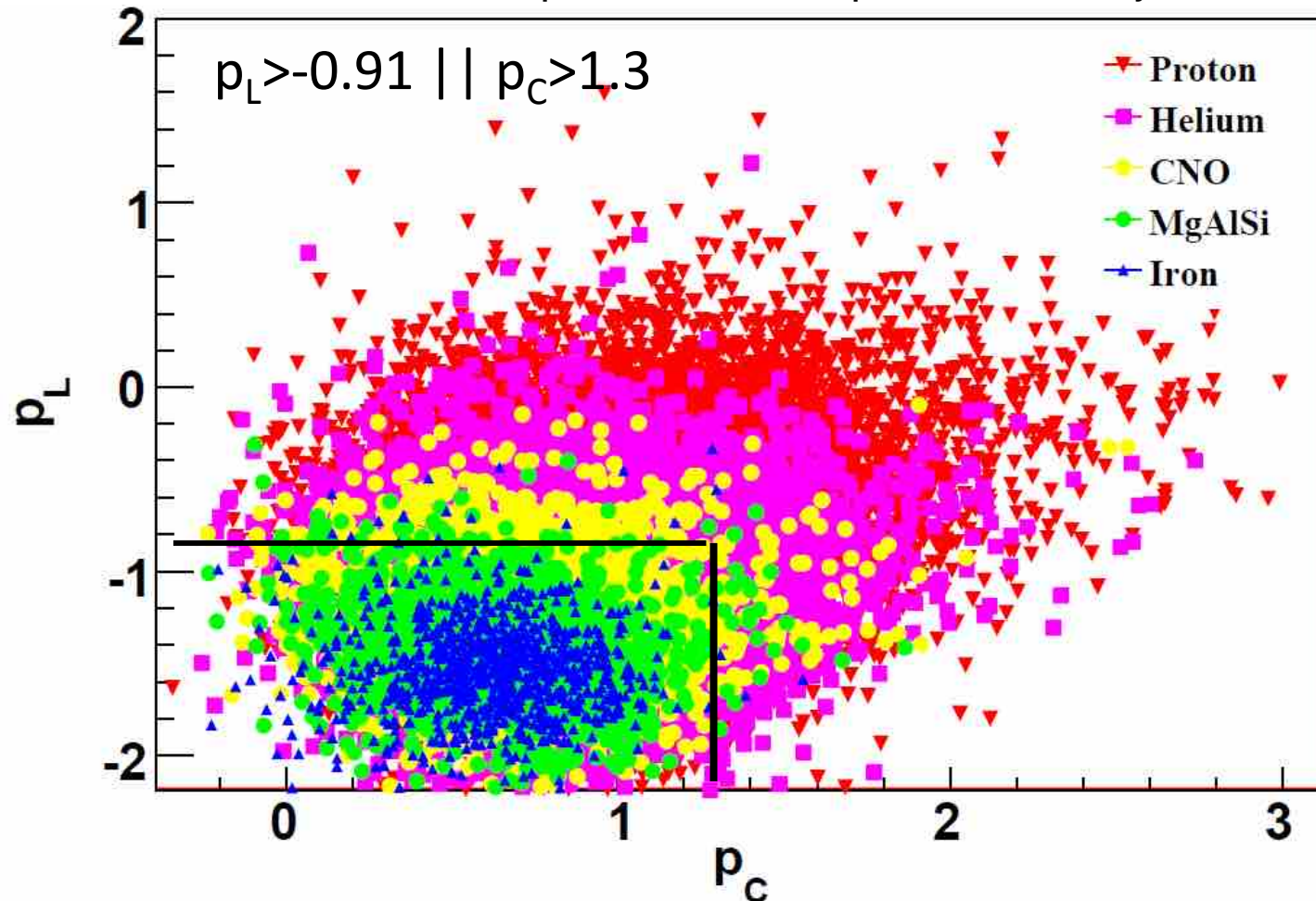
Chin. Phys. C 38, 045001 (2014)

The overall picture

A comment

Is not surprising that decades after the experimental discovery of the knee experimental results are still conflicting and there are still uncertainties on its interpretation.

This is the first time that we are actually probing this region with direct measurements on one side, and *the first time that we are studying EAS very close to the shower maximum (high altitude), and its core, with full coverage arrays.*

The proton spectrum is distinctly softer than that of Helium (and possibly other heavy elements) at all energies (Pamela,CREAM, AMS02).

"The harder He spectrum has the interesting consequence that by the time one gets to the knee energies it dominates hydrogen in the all-particle energy spectrum (though not in energy per nucleon or rigidity).

Thus the knee in the all-particle spectrum at 3×10^{15} eV is actually predominantly a Helium and CNO knee, and it is possible that the proton spectrum cuts off significantly before this as has been suggested by the Tibet ARGO-YBJ experiment".

Drury arXiv:1708.08858

Cosmic Ray diffusive propagation and anisotropy

CR anisotropy as fingerprint for their origin and propagation

Distribution of nearby SNRs in the Galaxy

Sveshnikova et al.
APP 50 (2013) 33
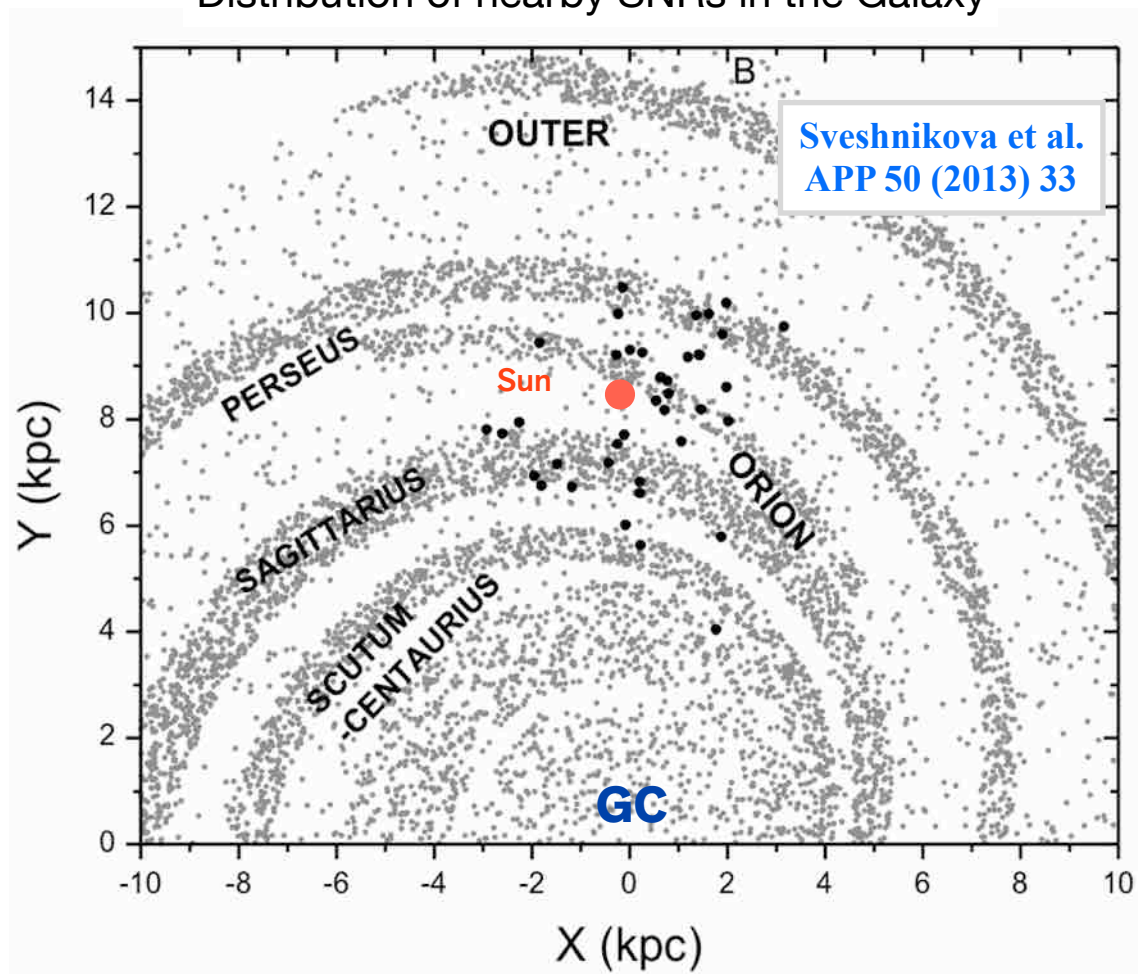
Galactic Cosmic Rays

- Accelerated in SNRs
- Propagate diffusively

Consequences for anisotropy

- CR density gradients are visible as anisotropy
- Anisotropy amplitude $\lesssim 10^{-2}$
- Amplitude increases with energy
- Dipole shape
- Phase pointing towards the most significant sources

A weak anisotropy is expected from the diffusion and/or drift of GCRs in GMF.
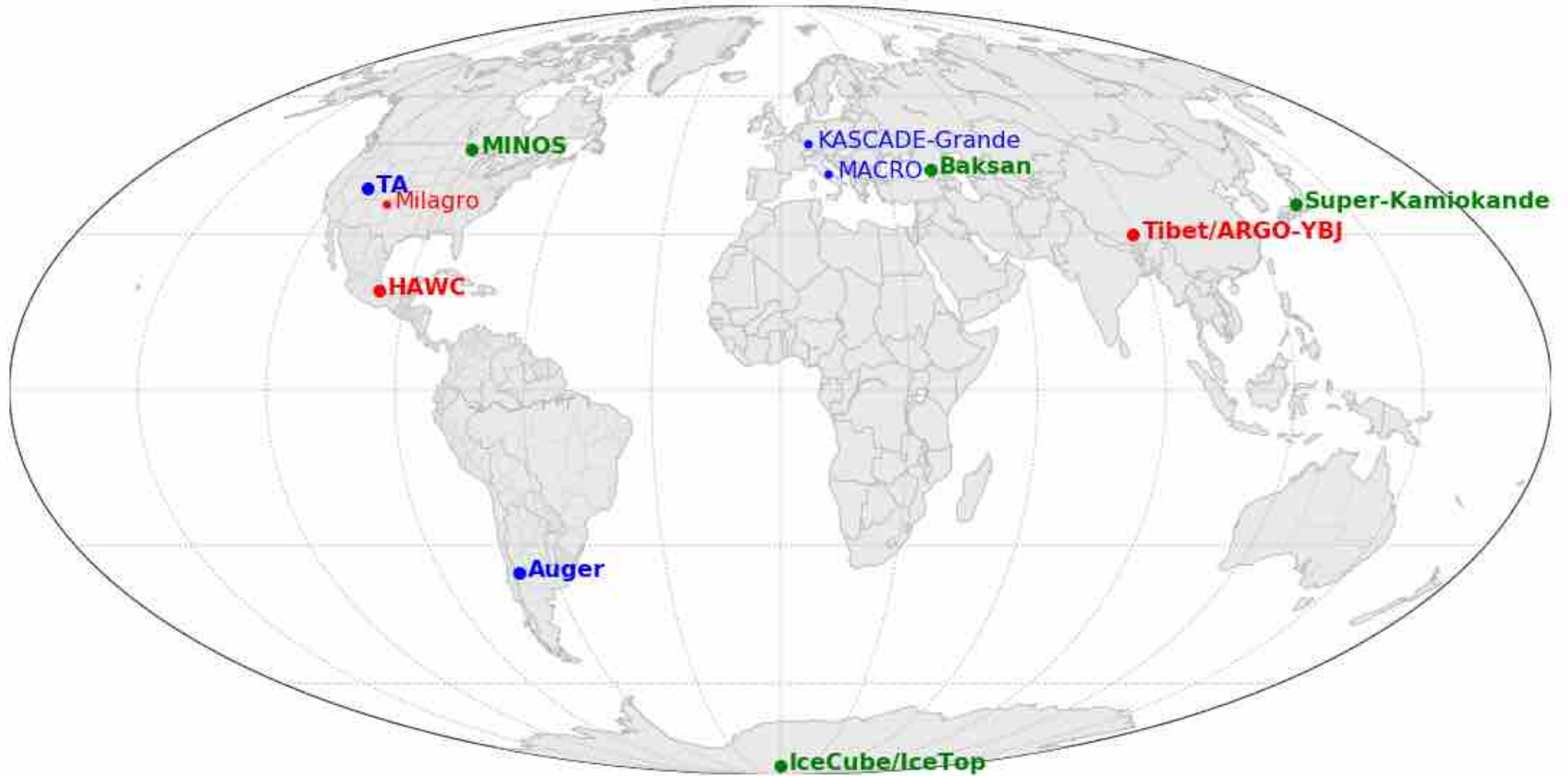
Generally speaking, the dipole component of the anisotropy is believed to be a tracer of the CR source distribution, with the largest contribution from the nearest ones.

Review:
G. Di Sciascio and R. Iuppa, arXiv:1407.2144
M. Ahlers & P. Mertsch, arXiv:1612.01873

Cosmic Ray Observatories

Large Data Sets

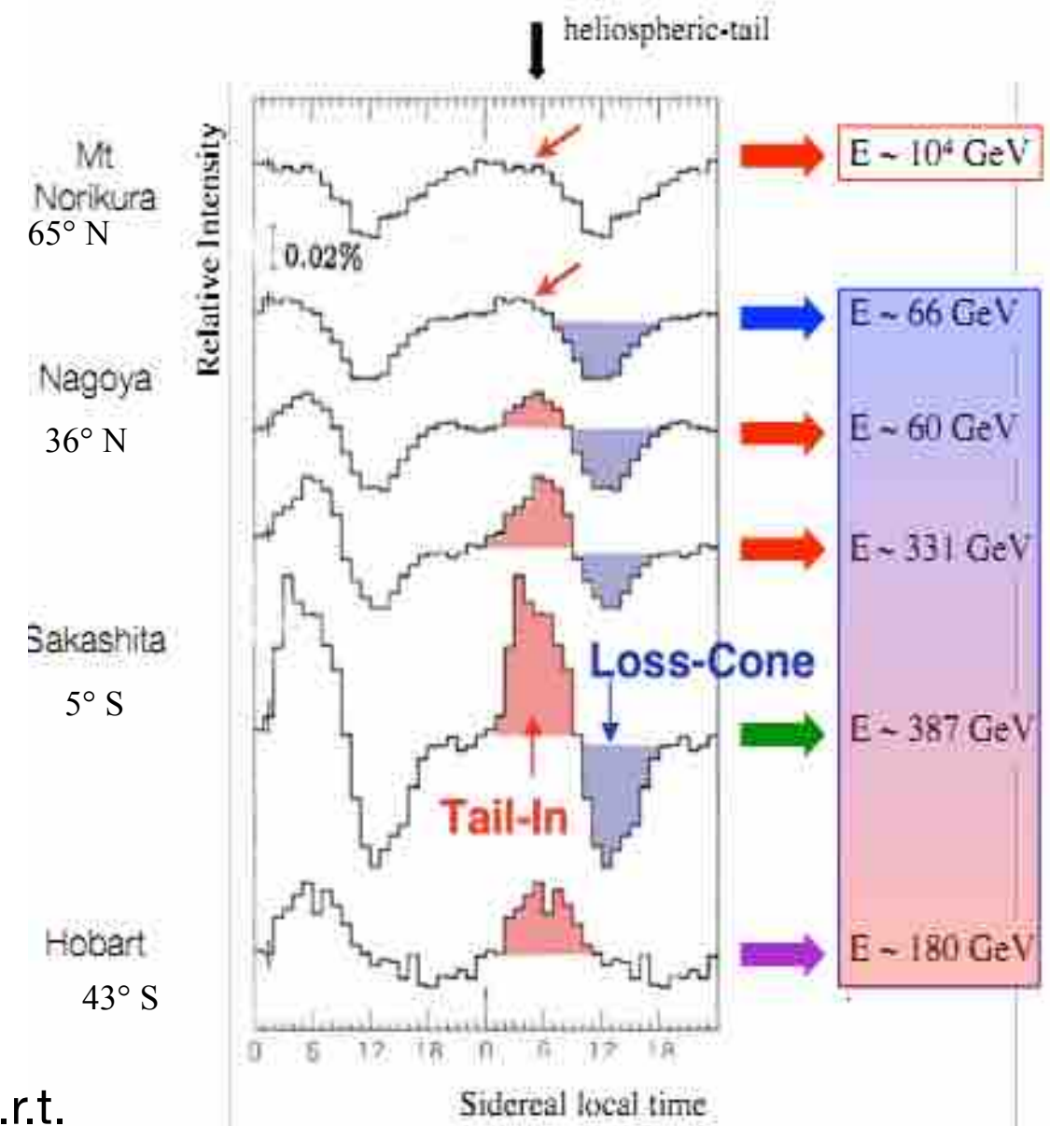| Detector	Altitude	Latitude	E_{median}	N_{events}	Run Date
Tibet ASγ	4300 m	30°S	~3 TeV	~4×10⁹	Feb. 1997 - Nov. 2005
Milagro	2630 m	36°S	~1 TeV	~220×10⁹	Jul. 2000 - Jul. 2007
ARGO-YBJ	4300 m	30°S	~1 TeV	~220×10⁹	Nov. 2007 - May 2012
HAWC	4100 m	19°N	~2 TeV	~110×10⁹	Jun. 2013 -
Auger	1400 m	35°S	~1 EeV	~0.001×10⁹	Nov. 2004 -
IceCube	—	90°S	~20 TeV	~360×10⁹	May 2009 -
IceTop	2835 m	90°S	~1.6 PeV	~0.23×10⁹	May 2009 -

BenZvi, CRA 2017

The largest CR datasets are being accumulated by *gamma-ray* and *neutrino detectors*

★ *Lesson*: if you want a really huge sample of cosmic rays, build a gamma-ray observatory !

Outline of Current Results

Anisotropy in the arrival directions of cosmic rays has been observed by a number of underground and surface detectors.

★ Total energy range covered: ~10 GeV to ~10 EeV.

★ *Large-scale structure*: > 60 degrees in extent, relative intensity 10^{-3}

★ *Small-scale structure*: < 10 degrees in extent, relative intensity $10^{-4} – 10^{-5}$

★ The large-scale anisotropy is *not described by a simple dipole*, though the dipole component is often shown when comparing across experiments.

★ Amplitude and phase change with latitude.

★ The anisotropy is *energy dependent*.

　● Shift in phase of large-scale structure >100 TeV.

　● Small-scale excesses seem to have hard spectrum w.r.t. isotropic background. Cut off >10 TeV

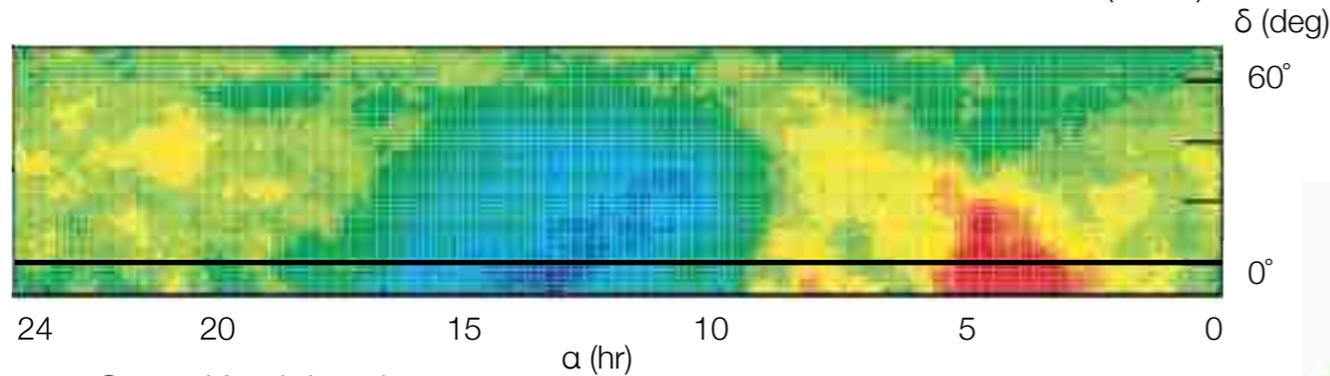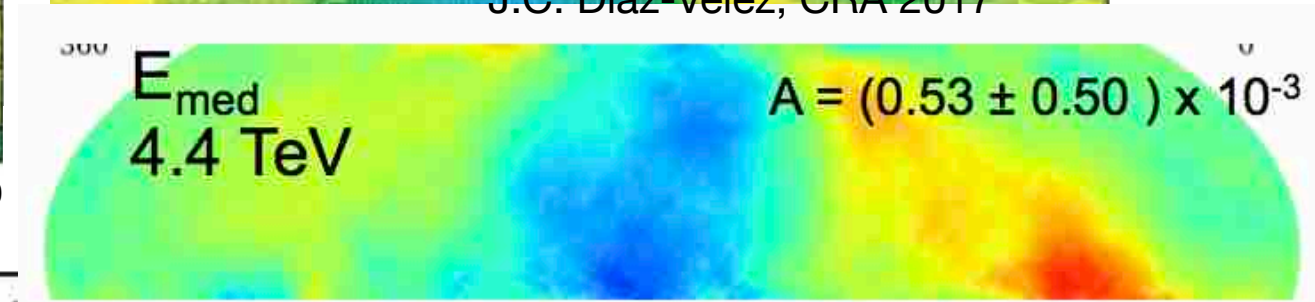★ At the few percent level, the anisotropy is *time-independent* going back almost 20 years.
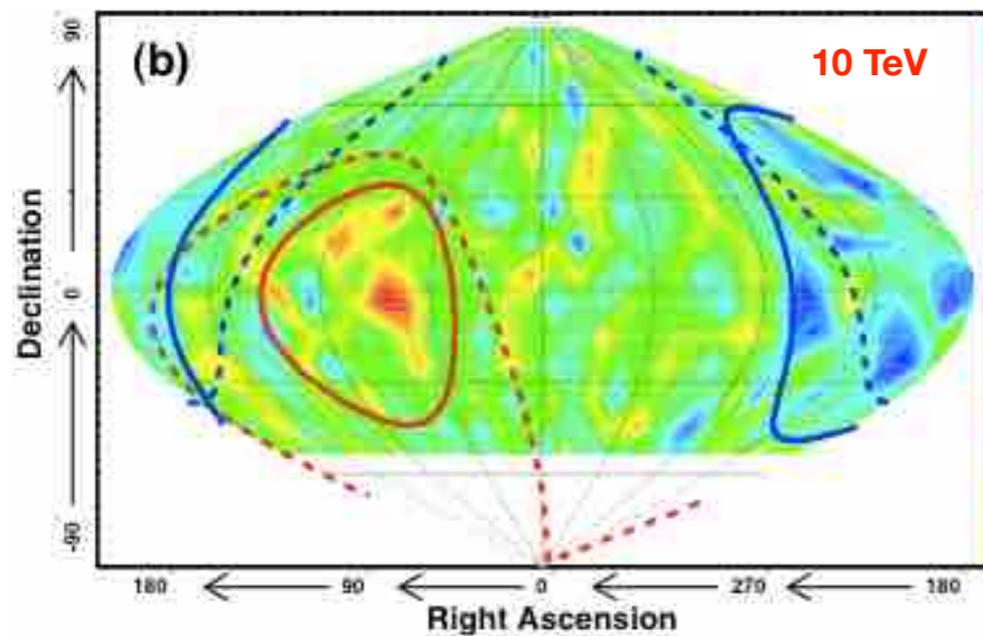

by Nagashima 1998

scale anisotropy ~10⁻³

Tibet ASγ
Amenomori et al. (2006)

TeV   4 TeV

Tibet ASγ
Amenomori et al. (2006)

Tibet ASγ
Amenomori et al. (2006)

δ (deg)
60°
0°

Tibet ASγ
Amenomori et al. (2006)

δ (deg)
60°

HAWC
J.C. Diaz-Velez, CRA 2017

E_{med}
4.4 TeV

$A = (0.53 \pm 0.50) \times 10^{-3}$

(b)   10 TeV
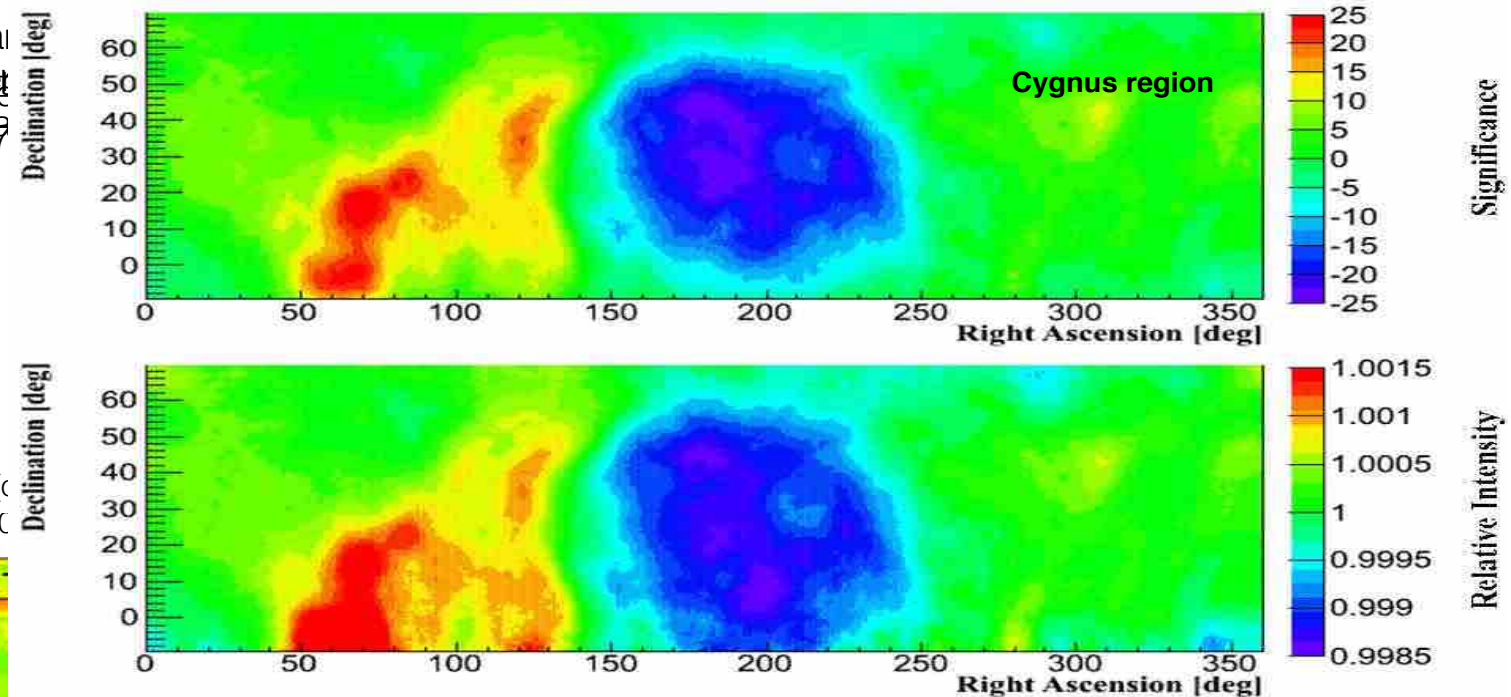
Super Kamiokande
Guillian et al. (2007)

(b)

Tail-in excess region   Loss-cone deficit region

ARGO-YBJ   1 TeV
ApJ 809 (2015) 90

Cygnus region

Right Ascension

Milagro
Abdo et al. (2009)

ARGO-YBJ
Zhang et al. (2009)

Bartoli et al. (2015)

4 TeV

38
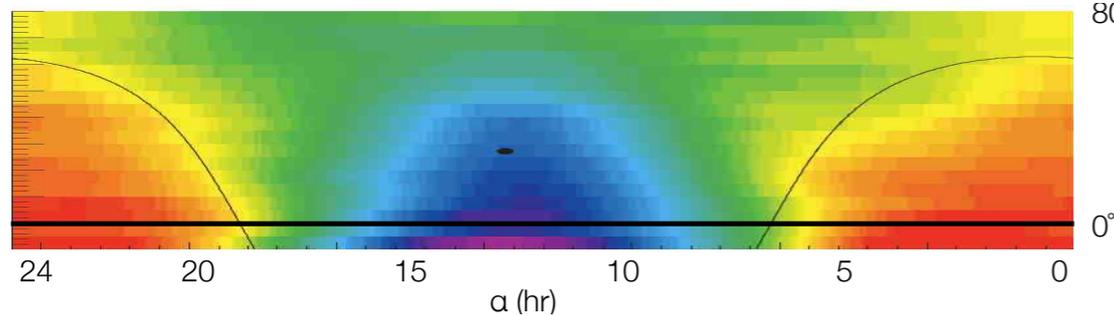
Energy dependence of anisotropy

- R.A. profile of anisotropy can be described with 2 harmonics

$$I = 1 + A_1 cos[2\pi(x - \phi_1)/360] + A_2 cos[2\pi(x - \phi_2)/180]$$
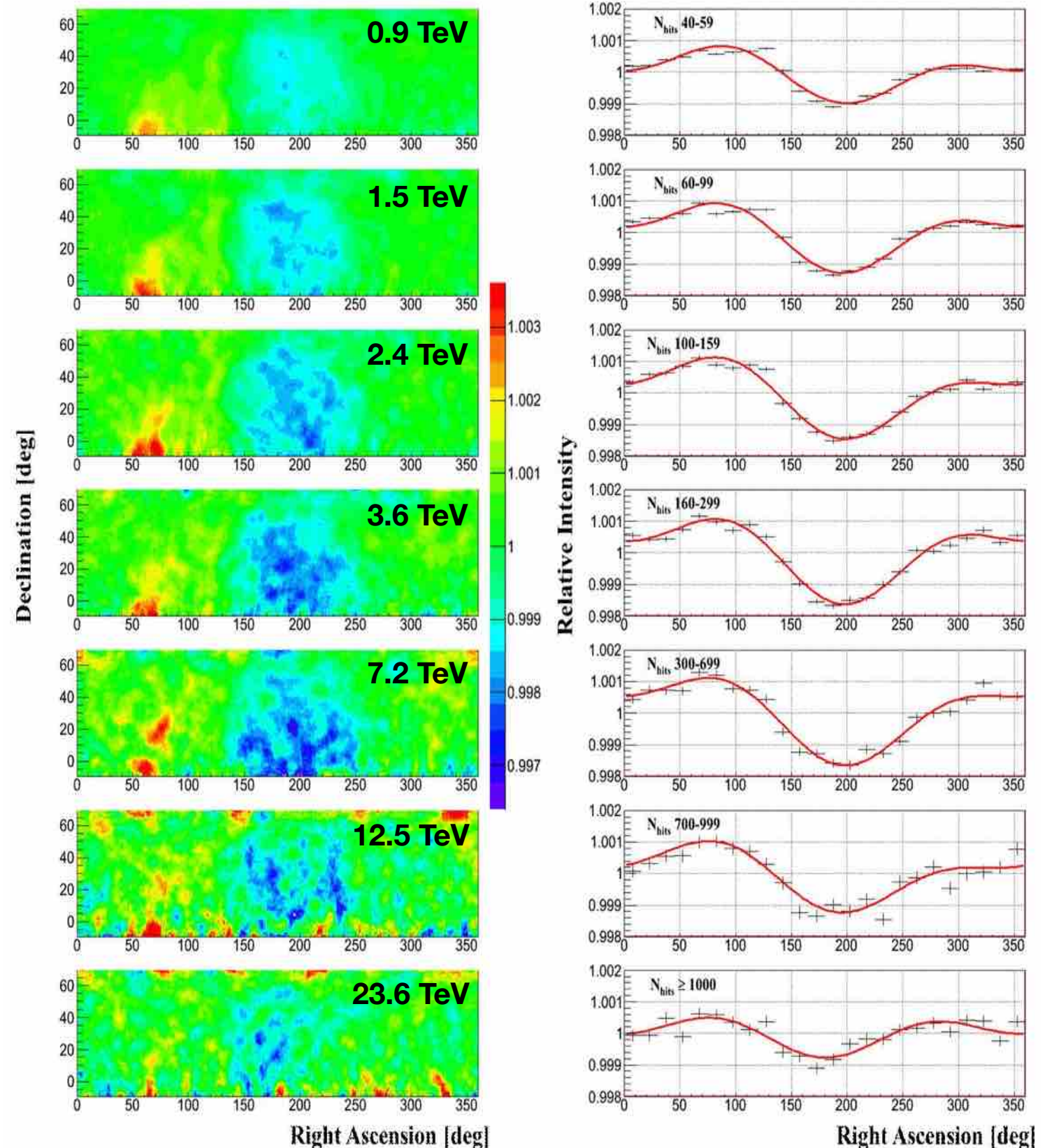
$A_1 = 6.8 \times 10^{-4}$, $\Phi_1 = 39.1°$
$A_2 = 4.9 \times 10^{-4}$, $\Phi_2 = 100.9°$

- The LSA cannot be described by a simple dipole.

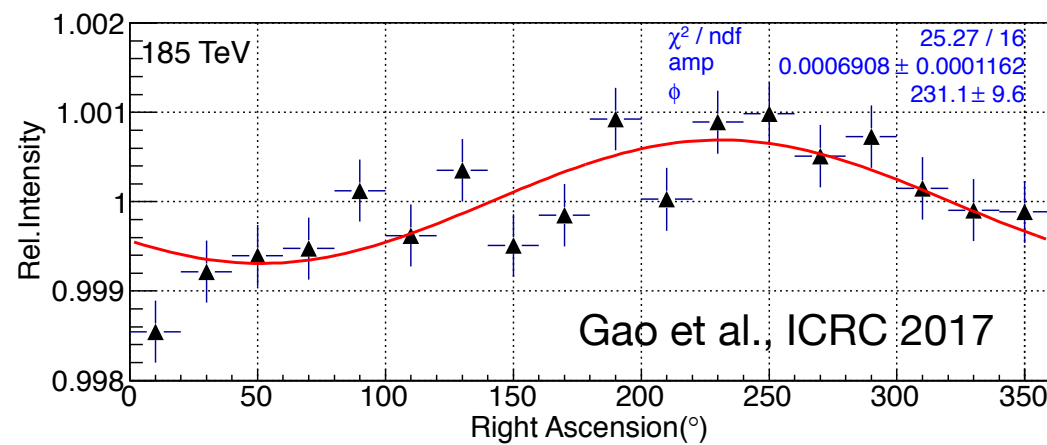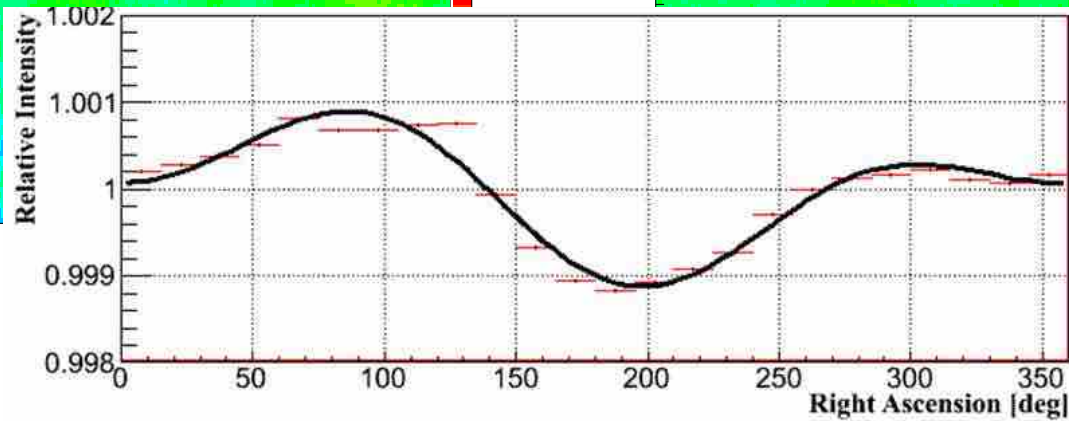Structures with complex morphologies are visible in all the maps, changing shape with energy.

The tail-in broad structure appears to dissolve to smaller angular scale spots with increasing energy.

ARGO-YBJ
ApJ 809 (2015) 90

High energies (>100 TeV) with ARGO—YBJ

At 185 TeV dramatic change of anisotropy !

Gao et al., ICRC 2017

excess region: $\alpha \approx 240°$
deficit region: $\alpha \approx 70°$

consistent with IceCube/IceTop and Tibet ASγ results

The origin of this feature cannot be explained with the conventional diffusion scenario of GCRs, and may provide us with a new hint for understanding the origin and propagation of GCRs.

1.4 TeV 10.6 TeV
2.4 TeV 18.0 TeV
3.5 TeV 29.9 TeV
6.1 TeV 70.0 TeV

Significance

Zig Hampel, PhD Thesis (2017)
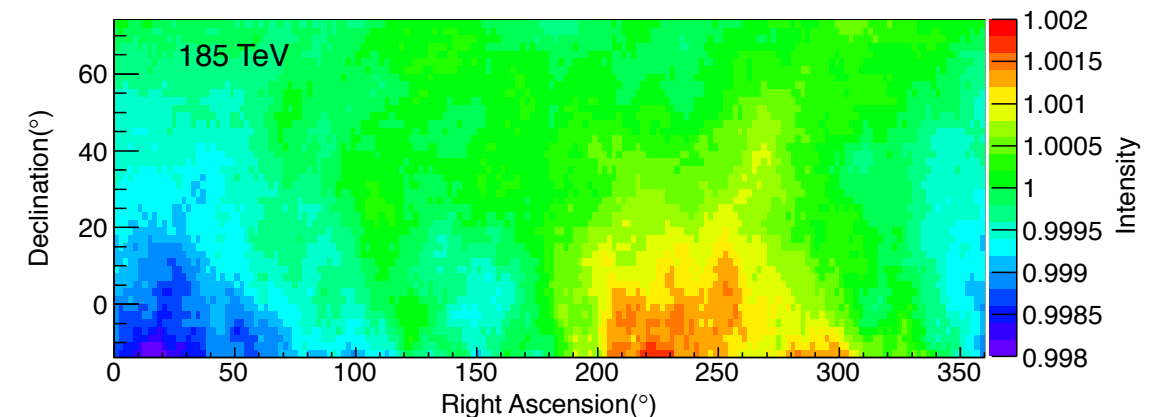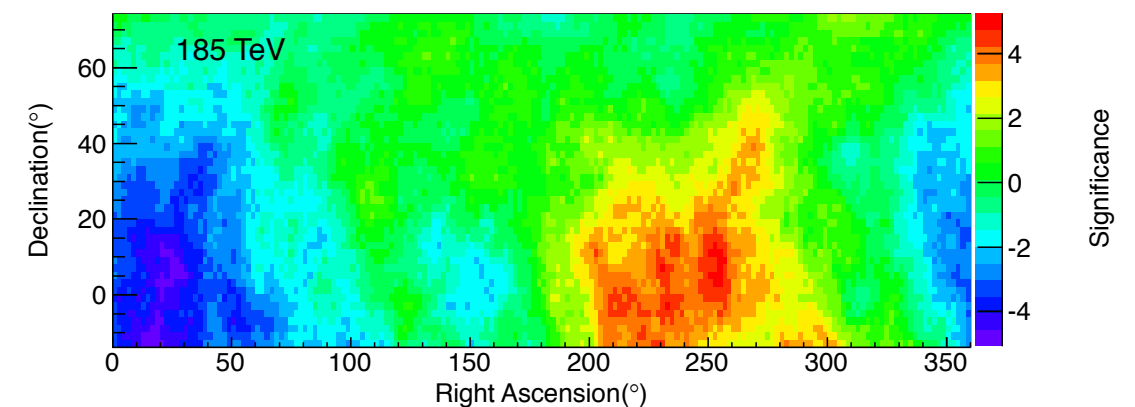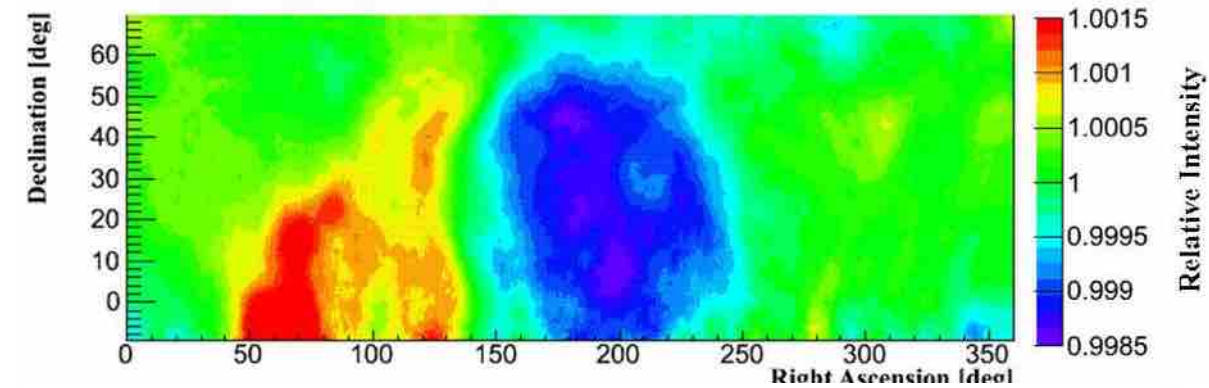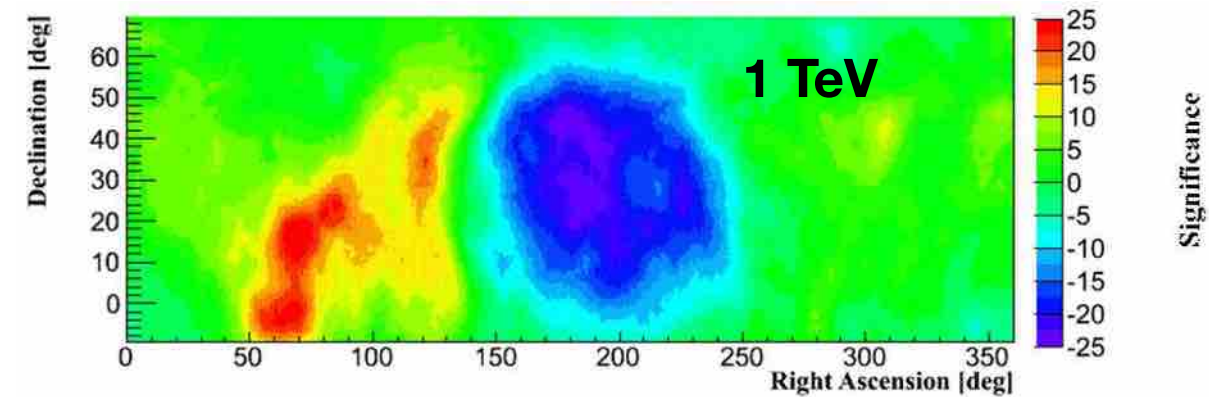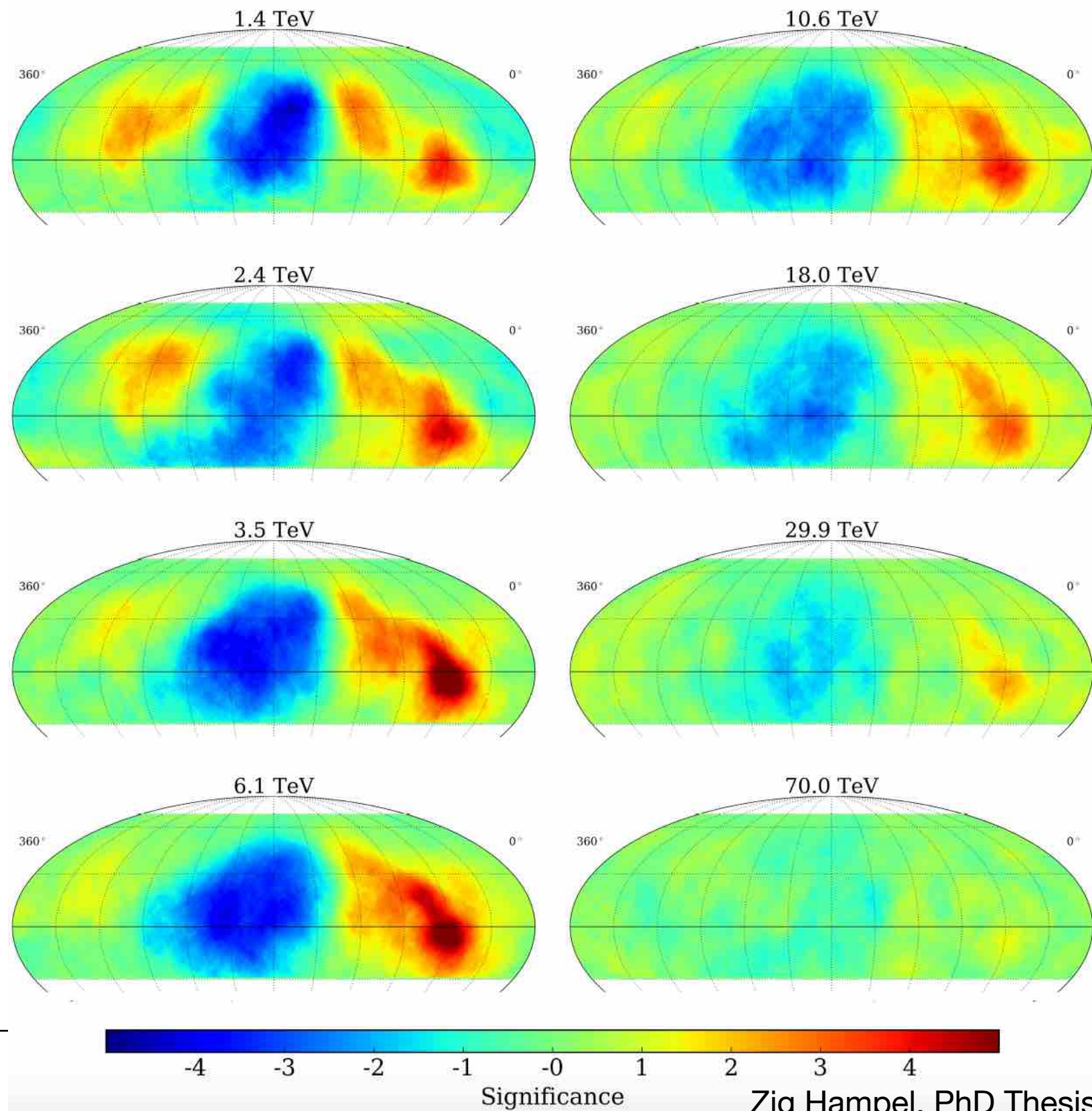
Energy dependence: IceCube

Note: *cosmic ray composition changes as well vs. energy*
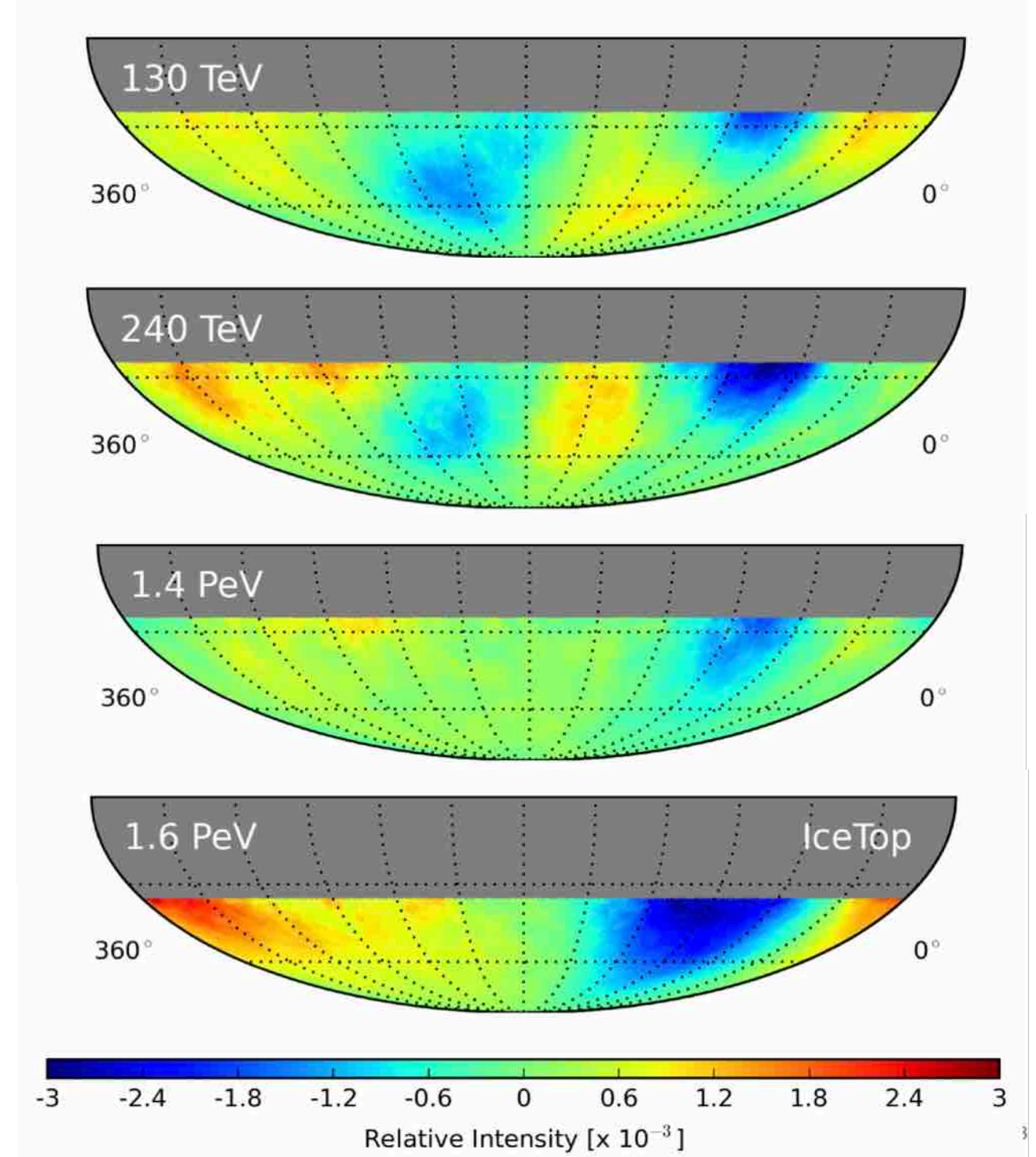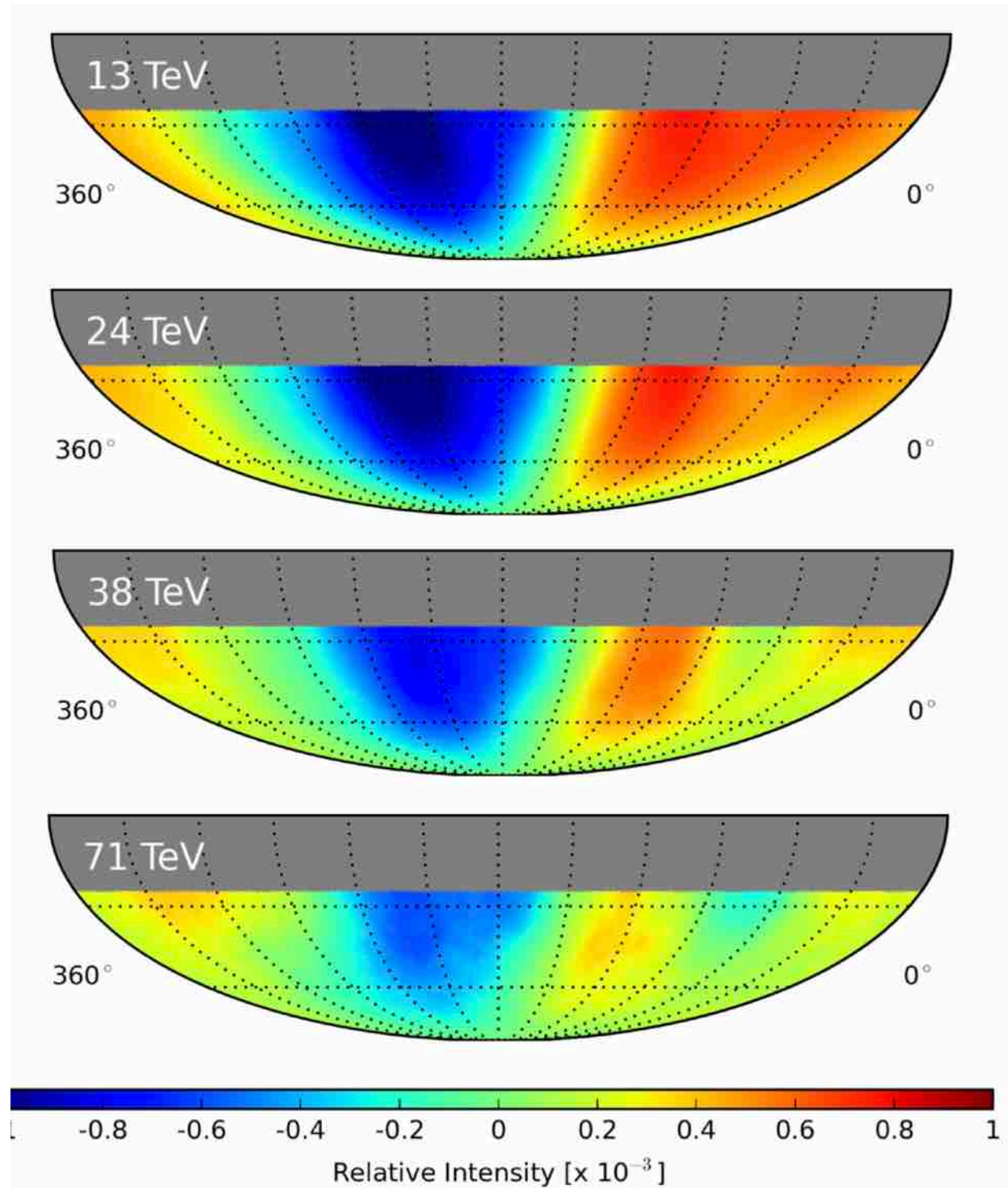
Amplitude and Phase of the first harmonic

dipole component as a tracer
of the CR source distribution

- Extremely small amplitude: $10^{-4} - 10^{-3}$

- Slow increase of A_1 with increasing energy to a maximum around 10 TeV.

- Slow fall of A_1 to a minimum at about 100 TeV.

- Evidence of increasing A above 100 TeV.

- Phase nearly constant around 0 hrs.

- Dramatic change of phase above 100 TeV.

The variation of the amplitude with energy seems to be difficult to interpret in terms of the conventional GCR diffusion model in the Galaxy.

G. Di Sciascio and R. Iuppa, arXiv:1407.2144
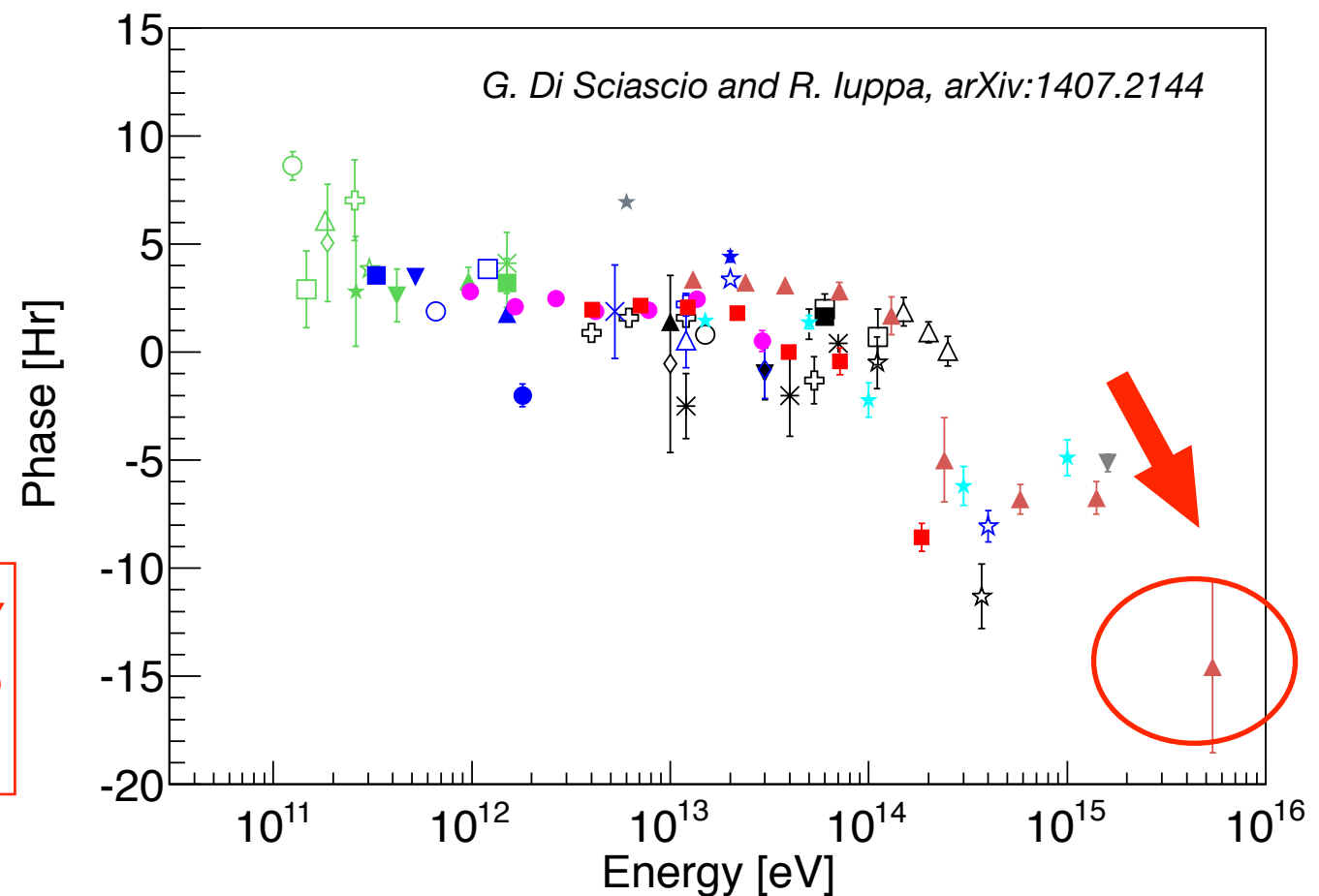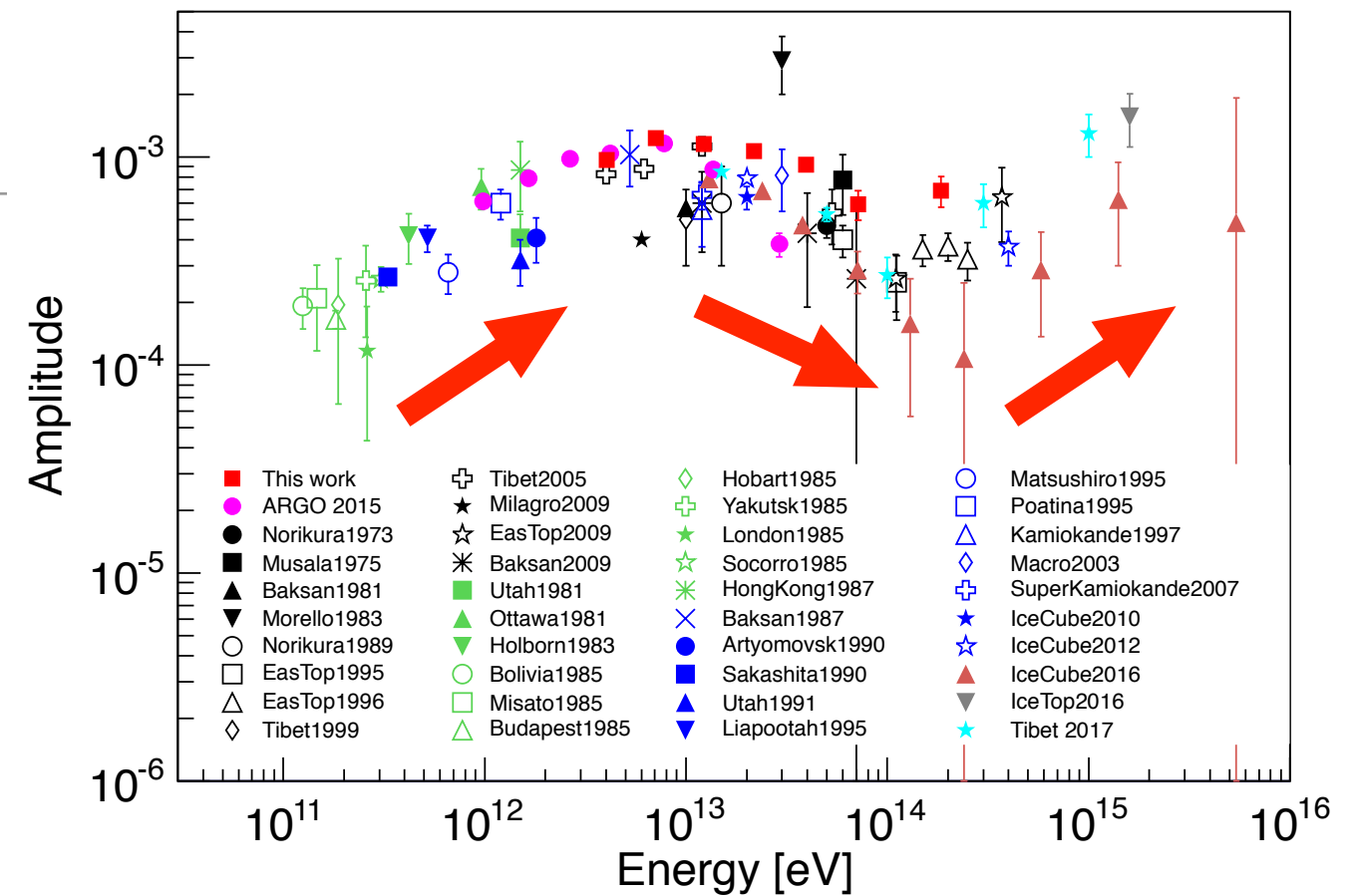
All-sky coverage of LSA

HAWC

IceCube

Small scale anisotropy

Tibet-III

Amenomori et al. ICRC (2007)

relative intensity

Vernetto et al., ICRC2009
Bartoli et al., PRD D88 (2013) 082001

ARGO-YBJ

statistical significance

Milagro

Abdo et al. (2008)

statistical significance

BenZvi et al., ICRC 2013
Abeysekara et al., ApJ 796 (2014) 108

HAWC

statistical significance
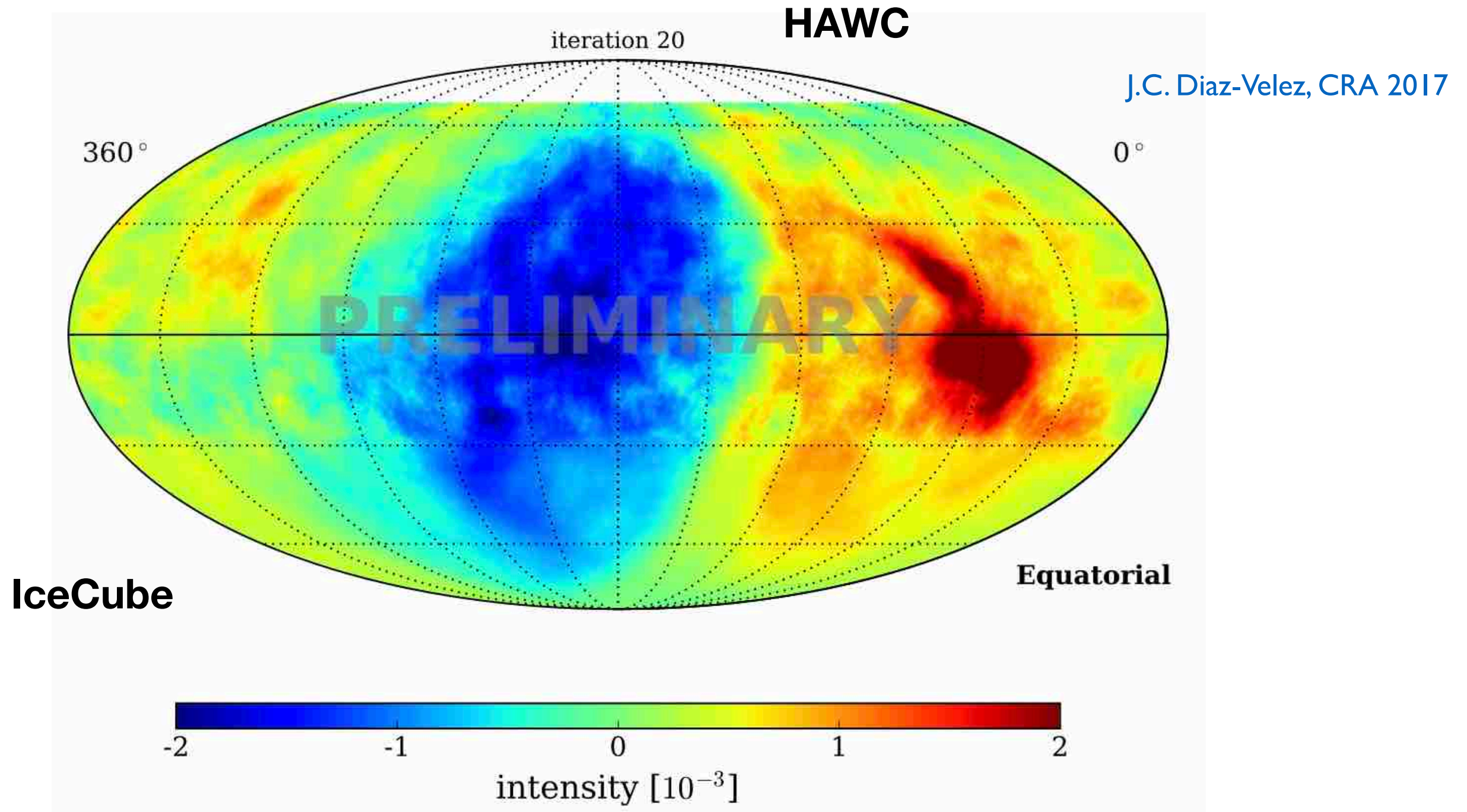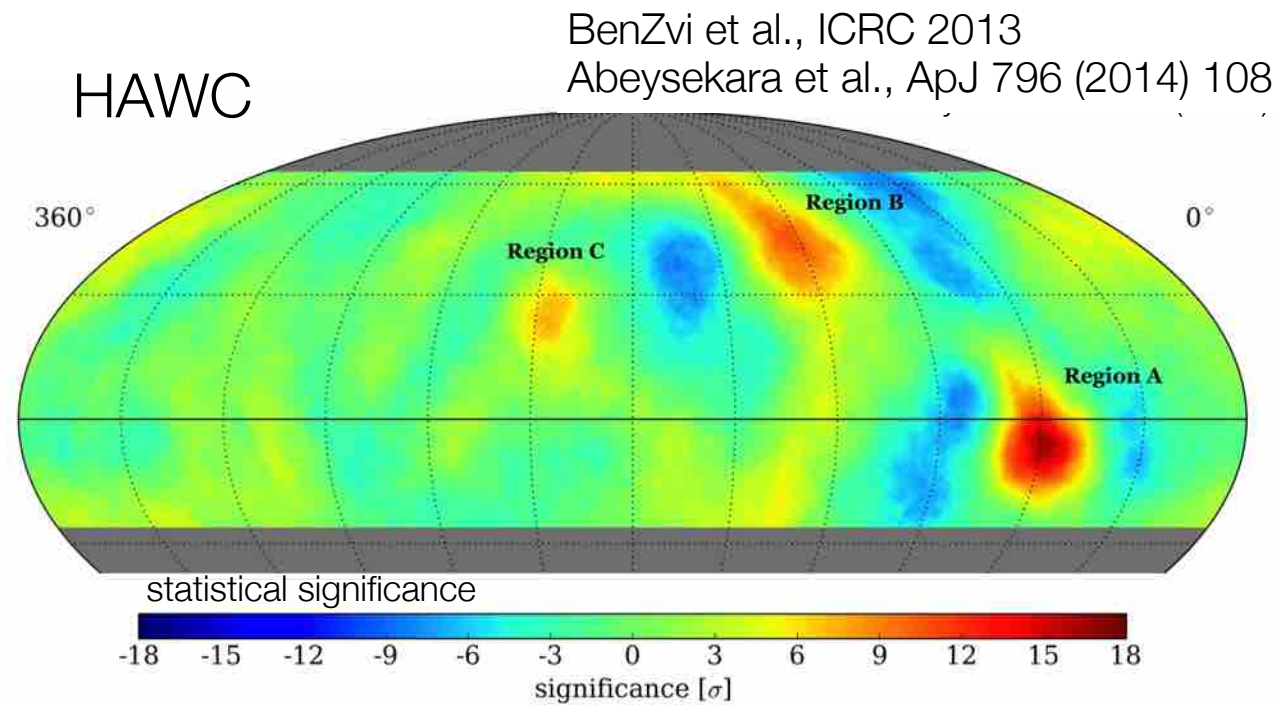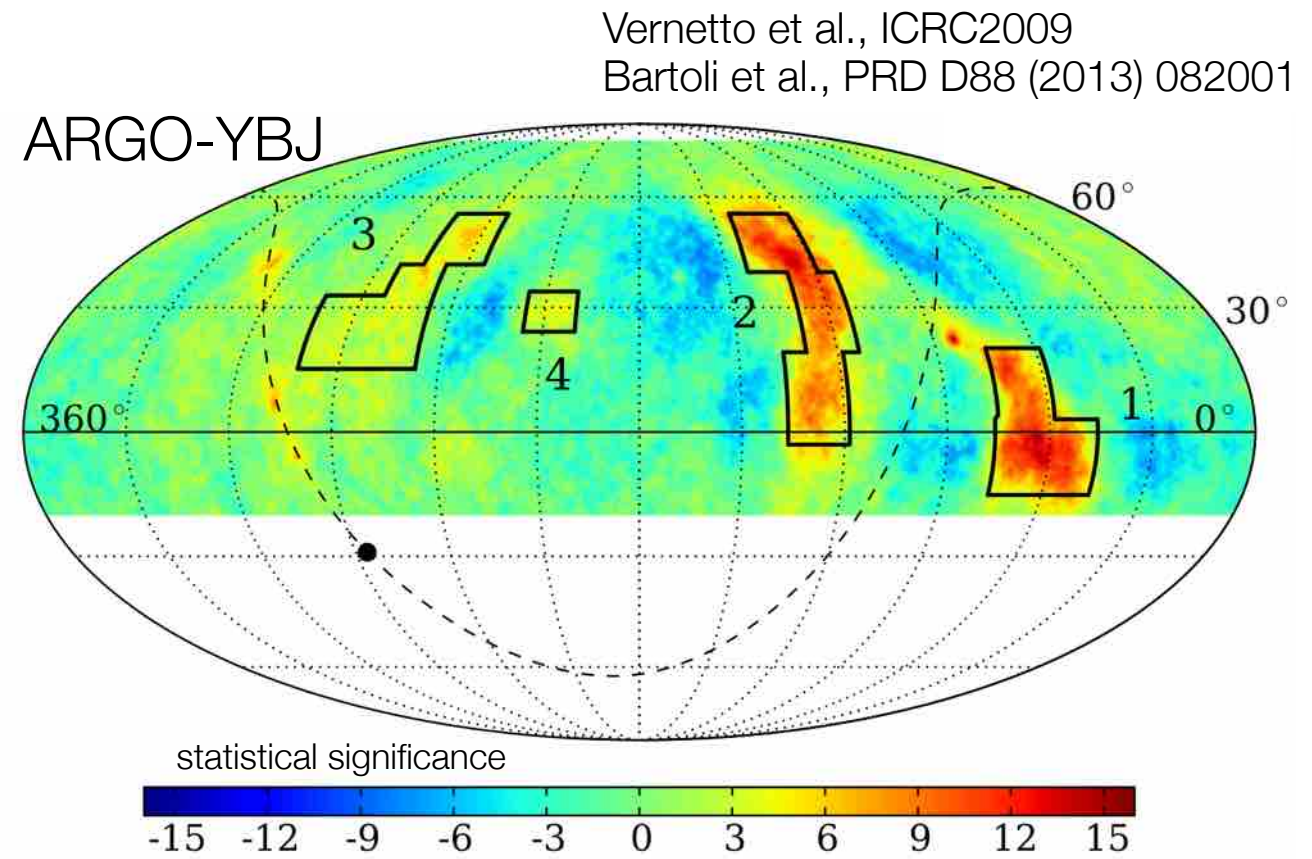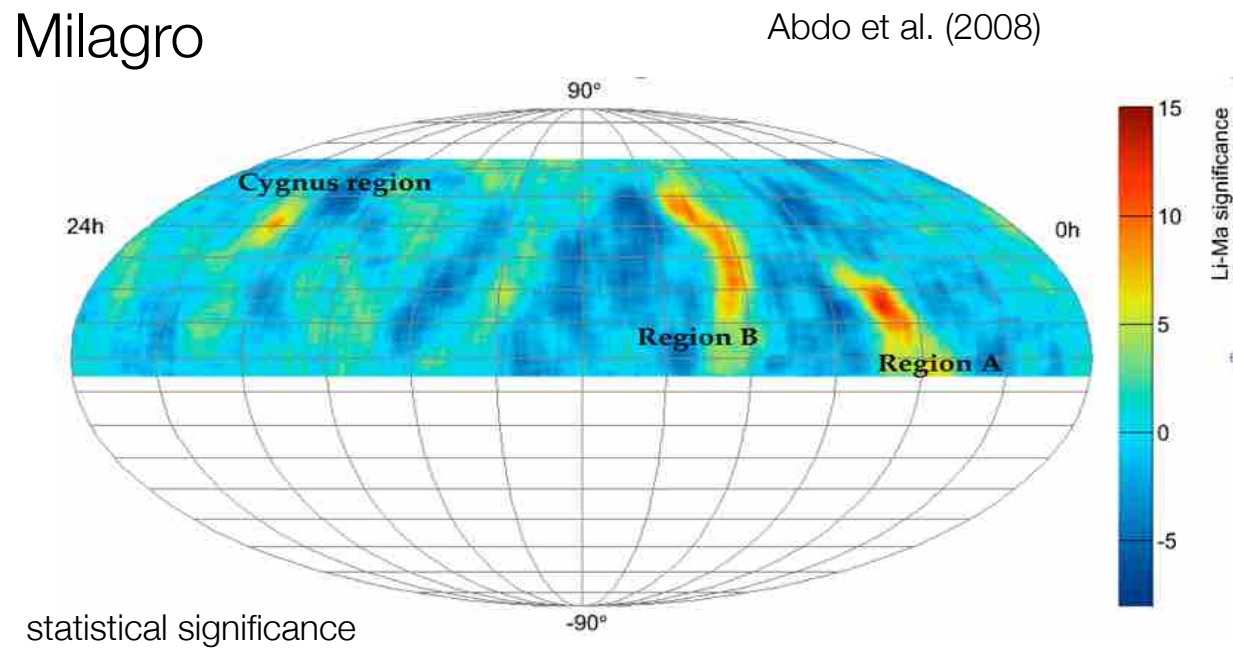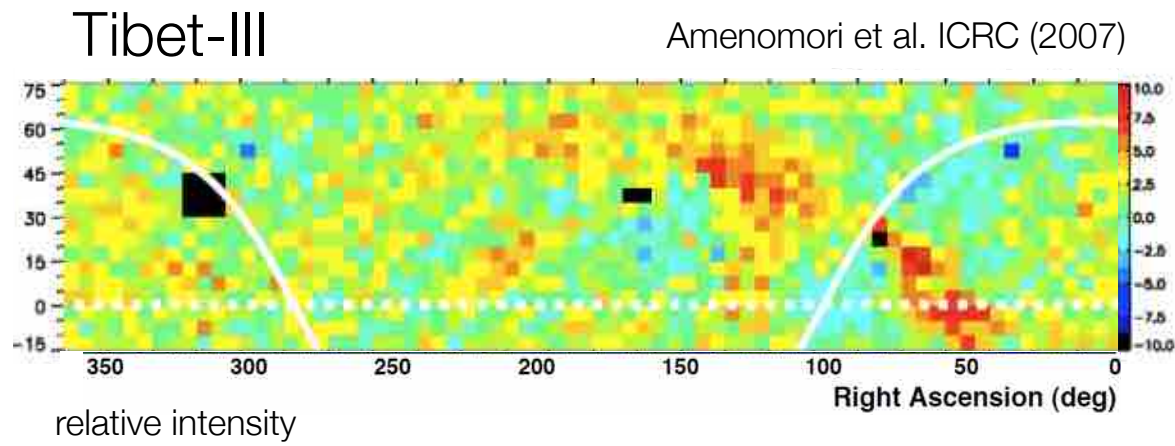
All-sky coverage of medium scale anisotropy

ARGO-YBJ

IceCube
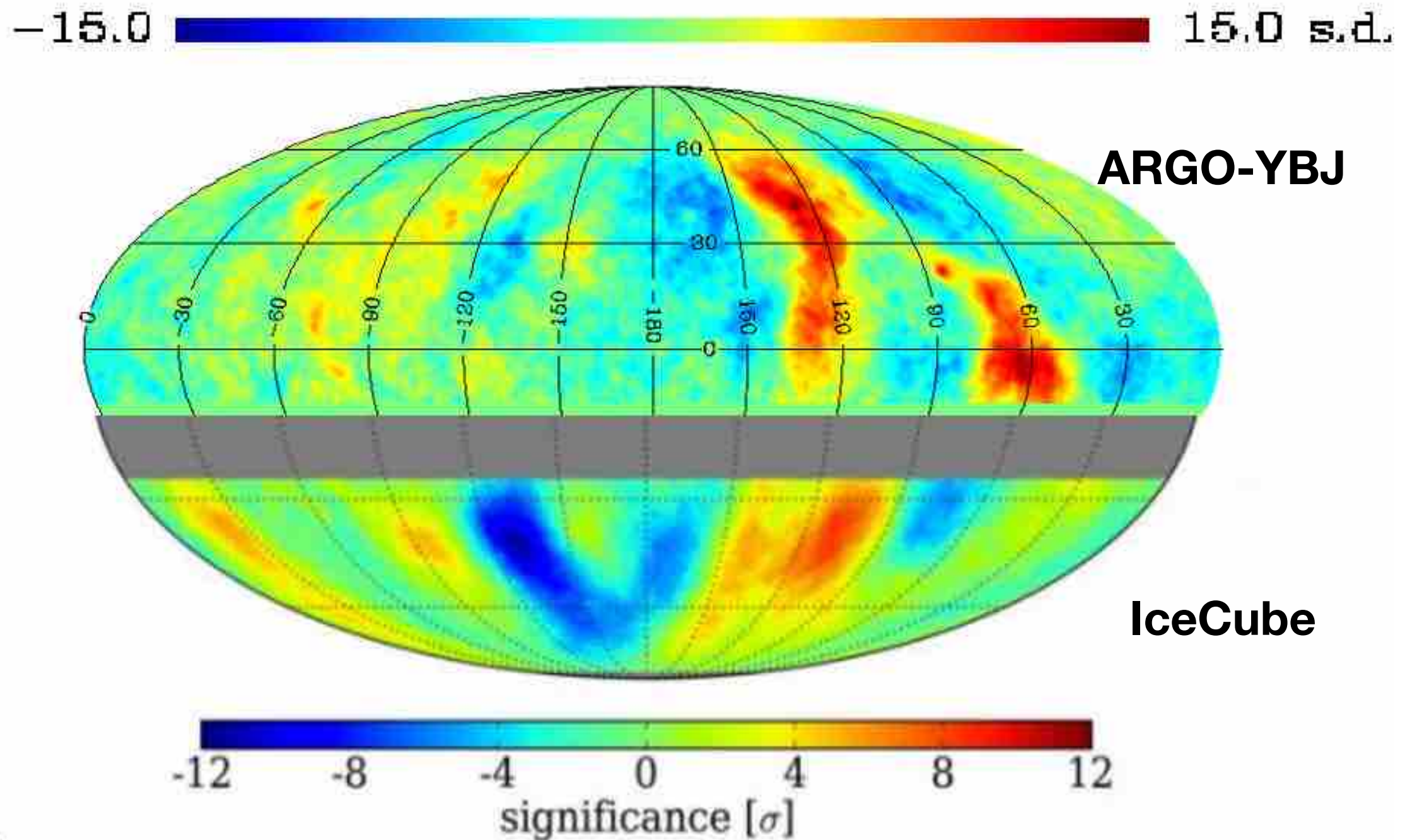
G. Di Sciascio and R. Iuppa, arXiv:1407.2144

A synoptic view of CR anisotropy

K. Nagashima, K. Fujimoto and R.M. Jacklyn,
J. Geophys. Res.103 (1998) 17429.
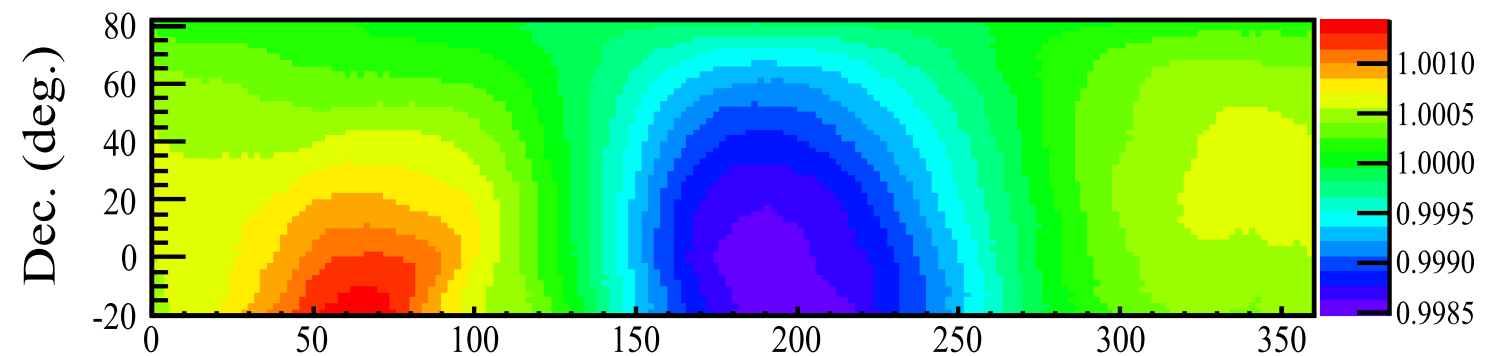
★ **Excess Region**, *"tail-in"*: an excess from the direction (40° - 90°, -24°) confined in a cone with a half opening angle of 68°, of non-galactic origin, supposed to be produced by the CR acceleration at the tail boundary of the *heliomagnetosphere* (HMS). Indeed, this direction approximately coincides with the *heliomagnetotail* direction. Disappeares at > 100 TeV.

★ **Deficit Region**, *"loss-cone"*: a galactic anisotropy consistent in a deficit flux from the direction (150° - 240°, 20°), confined in a cone with a half opening angle of 57°. The galactic origin is attributed since this feature is larger in the quiet period of the solar activity than in the active periods. Disappeares at > 100 TeV.

★ *"Nose-in"* (270° - 300°, 24° - 41°): heliospheric origin from the nose of HMS.
Observed only by muon telescopes and neutron monitor.

The evolution of the anisotropies of heliospheric origin is obviously related to the evolution of HMS. Indeed, since these anisotropies are considered to be produced by CR acceleration/interaction on the boundary surface of HMS, their magnitude, spectrum and direction would be variable in time. They are *unstable*, sometime in competition, *related to the solar activity and polarity and subject to seasonal variations.*

Conclusions

The origin of knee: the main open problem in Cosmic Ray Physics.

Understanding the origin of the "knee" is the key for a comprehensive theory of the origin of CRs up to the highest observed energies.

In fact, the knee is clearly connected with the issue of the end of the Galactic CR spectrum and the transition from Galactic to extra-galactic CRs.

The measurement of the energy spectrum of protons crucial to investigate the maximum energy of accelerated particles in CR sources.

What's next ?

★ Gamma-ray astronomy in the 100 - 1000 TeV energy range

★ High statistics measurement of energy spectra of different nuclei up to $10^{17} - 10^{18}$ eV

★ Evolution of the anisotropy across the knee energy range separately for different primary masses

★ Right altitude: close to the shower maximum ➜ > 4000 m asl

Outlook to the future: LHAASO

- **1.3 km² array**, including 5195 <u>scintillator</u> detectors 1 m² each, with 15 m spacing.

- An overlapping <u>1 km² array</u> of 1171, underground water Cherenkov tanks <u>36 m² each</u>, with 30 m spacing, for <u>muon detection</u> (total sensitive area ≈ <u>42,000</u> m²).
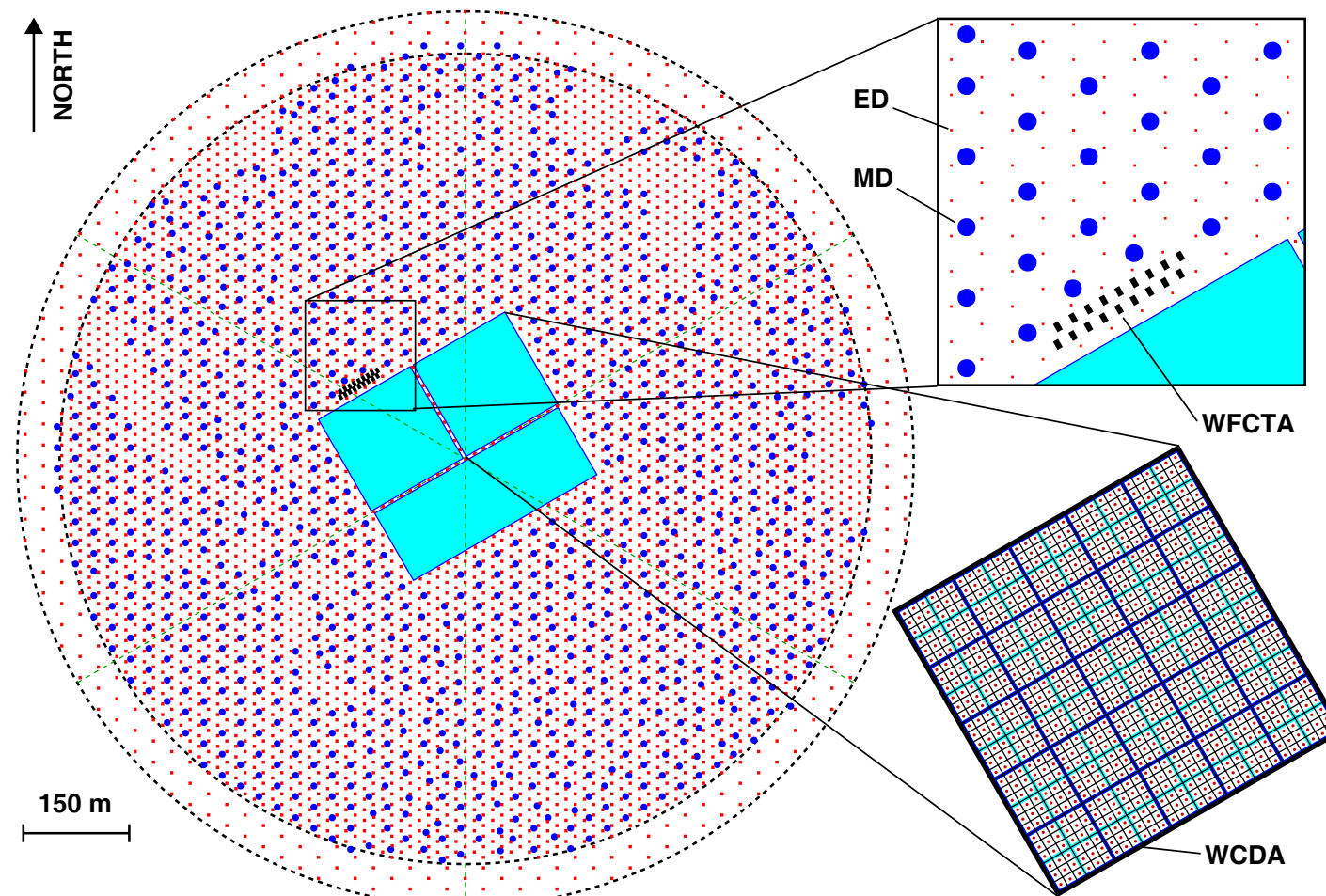
- A close-packed, surface <u>water Cherenkov detector</u> facility with a total area of <u>80,000 m²</u>.

- 18 wide field-of-view air Cherenkov (and fluorescence) telescopes.

- Neutron detectors

The LHAASO site

The experiment is located at 4400 m asl (600 g/cm^2) in the Haizishan (Lakes' Mountain) site, Sichuan province

Coordinates: 29° 21' 31'' N, 100° 08' 15'' E

700 km to Chengdu
50 km to Daocheng City (3700 m asl, guest house)
10 km to the highest airport in the world
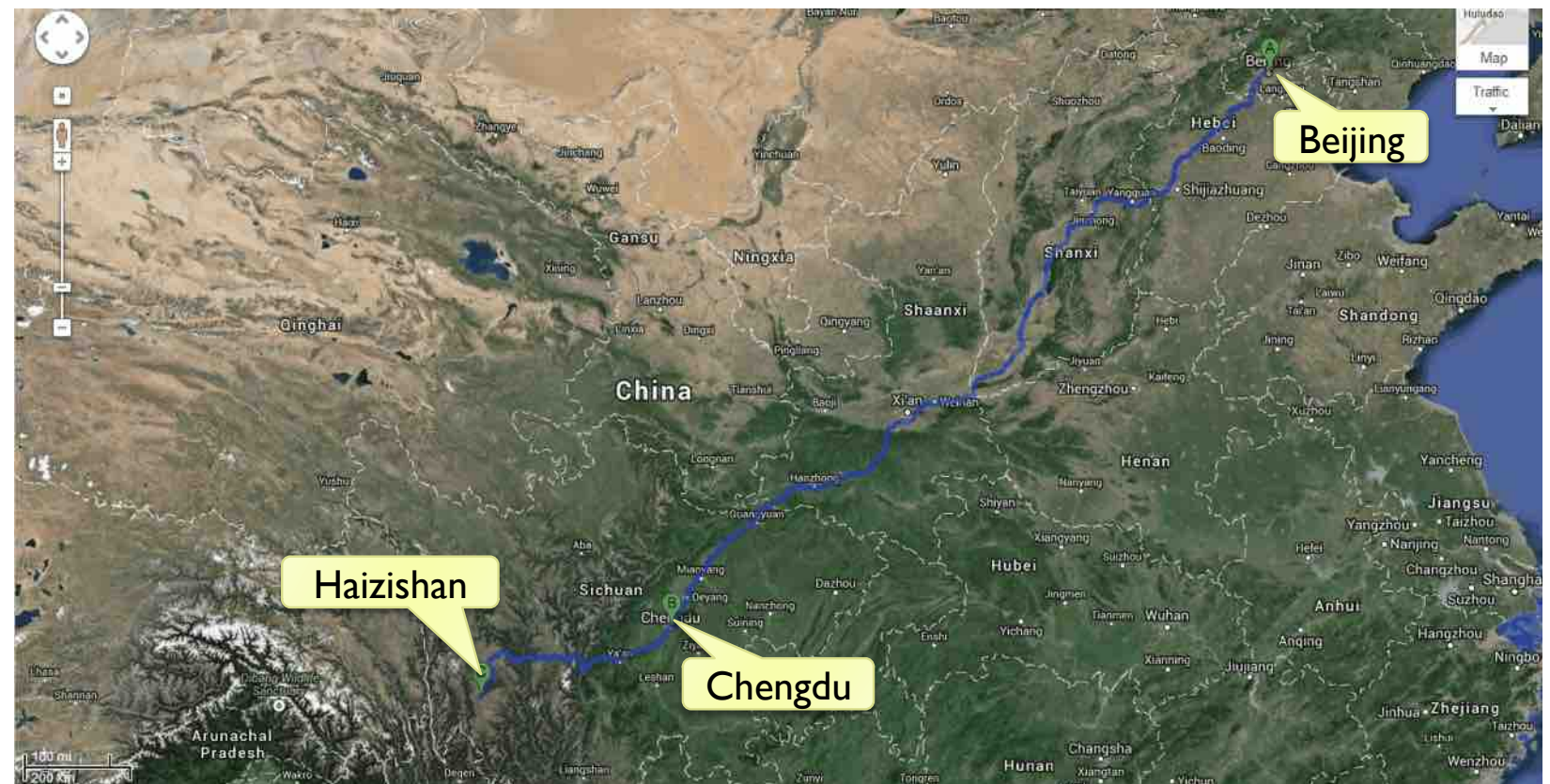
Status of the experiment

CATCHING RAYS
China's new observatory will intercept ultra-high-energy γ-ray particles and cosmic rays.

~25,000 m

12 wide-field-of-view air Cherenkov telescopes

80,000 m² surface-water Cherenkov detector

5,195 scintillator detectors

4,400 m

1,171 underground water Cherenkov tanks

©nature

Nature NEW 03/2017

China seeks cosmic-ray win
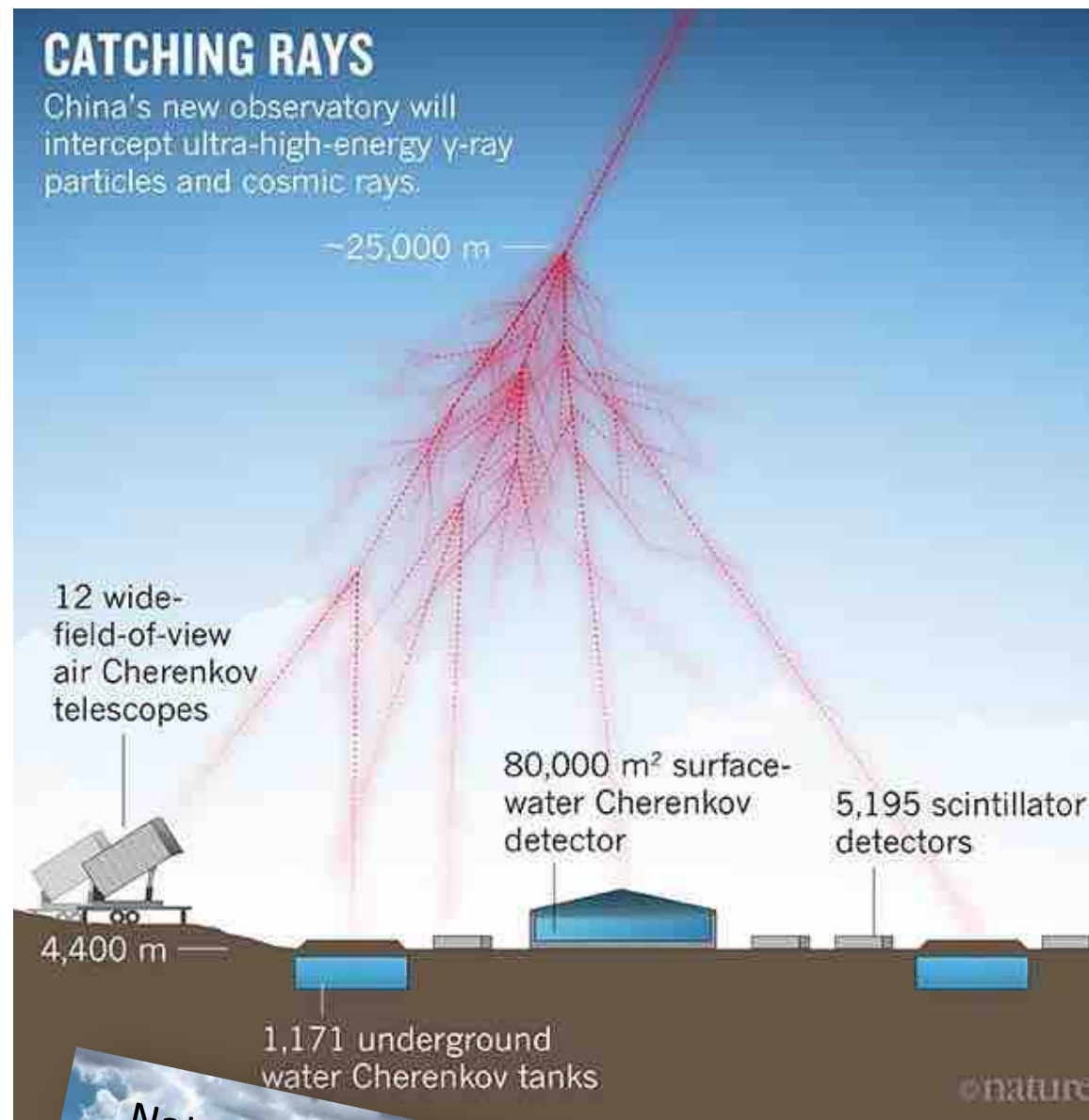
★ The first pond (HAWC-like) will be completed by the end of 2017 and instrumented in 2018.

The experiment will be located at 4400 m asl (600 g/cm²) in the Haizishan (Lakes Mountain) site, Sichuan province

★ 1/4 of the experiment in commissioning by the end of 2018 (sensitivity better than HAWC):

- 6 WFCTA telescopes
- 22,500 m² water Cherenkov detector
- ≈200 muon detectors

★ Completion of the installation in 2021.

LHAASO vs other EAS arrays

Experiment	Altitude (m)	e.m. Sensitive Area (m^2)	Instrumented Area (m^2)	Coverage
LHAASO	4410	5.2×10^3	1.3×10^6	4×10^{-3}
TIBET ASγ	4300	380	3.7×10^4	10^{-2}
IceTop	2835	4.2×10^2	10^6	4×10^{-4}
ARGO-YBJ	4300	6700	11,000	0.93 (central carpet)
KASCADE	110	5×10^2	4×10^4	1.2×10^{-2}
KASCADE-Grande	110	370	5×10^5	7×10^{-4}
CASA-MIA	1450	1.6×10^3	2.3×10^5	7×10^{-3}

		μ Sensitive Area (m^2)	Instrumented Area (m^2)	Coverage
LHAASO (✦)	4410	4.2×10^4	10^6	4.4×10^{-2}
TIBET ASγ	4300	4.5×10^3	3.7×10^4	1.2×10^{-1}
KASCADE	110	6×10^2	4×10^4	1.5×10^{-2}
CASA-MIA	1450	2.5×10^3	2.3×10^5	1.1×10^{-2}

✓ LHAASO will operate with a coverage similar to KASCADE (about %) over a much larger effective area.

✓ The detection area of muon detectors is about 70 times larger than KASCADE (coverage 5%) !

✓ Redundancy: different detectors to study hadronic models dependence

(✦) Muon detector area: 4.2 x 10⁴ m² + 8 x 10⁴ m² (WCDA)

"New excesses"

★ *Excess Region* (310° - 340°, 25°): 1 - 50 TeV ARGO-YBJ, Tibet ASγ. Cygnus region ???

★ *Excess Region* (230° - 260°, 0°): >100 TeV ARGO-YBJ, Tibet ASγ.

★ *Excess Region* (270°, <-20°): > 300 TeV IceCube, Tibet ASγ. CR streaming approximately from the Galactic Center direction.

The energy dependence of the anisotropy cannot be easily understood in a simple diffusion scenario with any types of GCR sources.

The knowledge of the propagation of GCRs needs to be further improved for our full understanding the properties of the anisotropy, especially in the high-energy region where the conventional diffusion/drift models may not work anymore.


Tibet ASγ
ApJ 836 (2017) 153
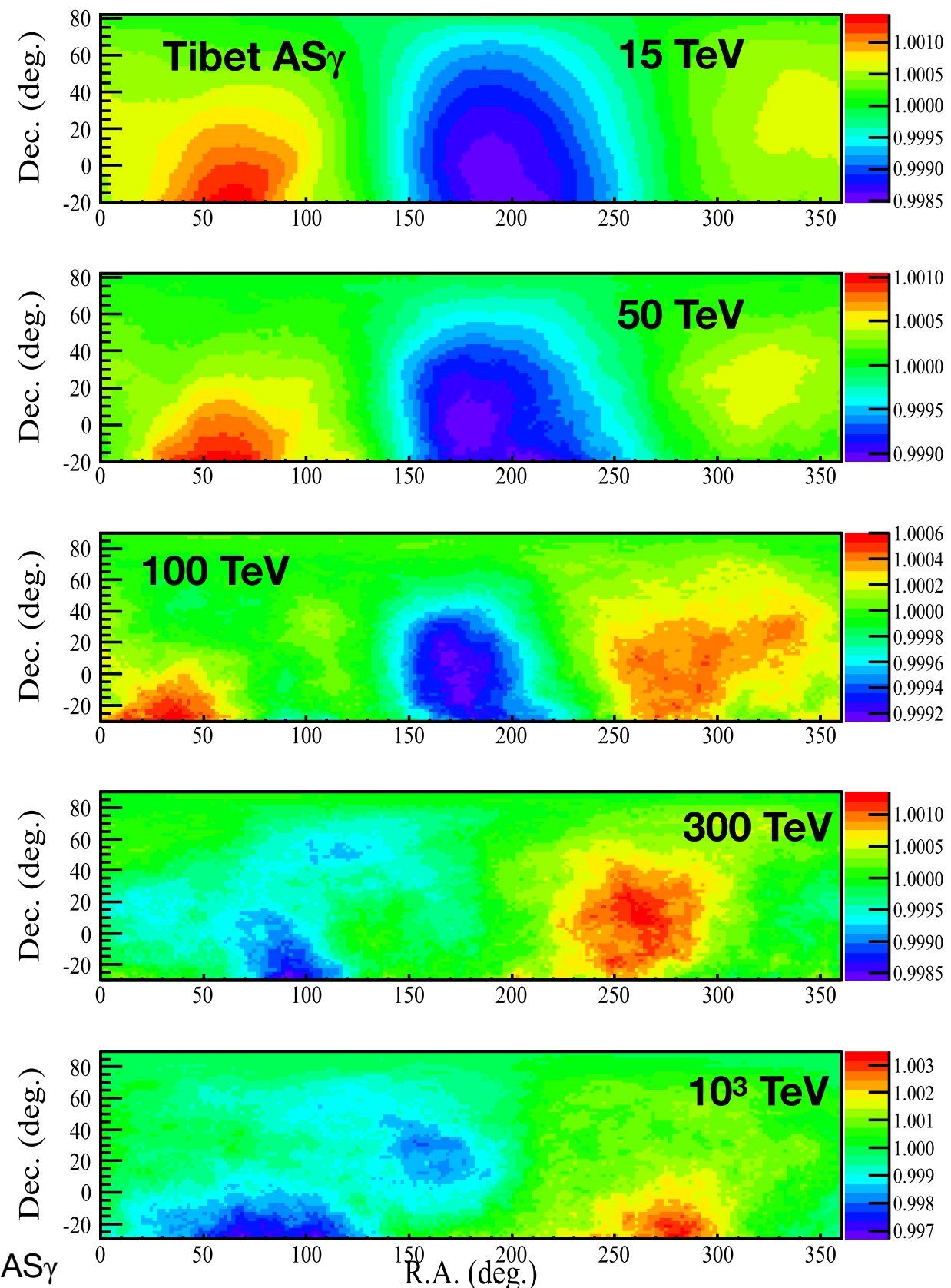
Solar vs Sidereal day

★ Sidereal day – time it takes a star at the meridian to return to the meridian. 23 hours 56 min 4 sec

★ Solar day – time it takes the Sun at meridian (noon) to return to the meridian. noon to noon or 24 hours

Why the 4-minute difference?

as it rotates, the Earth also orbits the Sun.
Earth must rotate an extra degree (4 min) each day…
for any observer on Earth to be at noon again
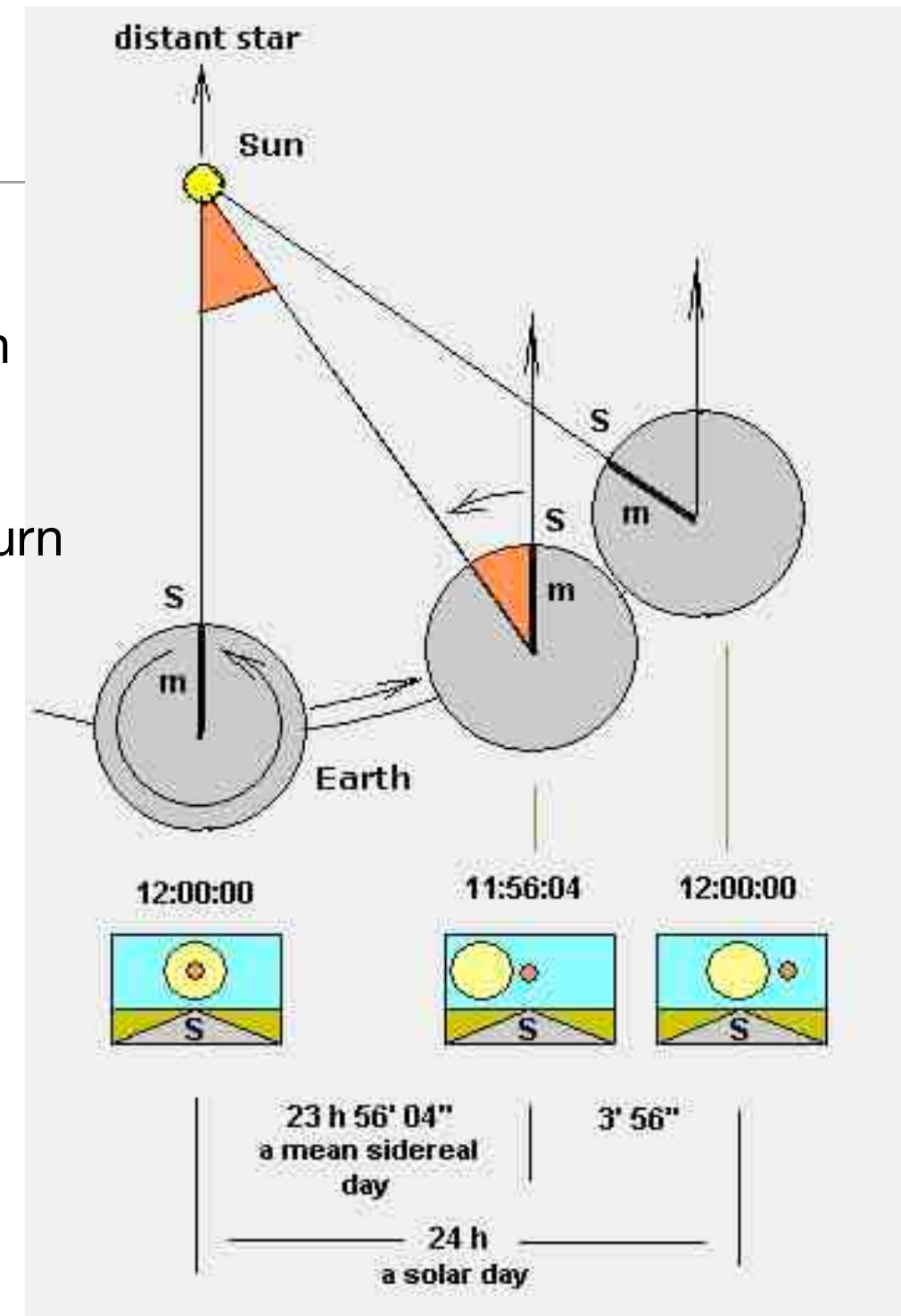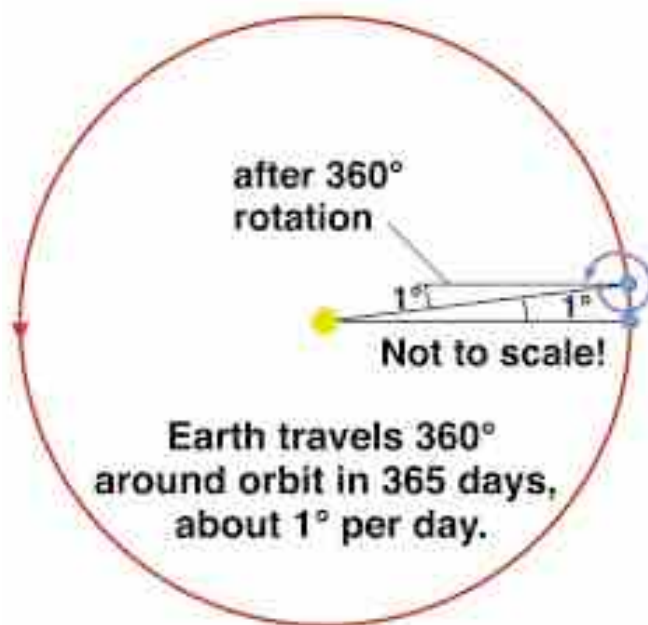
Probing heliospheric magnetic structure

TeV CRs can be used to probe the far reaches of heliosphere (e.g. the heliotail)

The *heliosphere* is the bubble-like region of space dominated by material emanating from the Sun (solar wind particles), which extends far beyond the orbit of Pluto.

Solar wind particles reach escape velocity, streaming outwards at 300 to 800 km/s.
As it begins to interact with the interstellar medium, its velocity slows to a stop. The point where the solar wind becomes slower than the speed of sound is called the *termination shock.*
The solar wind continues to slow as it passes through the *heliosheath* leading to a boundary called the *heliopause*, where the interstellar medium and solar wind pressures balance.

Cosmic rays, fast-moving neutral atoms, and cosmic dust can penetrate the heliosphere from the outside.

The *heliotail* is the tail of the heliosphere, and thus the solar system's tail. It can be compared to the tail of a comet.
The tail is a region where the Sun's solar wind slows down and ultimately escapes the heliosphere, slowly evaporating.
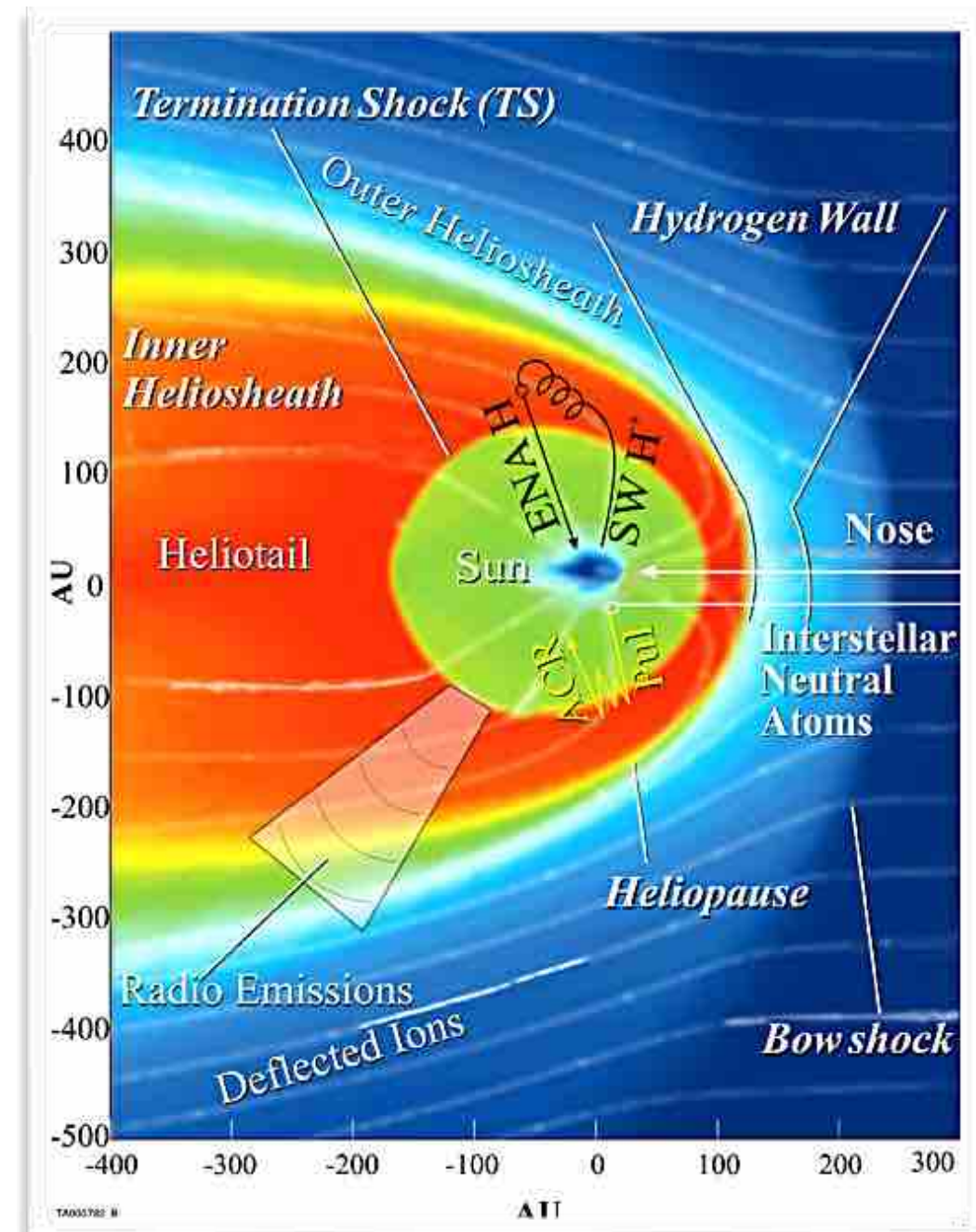
The Compton-Getting effect
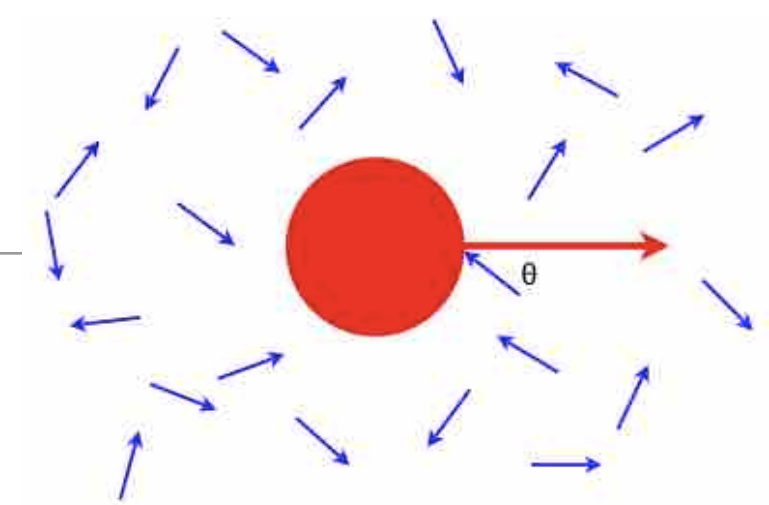
★ **Expected CR anisotropy due to Earth's orbital motion around the Sun**: when an observer (CR detector) moves through a gas which is isotropic in the rest frame (CR "gas"), he sees a current of particles from the direction opposite to that of its own motion.

Compton, A. H., & Getting, I. A. 1935, PhRv, 47, 817

A benchmark for the reliability of the detector and the analysis method. In fact, all the features (period, amplitude and phase) of the signal are predictable without uncertainty, due to the exquisitely kinetic nature of the effect.

$$\frac{\Delta I}{\langle I \rangle} = (\gamma + 2)\frac{v}{c}\cos\vartheta$$

I = CR intensity
γ = power-law index of CR spectrum (2.7)
v = detector velocity ≈ 30 km/s
θ = angle between detector motion and CR arrival direction

0°

A detector on the Earth moving around the Sun scans various directions in space while Earth spins.
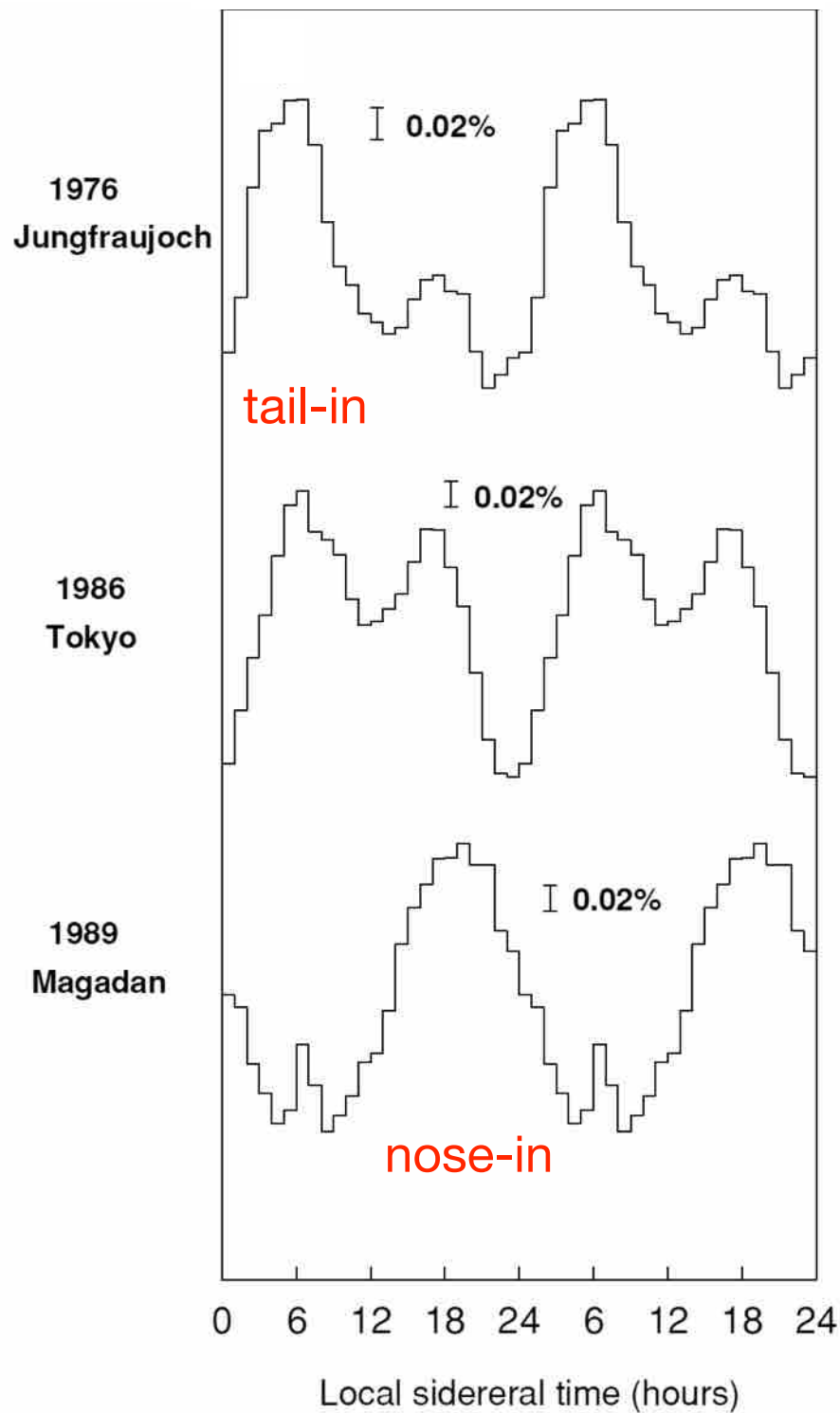Maximum at 6 hr solar time (when the detector is sensitive to a direction parallel to 's orbit)

270°

$$\frac{\Delta I}{\langle I \rangle}(\exp): 0.047\%$$

$$\varphi(\exp): 6hr$$

The first clear observation of the SCG effect with an EAS array was reported by EAS-TOP (LNGS) in 1996 at about 10^{14} eV.

The *'nose-in'* anisotropy

1976
Jungfraujoch

tail-in

1986
Tokyo

1989
Magadan

nose-in

Local sidereal time (hours)

Nagashima 2005, 2012

**Sharply concentrated cosmic-ray excess fluxes from heliomagnetospheric nose
and tail boundaries observed with neutron monitors on the ground**

K. Nagashima[1], I. Kondo[2], and Z. Fujii[1]

Two kinds of sharply concentrated excess flux of cosmic rays from heliomagnetospheric nose and tail directions (right ascension $\alpha \sim 18$ hours and ~ 6 hours) are found by the analysis of sidereal daily variation of neutron intensity (median energy $E_m \sim 20$ GeV) on the ground.

Table 1. Modulation pattern of sidereal anisotropy by GA, TA, and HA.

	Polarity 22 yr period		Solar activity 11 yr period		Direction Φ		
	P	N	A	Q	α (hr)	$\delta(°)$	Origin
GA	<		<		0	−20	Galactic
TA	>		>		6	−24	Solar (Tail boundary)
HA	<		>		18	>0	Solar (Nose boundary)

It is shown that the sidereal anisotropy (S_iA) of cosmic rays (CRs) with energies smaller than 10^4 GeV consists of three kinds: one (GA) is of galactic origin from the direction Φ_G ($\alpha_G = 0$ hr; $\delta_G = -20°$), and the other two (tail-in TA and nose-in HA) are of solar origin from the respective directions Φ_T ($\alpha_T = 6$ hr; $\delta_T \sim -24°$) and Φ_H ($\alpha_H = 18$ hr; $\delta_H > 0°$) and supposed to be produced by the acceleration of CRs on the tail and nose boundaries of the heliomagnetosphere (HMS). This conclusion was arrived at in 1995 after a long-term delay since the

so far observed only by neutron monitor and muon detectors

The ARGO-YBJ experiment

ARGO-YBJ is a telescope optimized for the detection of small size air showers
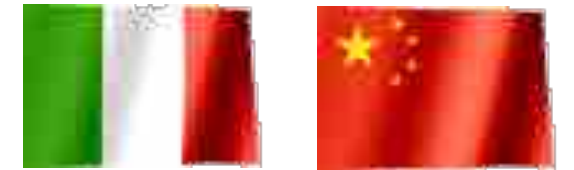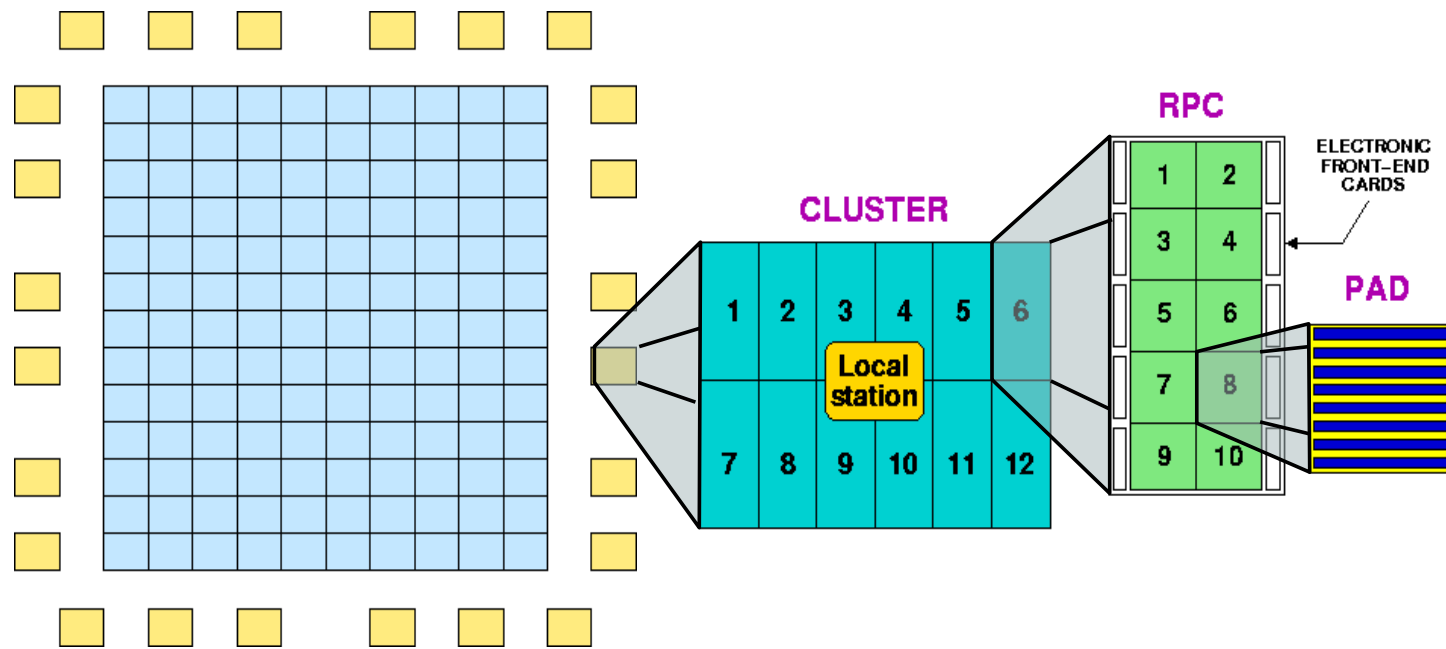
INFN   IHEP/CAS

Longitude: 90° 31' 50'' East
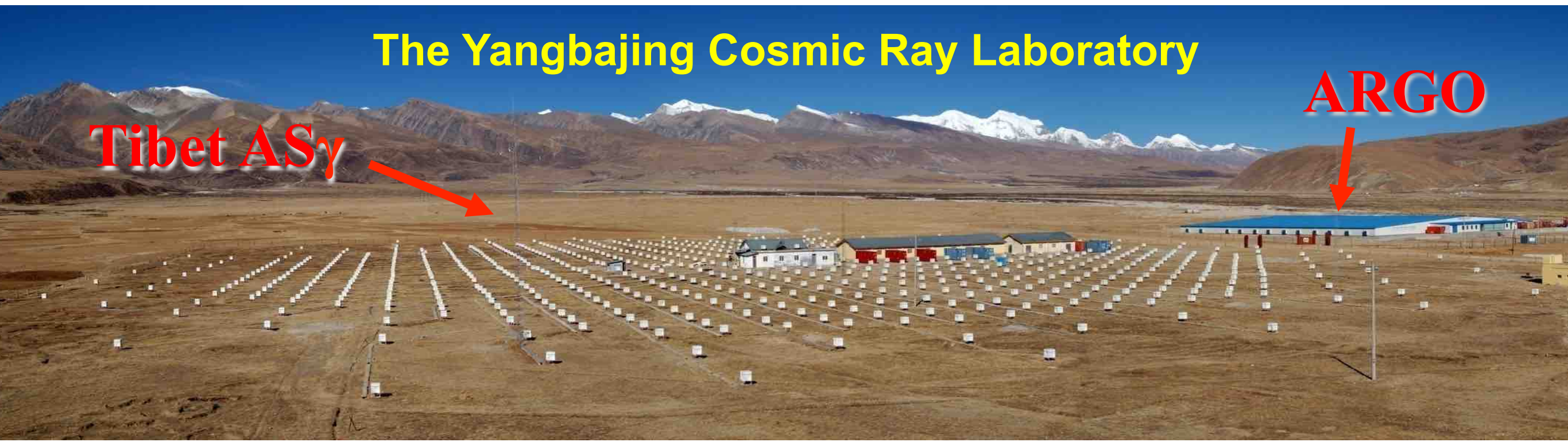Latitude: 30° 06' 38'' North
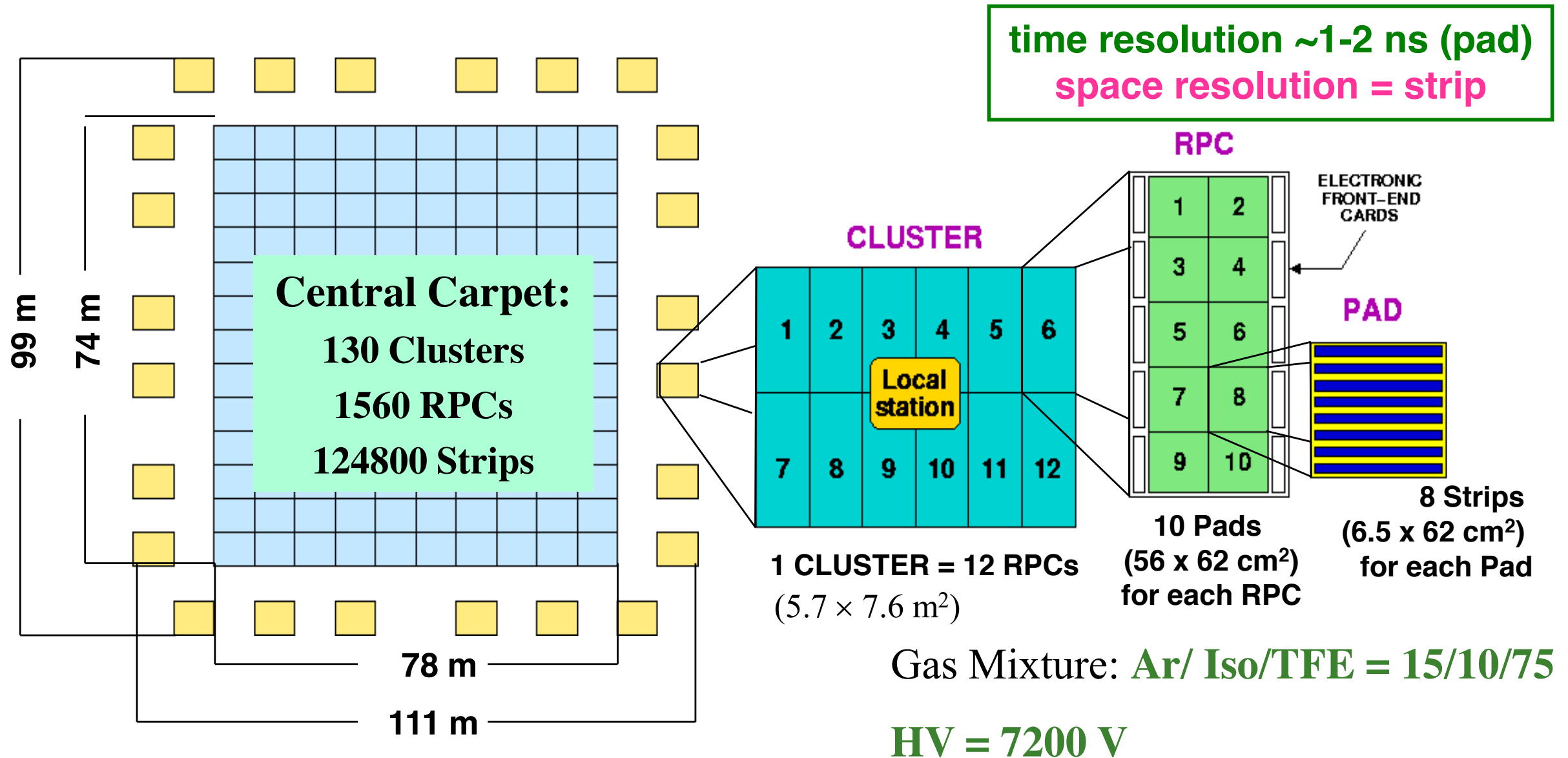
90 km North from Lhasa (Tibet)

4300 m above sea level
$\sim 600\ g/cm^2$

The Yangbajing Cosmic Ray Laboratory

Tibet ASγ

ARGO

The ARGO-YBJ layout

Central Carpet:
130 Clusters
1560 RPCs
124800 Strips

99 m
74 m
78 m
111 m

RPC

ELECTRONIC FRONT–END CARDS

CLUSTER

| 1 | 2 | 3 | 4 | 5 | 6 |
| Local station |
| 7 | 8 | 9 | 10 | 11 | 12 |

1	2
3	4
5	6
7	8
9	10

PAD

1 CLUSTER = 12 RPCs
(5.7 × 7.6 m²)

10 Pads
(56 x 62 cm²)
for each RPC

8 Strips
(6.5 x 62 cm²)
for each Pad

Gas Mixture: **Ar/ Iso/TFE = 15/10/75**

HV = 7200 V

**Single layer of Resistive Plate Chambers (RPCs)
with a full coverage (92% active surface) of a large area (5600 m²)
+ sampling guard ring (6700 m² in total)**
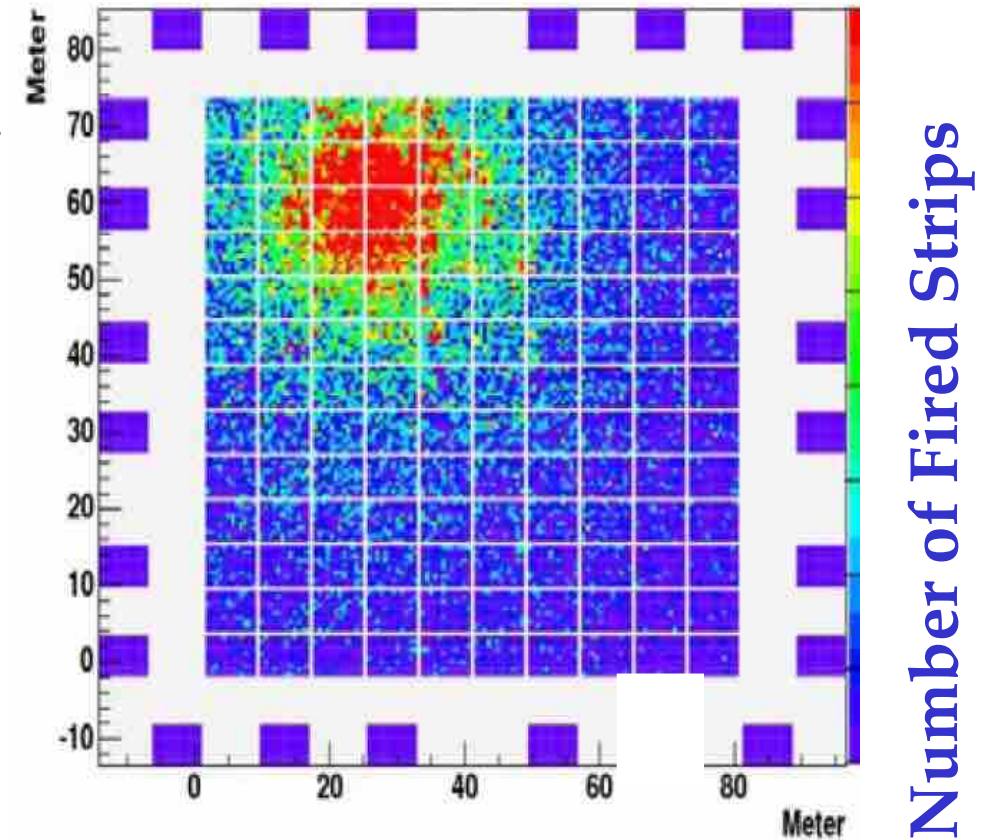
The basic concepts

…for an unconventional air shower detector

❖ **HIGH ALTITUDE SITE**
(YBJ - Tibet 4300 m asl - 600 g/cm2)

❖ **FULL COVERAGE**
(RPC technology, 92% covering factor)

❖ **HIGH SEGMENTATION OF THE READOUT**
(small space-time pixels)

Space pixels: 146,880 strips (7×62 cm2)
Time pixels: 18,360 pads (56×62 cm2)

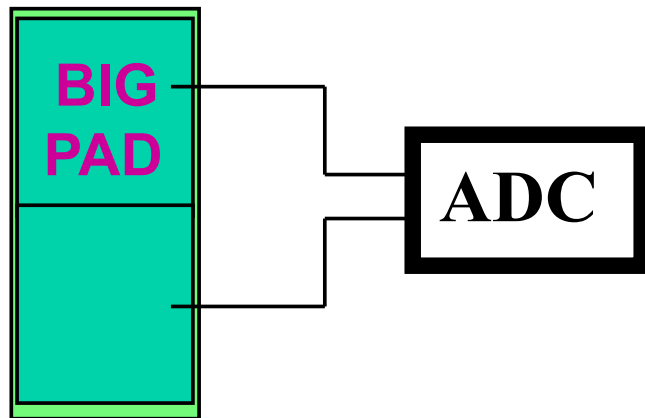*… in order to*

• image the shower front with unprecedented details

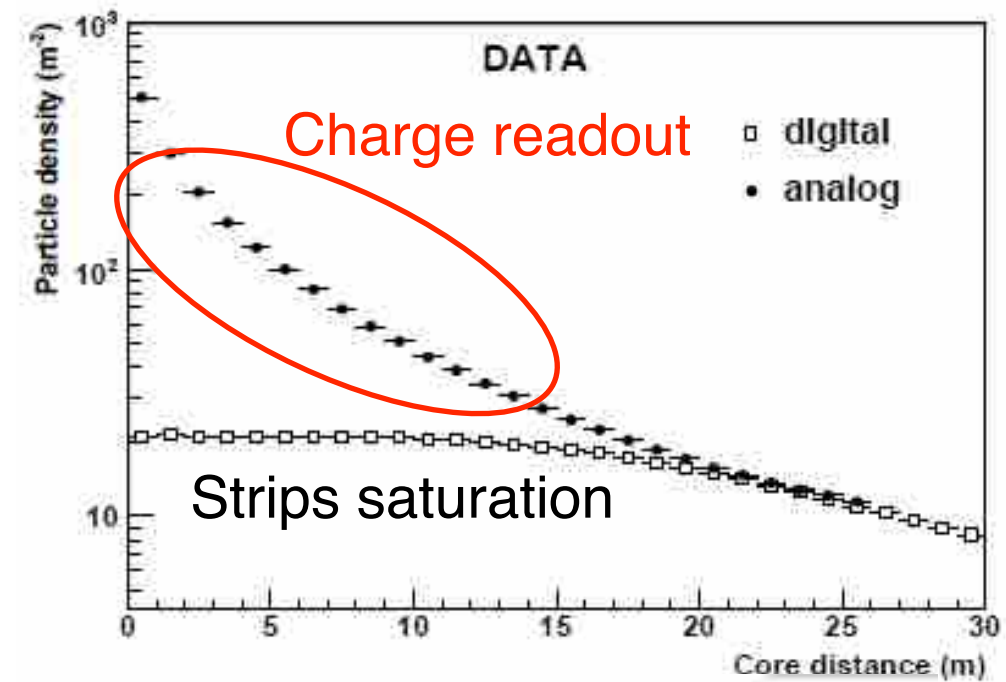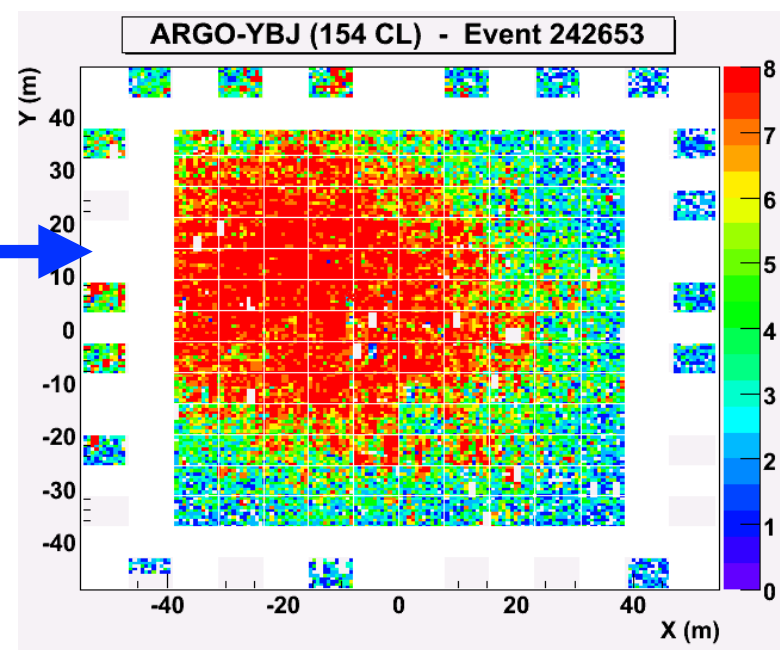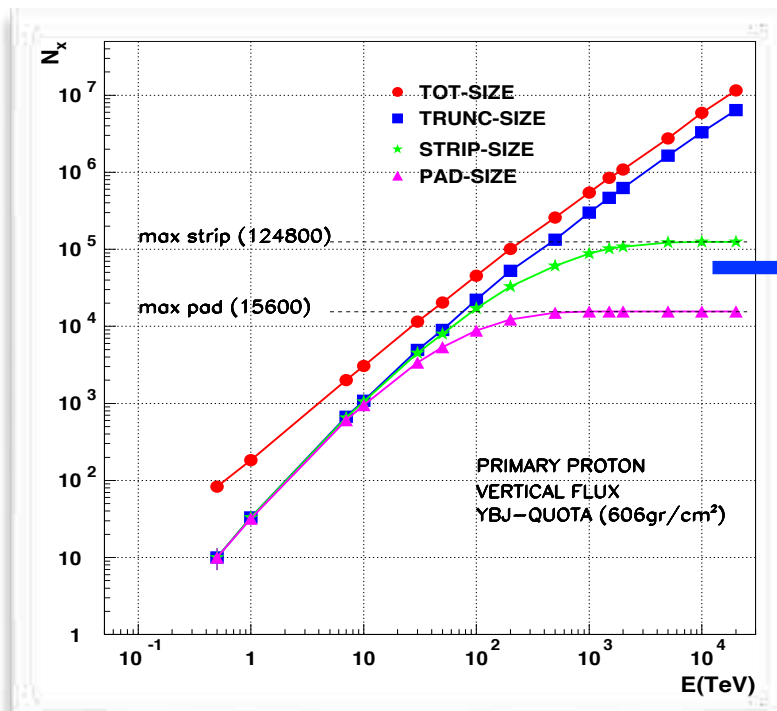• get an energy threshold of a few hundreds of GeV

Number of Fired Strips

Real event
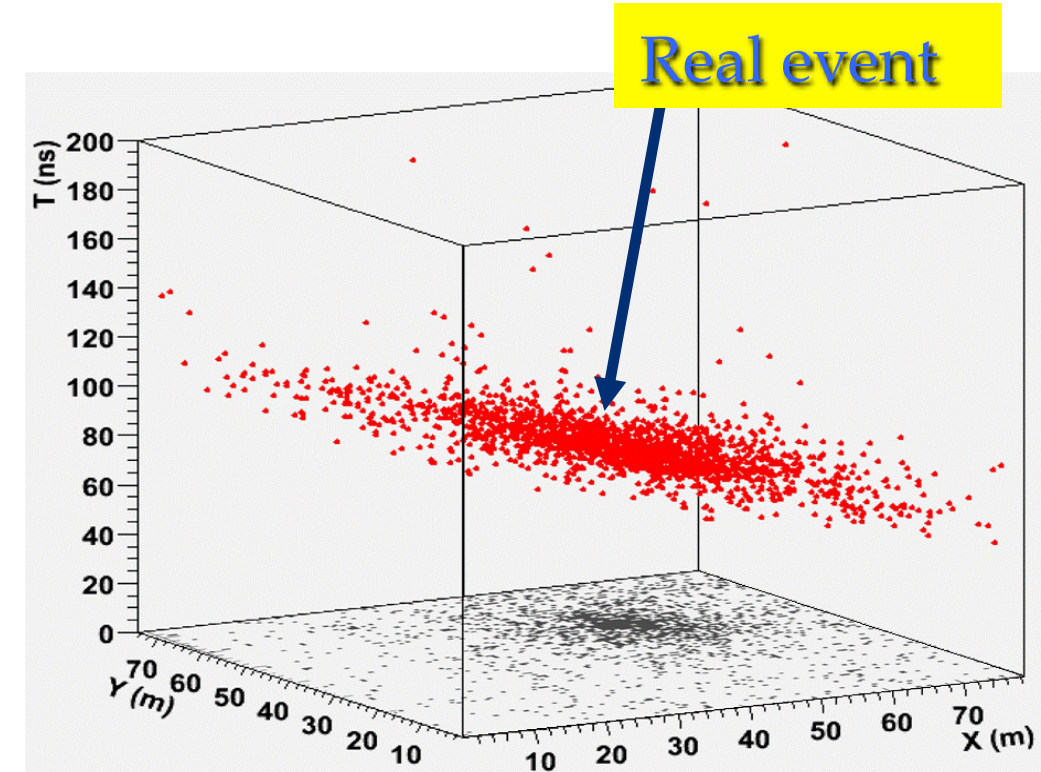
The RPC charge readout

…extending the dynamical range up to 10 PeV

Time pixel
(56 x 62 cm²)
#18360

.5

Space (digital) pixel
(6.7 x 62 cm²)
#146880

BIG PAD — **ADC**

4 different gain scales used to cover
a wide range in particle density:

$$\rho_{max-strip} \approx 20 \text{ particles/m}^2$$

$$\rho_{max-analog} \approx 10^4 \text{ particles/m}^2$$

ARGO-YBJ (154 CL) - Event 242653

DATA

Charge readout

□ digital
● analog

Strips saturation
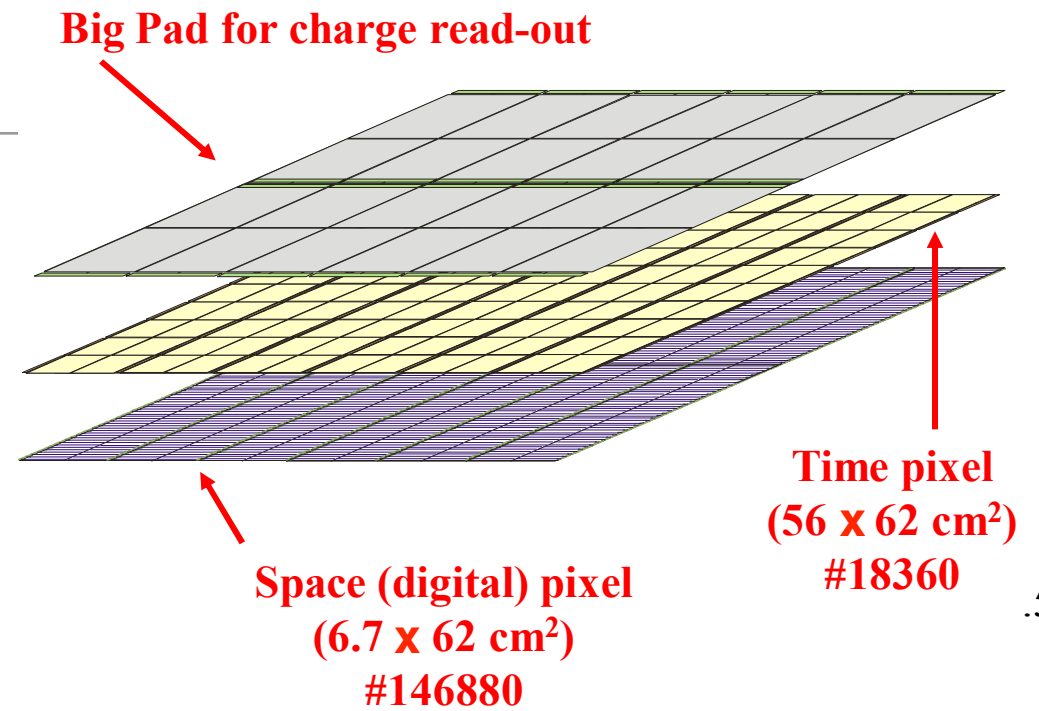
ARGO-YBJ milestones

- In data taking since July 2004 (with increasing portions of the detector)
- Commissioning of the central carpet in June 2006
- Stable data taking with full apparatus since November 2007
- End/Stop data taking: February 2013

- Average duty cycle ~87%
- Trigger rate ~3.5 kHz @ 20 pad threshold
- N. recorded events: ≈ $5 \cdot 10^{11}$ from 100 GeV to 10 PeV
- 100 TB/year data
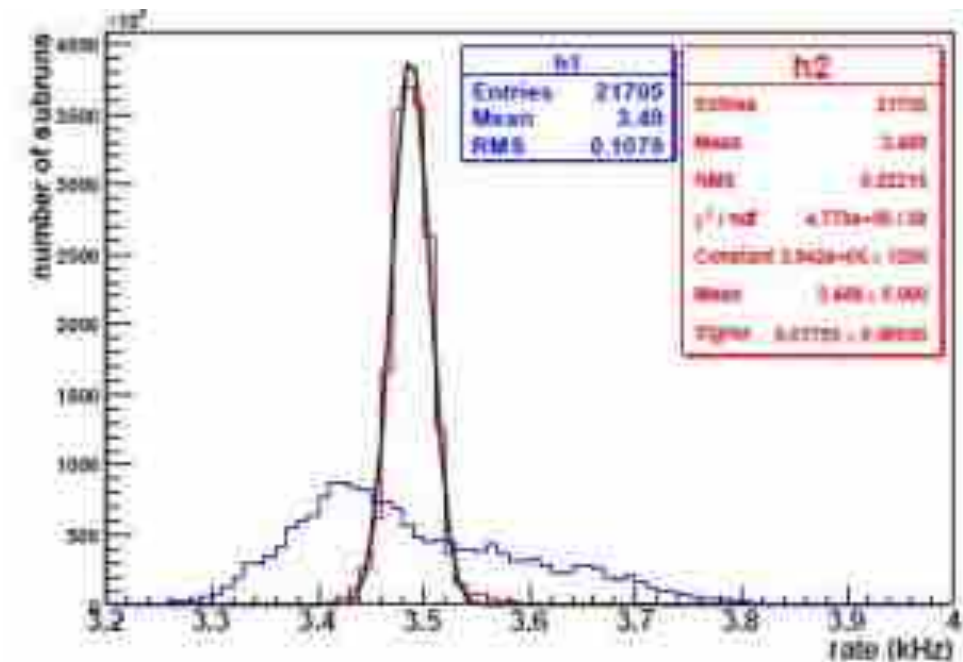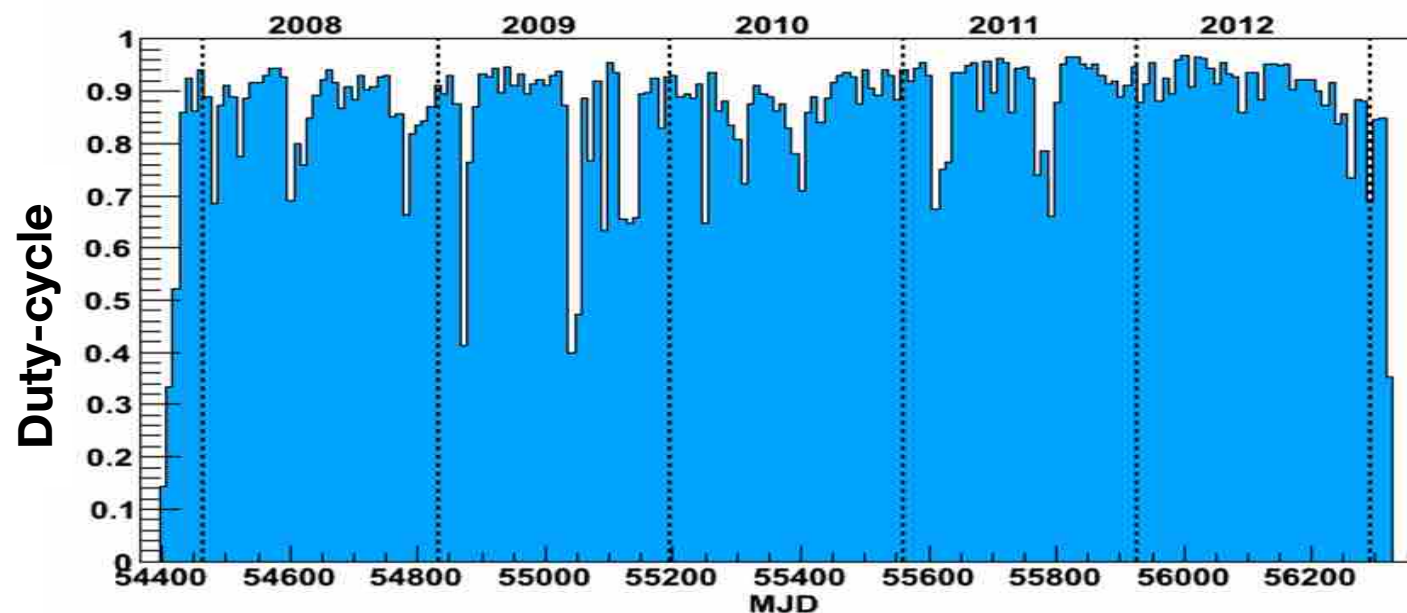
Intrinsic Trigger Rate stability 0.5%
(after corrections for T/p effects)

Measurement of CR energy spectrum with ARGO-YBJ

- Measurement of the CR energy spectrum (all-particle and light component) in the energy range TeV - 20 PeV by ARGO-YBJ with *different 'eyes'*

  ▶ *'Digital readout'* (based on *strip multiplicity*) below 300 TeV
  ▶ *'Analog readout'* (based on the *shower core density*) up to 20 PeV
  ▶ *'Hybrid'* measurement with a *Wide Field of view Cherenkov Telescope* 200 TeV - few PeV

- Working at high altitude (4300 m asl):

  1. p and Fe produce showers with similar size
  2. Small fluctuations: shower maximum
  3. Low energy threshold: absolute energy scale calibration with the Moon Shadow technique and overposition with direct measurements
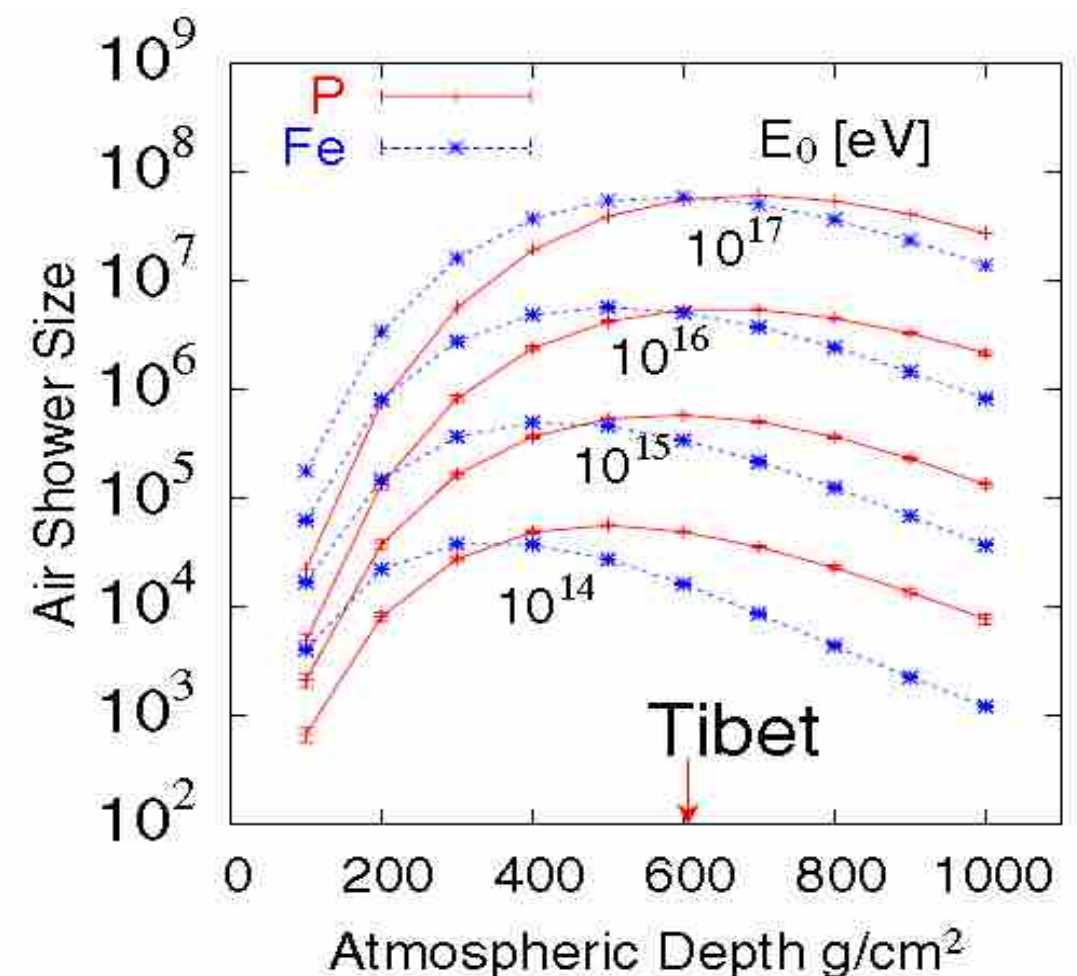
Selection of light (p+He)

- Selection of (p+He)-induced showers: **NOT** by means of an unfolding procedure after the measurement of electronic and muonic sizes, but on an event-by-event basis exploiting showers topology, i.e. the lateral distribution of charged secondary particles.

- Energy reconstruction is based on the N_p^{8m} parameter: the *number of particle within 8 m from the shower core position.*

This truncated size is

- well correlated with primary energy
- not biased by finite detector effects
- weakly affected by shower fluctuations

Energy resolution
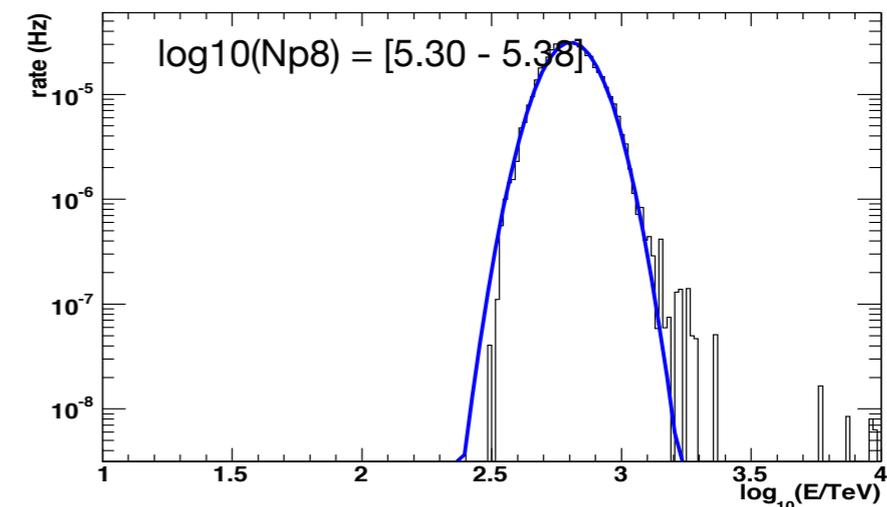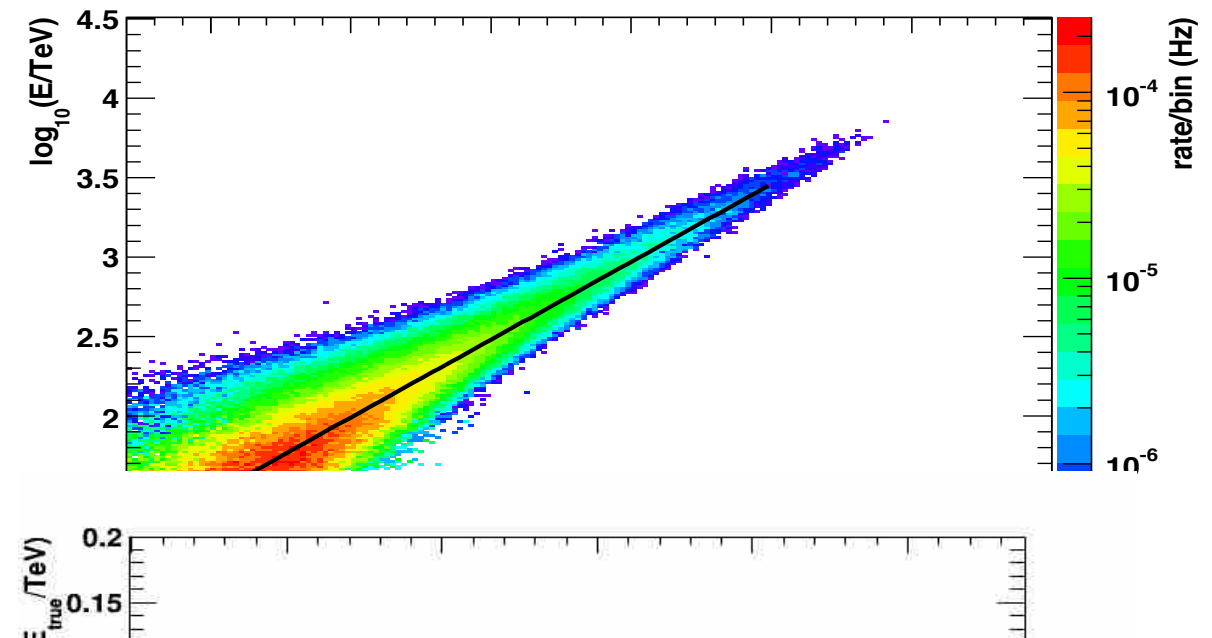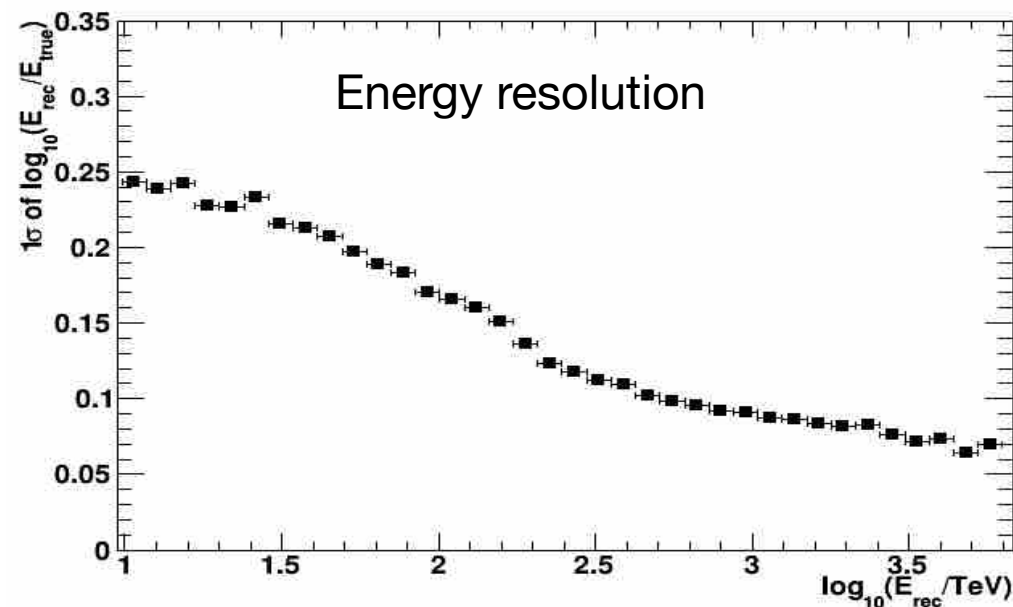
Comparison with other experiments